EUROPEAN ORGANIZATION FOR NUCLEAR RESEARCH

CERN/SPSC/74-46
SPSC/P 4 / Add 1
4.4.1974

MEMORANDUM

TO: S.P.S.C.

FROM: Bari-CAEN-CERN(NP/TC)-Liverpool-Milan Collaboration

RE: Addendum to "Proposal for a detailed study of high - p_t events at the SPS". (SPSC/P4)

BF/mk

I. INTRODUCTION

Having taken note of the points raised during our presentation of the proposal to the open session of the SPSC, we give here our present ideas as regards the trigger along with more detailed information on the various parts of the apparatus. The following points will be discussed.

Sec. II : The time schedule and the manpower needed to be on the SPS floor by September 1976.

Sec. III : The modified trigger system (the scintillator hodoscope and the Cerenkov system is now backed up by two calorimeters so as to allow an independent selection on the momentum of the wanted particles while reducing the background of unwanted triggers).

Sec. IV : The Cerenkov counter design.

Sec. V : The vertex detector design (details on the MWPC's).

Sec. VI : The forward detector design (details on the drift chambers).

Sec. VII : The data acquisition system.

Sec. VIII : The pattern recognition.

This completes our White Book on the specific apparatus needed to study in detail the high transverse momentum phenomena at the SPS.

II. THE SCHEDULE AND MANPOWER

According to the project schedule (Table I) the year 1974 will be devoted to studies, tests and fabrication of prototypes. Production should start at the beginning of 1975 and be completed by 1976. Installation at the SPS will commence somewhat earlier than July 1976. The achievement of such a schedule requires the technical support listed below.

Mechanical construction of the vertex MWPC's forward drift chambers and Cerenkov counters

	MAN-YEARS			
	1974	1975	1976	
1. Designers and laboratory technicians for design, development, tests, production control, assembly, etc.	6	4	3	
2. Machinists (CERN)	2	2	2	
3. Cablers for MWPC's and drift chambers (Regie)	1	3	2	
Total	9	9	7	25

4. Technicians (Regie). These will be necessary for the fabrication and assembly. Their importance will vary depending on the division of work in the CERN and outside workshops. The estimated total cost of the MWPC and drift chamber system includes the cost of all sources of manpower.

Electronics

MAN-YEARS

	1974	1975	1976	
1. Engineers and technicians				
a) MWPC's and drift chambers..............	4	4	3	
b) Fast electronics and trigger...........	1	1	1	
c) Reading and coding logic and interface............................	1	1	1	
d) Software for data acquisition..........	½	1	½	
2. Cablers (Regie)	3	5	5	
3. Designers for printed circuits	½	1	½	
Total	10	13	11	34

Cerenkov optics

1. Study and design (Engineer) and assembly	½	½	½	
2. Fabrication of mirrors and light catchers	¼	½	¼	
3. Mirror coating	¼	1	¼	
Total	1	2	1	4

Counters

1. Scintillators: fabrication and assembly of hodoscopes (West Workshop)	0	¼	¼	
2. Calorimeters (West Workshop)*)	½	1½	½	
Total	½	1 3/4	3/4	3

*) Scintillators and light guides will be purchased from outside sources.

Hence we arrive at a grand total of 66 man-years. Of these, 19 are from outside regie and 47 from CERN. The CERN load would then amount to a total of 18 men over ∿ 2.5 years.

Magnet

The possibility of building a copy of the Saclay magnet "GOLIATH" has been examined during a visit to ALSTHOM (Belfort) on 3/4/1974. The company confirms that the construction schedule given in Table I is realistic provided an order for the coils is submitted not later than September 1st, 1974.

TABLE 1

Time schedule of the project. The names of the rsons responsible for the various items are shown in parenthesis.

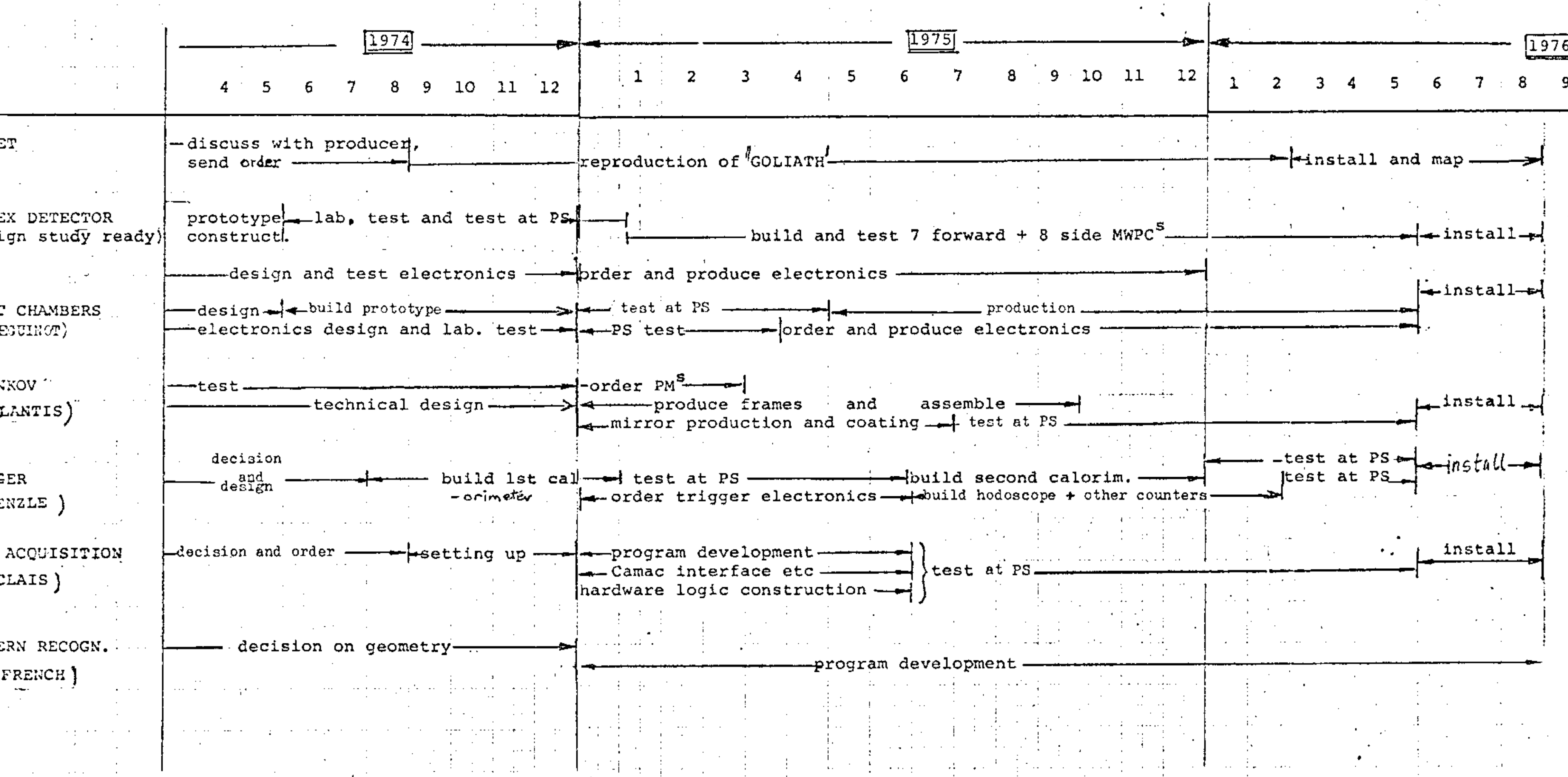

III. TRIGGER

In order to improve the selectivity of the system for the very low cross section of the high-p_t events, a more flexible multi-level trigger system has been designed by introducing calorimeters. We still require, as before, one high-p_t charged particle emitted near 90° in the c.m. However, we now perform the selection by means of three independent requirements : (a) the coincidence of the scintillation hodoscope, (b) the required combination of signals from the Cerenkov system and (c) the indication that a particle with momentum equal or larger than a pre-set value has entered one of two calorimeters situated downstream of the scintillation hodoscope.

These three components of the trigger signal are discussed below. They are followed by a re-examination of the expected trigger rates and by an analysis of the possible backgrounds.

1. Scintillation hodoscopes.

A first definition of p_t is done with the set of hodoscopes M_1M_2 consisting of vertical slabs of scintillators used in fast coincidence (fig. 1). One pair of hodoscopes is above and one below the beam, at an angle of $\sim 6^\circ$ with respect to the target. Each hodoscope has a rectangular shape (fig. 2) and covers the c.m. angle $80^\circ - 100^\circ$ (fig. 3) over the azimuthal interval $-45^\circ \lesssim \phi \leqslant +45^\circ$. The total solid angle covered by the hodoscope is ~ 1 sr.

The reason for having the M_1M_2 hodoscopes in the up-down regions only, rather than in the circular arrangement quoted in the original proposal, comes from a more extensive study of the peripheral events distribution. Fig. 4 shows the spread of track intersections at 10 m from the target (position of the calorimeter; see sect. 3) as obtained from Monte Carlo events after deflection through the magnet. Fig. 4 also shows the position of M_3 which defines the solid angle of the trigger. The peripheral Monte Carlo events have been plotted in Fig. 5 to show the correlation between the vertical coordinate Z in a plane 10 m from the target and their momentum; the trigger acceptance region can be seen to be well outside the peripheral spread.

By cabling suitable combinations of the hodoscope elements one can adjust the acceptance, selecting for example a lower cut-off in p_t. A situation that can be obtained if a uniform p_t acceptance is desired above $p_t \sim 3.5$ GeV/c appears in fig. 6; introducing the known $d\sigma/dp_t$ distribution at 150 GeV/c the acceptance function becomes as in Fig. 7. More details about M_1M_2 correlations can be found in the original proposal.

2. Cerenkov counters

As described in the proposal, the four Cerenkov counters $\check{C}_1 - \check{C}_4$ are used in the trigger in the following combinations according to the particle selection requirement :

$\check{C}_1\ \check{C}_2\ \check{C}_3\ \check{C}_4$ for π's

$\check{C}_1\ \check{C}_2\ \overline{\check{C}_4}$ for K's

$\check{C}_1\ \overline{\check{C}_3}\ \overline{\check{C}_4}$ for p and $\bar{p}$'s.

One can notice that the trigger condition is quite tight for π's, less so for K's and somewhat loose for p and $\bar{p}$'s ($\check{C}_1$ accepts π's already from ~ 2.5 GeV/c).

3. Calorimeters

In order to further improve the selectivity of our trigger and thus avoid certain backgrounds discussed below we have added calorimeters to the original set-up. In addition to reducing the background they give an independent definition of p_t.

We propose to use two calorimeters, positioned as in Fig. 1, covering the solid angle of the M_1M_2 hodoscope. Their position with respect to the peripheral events at 10 m from the target is shown in figs.4 and 5.

Their design is a straightforward extrapolation of the existing STAC developed by Engler et al (1). Each calorimeter consists of 6 equal modules and is 9 collision lengths deep (see Fig. 8). The construction of one module is illustrated in Fig. 9. It consists of 8 plastic scintillators (1 cm thick) sandwiched between 8 iron sheets (3 cm thick). The area is 1x2 m^2 and the thickness per module corresponds to 1.5 collision lengths (200 gr/cm^2). Each module is viewed from both sides by a large area fast photomultiplier (60 DVP) to assure uniform light collection and fast response (5 ns by mean-timer method) for use in the fast logic.

The expected energy resolution is ± 8% at 30 GeV (Fig. 10) with good linearity (Fig. 11). The drift in amplitude quoted by ref. (1) is less than 10% per week; however, this drift is continuously monitored and corrected by means of calibrated photodiode pulses thus ensuring permanent stability. Fig. 12 shows the expected cut-off efficiency of the calorimeters for a setting at $p_t = 2.5$ GeV/c (the corresponding lab. momentum at 150 GeV/c incident momentum is $\sim$ 22 GeV/c). We then arrive, for instance, at a rejection efficiency larger than 100 for $p_t \lesssim 1.5$ GeV/c. This efficiency should be folded into the hodoscope triggering function of Fig. 6 thus greatly improving the overall rejection. The relative adjustment between the hodoscope acceptance and the calorimeter rejection is obtained by the discriminator setting of the latter.

Each calorimeter is triggered by the counter M_3 located in front of it and which also defines the sensitive area. M_3 consists of vertical scintillator strips which can be used as an additional hodoscope system to check and reinforce the M_1M_2 coincidence. An anticounter $\bar{S}$ can be placed at the back of the calorimeter to ensure that the hadron shower has been contained. The effects of shower leakage and containment are illustrated in Fig. 13.

If we require that in the first 3 collision lengths the hadron shower has started to develop (by using module No. 3 of the calorimeter as a

---

(1) J. Engler et al., Nucl. Instr. and Meth. 106, (1973) 189 and measurements by the same authors at Serpukhov (1973), private communication.

probe counter) and that after another 6 collision lengths it is contained, then we expect a calorimeter efficiency larger than 90% (see Fig. 14).

Noticing that 1 collision length is approximately equivalent to 10 radiation lengths, we can use the first module of each calorimeter for an efficient rejection of the electromagnetic showers introducing a pulse height discrimination, (thus suppressing the γ background).

We would like to point out a further possible gain in rejection power if such need should arise. Calorimeter No. 2 can be shifted into the beam line and used as an antiperipheral trigger. This is shown as cal. 2'dashed in Fig. 1. Thus one could, for example, reject events where more than 100 GeV out of 150 GeV incident have been absorbed by cal. 2. For this "missing energy" trigger operation we could easily insert additional iron plates between the modules (each plate would have a small hole in the center to allow the passage of the beam). Rejections of the order of 10 or larger would be provided by this mode of triggering. At this stage, however, we cannot prove that such an anticalorimeter alone would give enough rejection (see, for example the NAL proposal No. 222 by Frisch et al, 1973). Thus the reason for starting by triggering on one high-p_t particle.

The effects of backscattering from the calorimeters into the trigger hodoscopes are, according to measurements by ref. (1), of the order of 10%. They can be avoided, in our case, by introducing a sufficient distance between M_2 and the calorimeters. The solid angle available to the backscattered particles would then be reduced. Also, a time-of-flight separation may become feasible.

In order to keep the rate of accidental triggers due to backscattering of beam-halo particles at an acceptable level, some shielding may be necessary beside that provided by the iron of the magnet (which already shadows most of the calorimeter volume). We require that the flux of the hadronic halo at 1 m from the beam and with energy larger than ∿ 25 GeV should not exceed 10^5 particles x m^{-2} x sec^{-1}.

Finally, we estimate the cost of each calorimeter module to be 50 KSF as indicated by up-to-date information from various manufacturers. A total of 0.6 MSF is thus necessary for the 50-ton complete calorimeter system.

4. Rates.

The rates expected with the new geometry at 150 GeV/c incident momentum have been calculated using the "universal CCR fit" of the ISR data :

$$E\, d\sigma/d^3p = 1.54 \times 10^{-26}\, p_t^{-8.24}\, e^{-26.1\, p_t/\sqrt{s}}\ [\mathrm{mb/GeV}^2]$$

The above refers to the π^o of the inclusive reaction $pp \rightarrow \pi^o$ + anything. Applying this to our conditions (10^7 incident particles per burst, 10^4 bursts per day, 30 cm liquid hydrogen target) and triggering on all charged particles in our solid angle, we expect the following rates :

p_t (GeV/c)	2.5 - 3.5	3.5 - 4.5	4.5 - 5.5
events/day	22400	975	44

These rates could probably be improved substantially if, as discussed earlier, one succeeds in triggering on the missing energy alone, i.e. with the calorimeter No. 2 in the anticoincidence position (the gain could be a factor p_t^4 and would result in ∿ 600 times more events at p_t = 5 GeV/c).

5. Background.

Three possible sources of background have been estimated. They are all strongly suppressed by the use of the calorimeters. They are :

i) A single charged particle of low momentum (less than 9 GeV/c) impinges on the first hodoscope M_1, interacts and gives rise to a particle going into the second hodoscope M_2 satisfying the M_1M_2 correlation condition. From a sample of Monte Carlo events we find a 2% probability for one such particle to enter M_1. The interaction rate in the M_1 scintillators being $\sim$ 1%, we see that at most (i.e. with the secondary particle entering the correct M_2 section each time) the probability for such a background is 2×10^{-4}. With 5×10^5 interactions per burst in the target this results in 100 background triggers per burst. The calorimeter trigger condition rejects them all. It should be noticed that - in the absence of a calorimeter - this background could also be rejected by an on-line rough straight track reconstruction on the PDP 11 computer (the computational capacity is of the order of 2000 per second).

ii) Two charged particles of low momentum, one hitting M_1 the other hitting M_2, can simulate a good trigger. This background occurs with a probability of 2×10^{-4} and is also eliminated by the calorimeter. Alternatively, a fast reconstruction on the on-line computer could also take care of it.

iii) The γ-rays emitted by the π^o's which are produced in large number (5×10^5 per burst of 10^7 incident particles) among the peripheral events are an important source of background. They materialise in a region before, or just inside, the first Čerenkov counter ($\check{C}_1$ in fig. 1). In this region the influence of the magnetic field is minimal and the electrons from the γ conversion can simulate charged tracks of high momentum - and hence high-p_t - in the M_1M_2 hodoscope. We have estimated the size of this background by generating Monte Carlo events of a peripheral type with 8 charged tracks and 4 π^o's. The γ's from the π^o's have been allowed to materialise with a 40 m radiation length. The effective amount of material which is responsible for the conversion is 3×10^{-3} radiation lengths, mainly concentrated in the region of the 6th MWPC of the vertex detector. We find a total of 600 simulated high-p_t events per burst. Most of them are rejected by the calorimeter. An independent reduction can also be achieved by interrogating specific sets of wires in the 5th MWPC so as to insure that a charged track is already present inside the magnet (one could probably gain a factor 10 in this way thus reducing the false triggers to only 60 per burst). A check on the above estimates has been done by using real events as observed in the OMEGA spectrometer. Fig. 15a shows the correlation observed in two hodoscopes for events with one track in the spark chambers: these are the good triggers. Fig. 15b shows instead the same hodoscope correlation for 2750 background triggers, i.e. events which had no charged track in the spark chambers. From the density on the latter plot and scaling to the size of our hodoscopes we find a background of 700 triggers per 5 x 10^5 interactions, to be compared to the 600 estimated above.

We conclude by stressing that, although alternative or complementary methods such as those originally proposed can also be construed, the use of the calorimeter by itself will eliminate all sources of background.

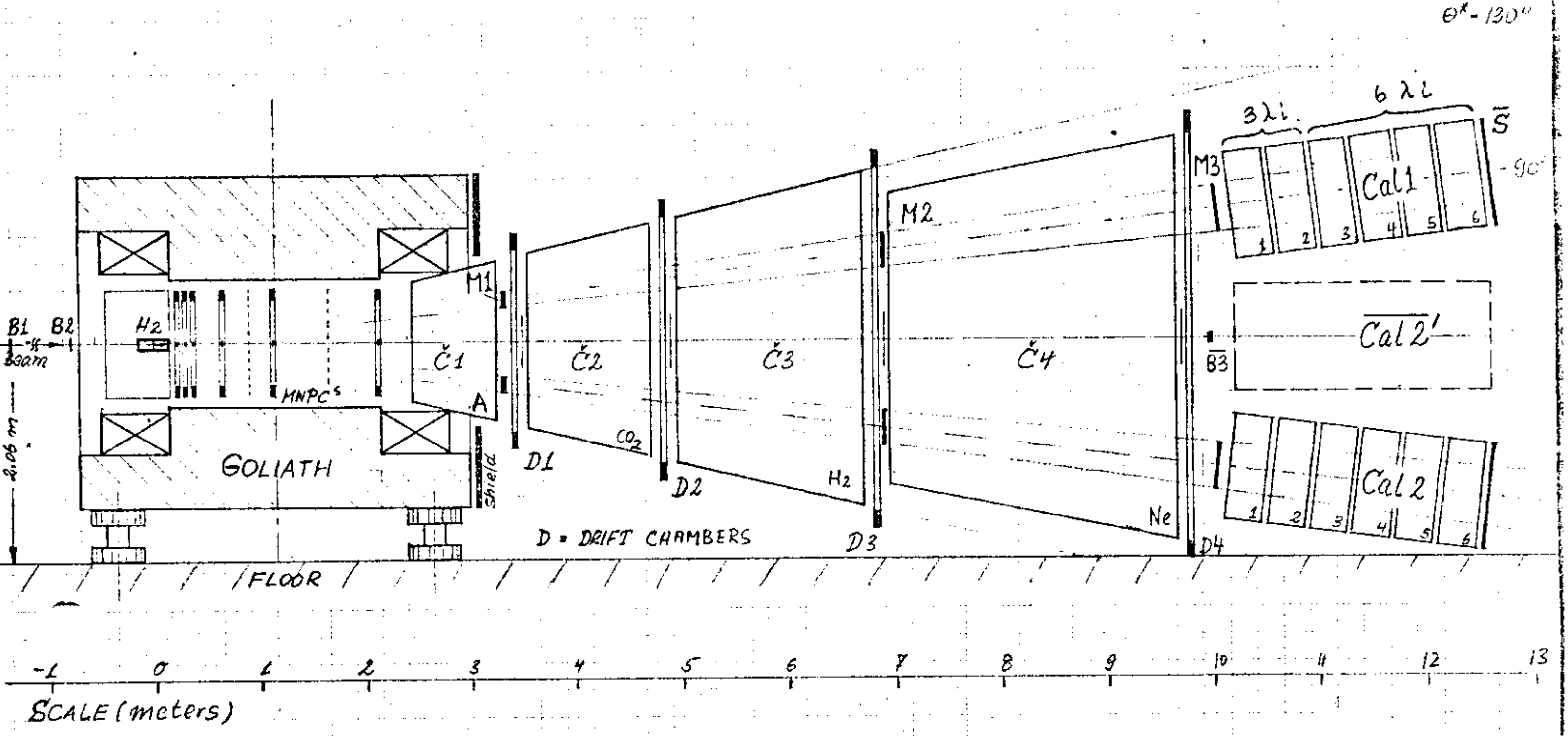

TRIGGER: $B1B2\overline{B3}$
$M1H2\,\bar{C}_i$
Cal1/Cal2
OR: Cal1 $\overline{Cal2}'$

Fig.1: HIGH $P_\perp$ SPECTROMETER
(elevation)

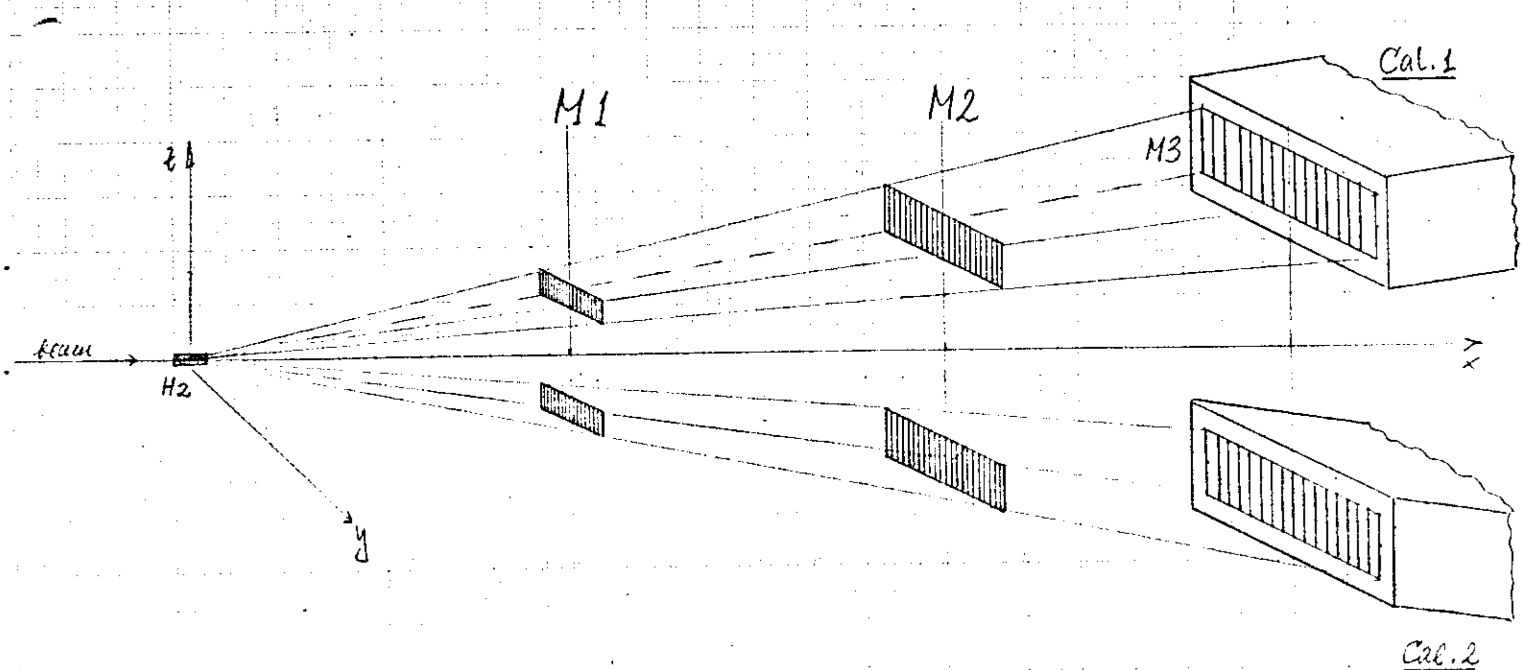

Fig. 3: Acceptance of trigger hodoscopes in c.m.s. (Θ^* = polar angle).

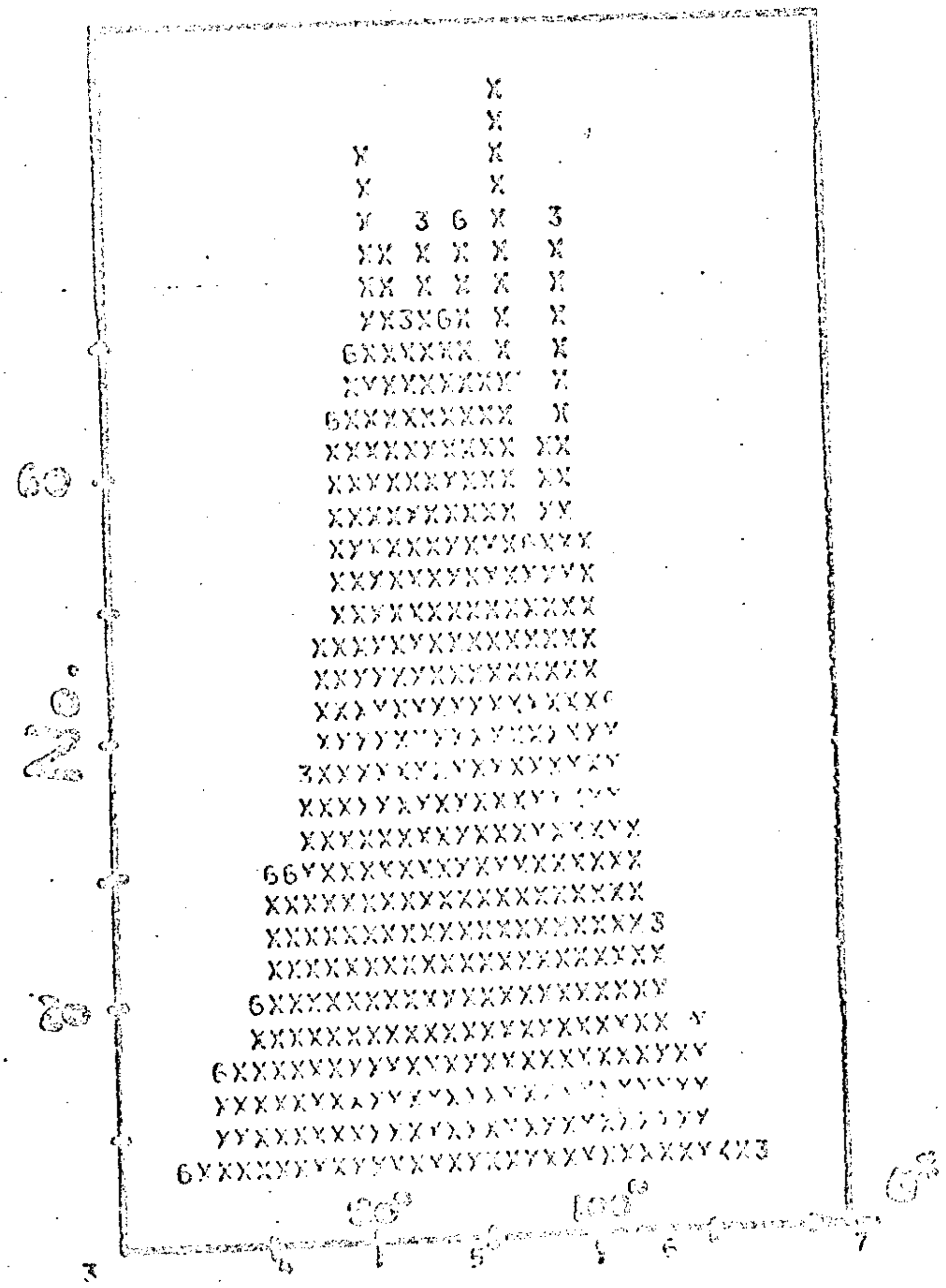

Fig 4: POSITION OF CALORIMETERS WITH RESPECT TO TYPICAL EVENT
(at 15 metres from origin)

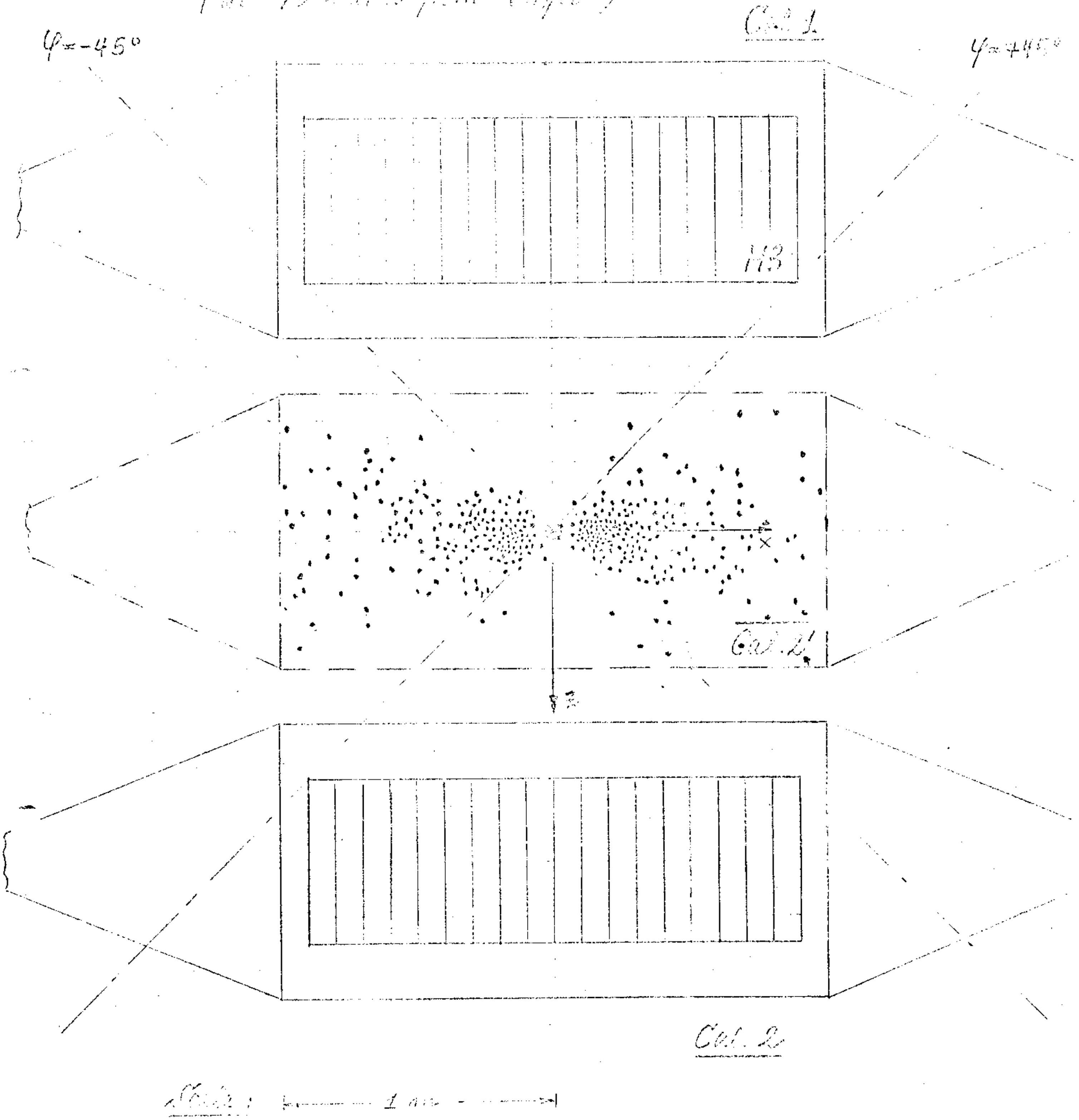

Fig. 5:

P_{lab} vs. z for peripheral events at 10 m from target

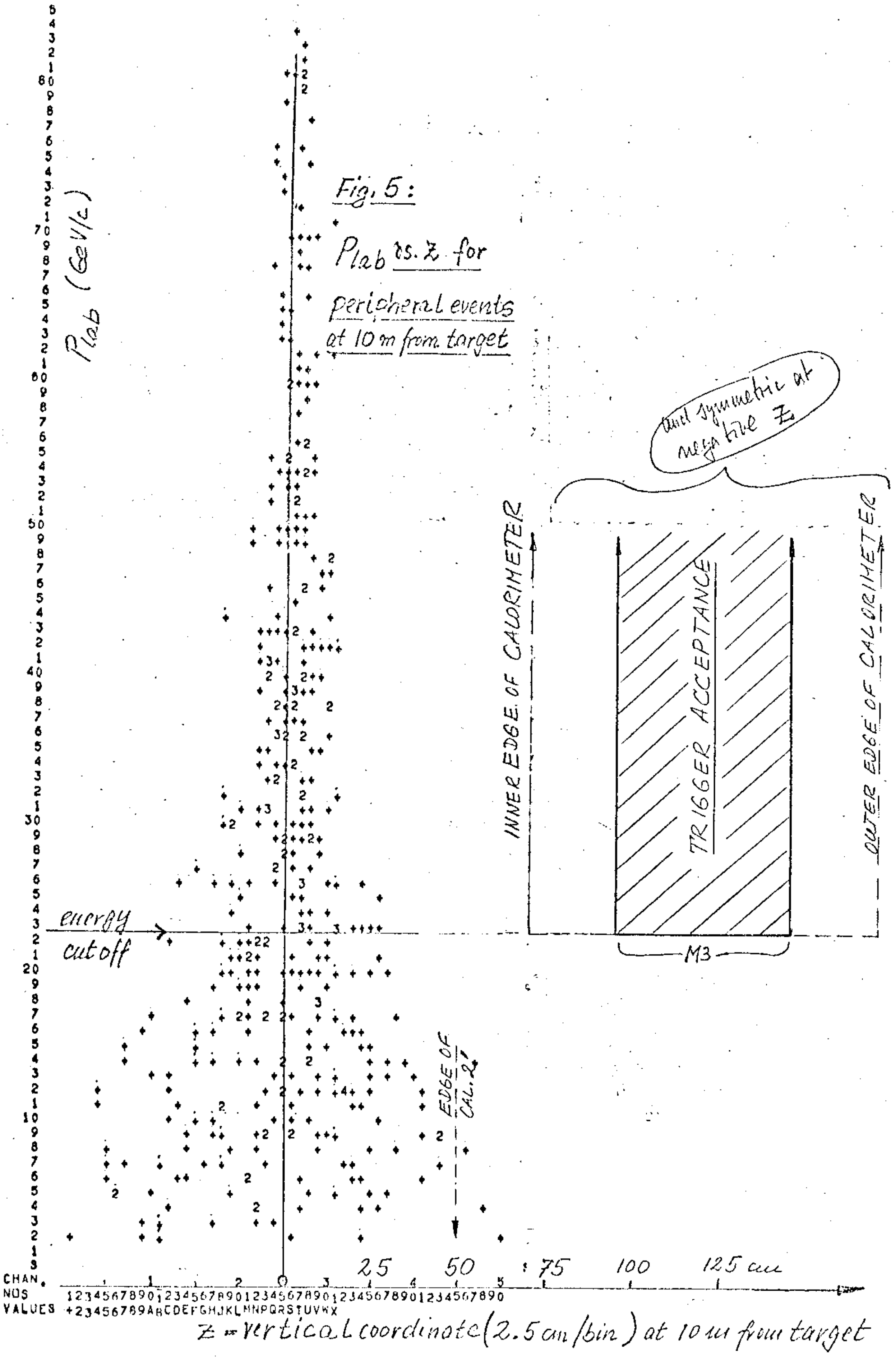

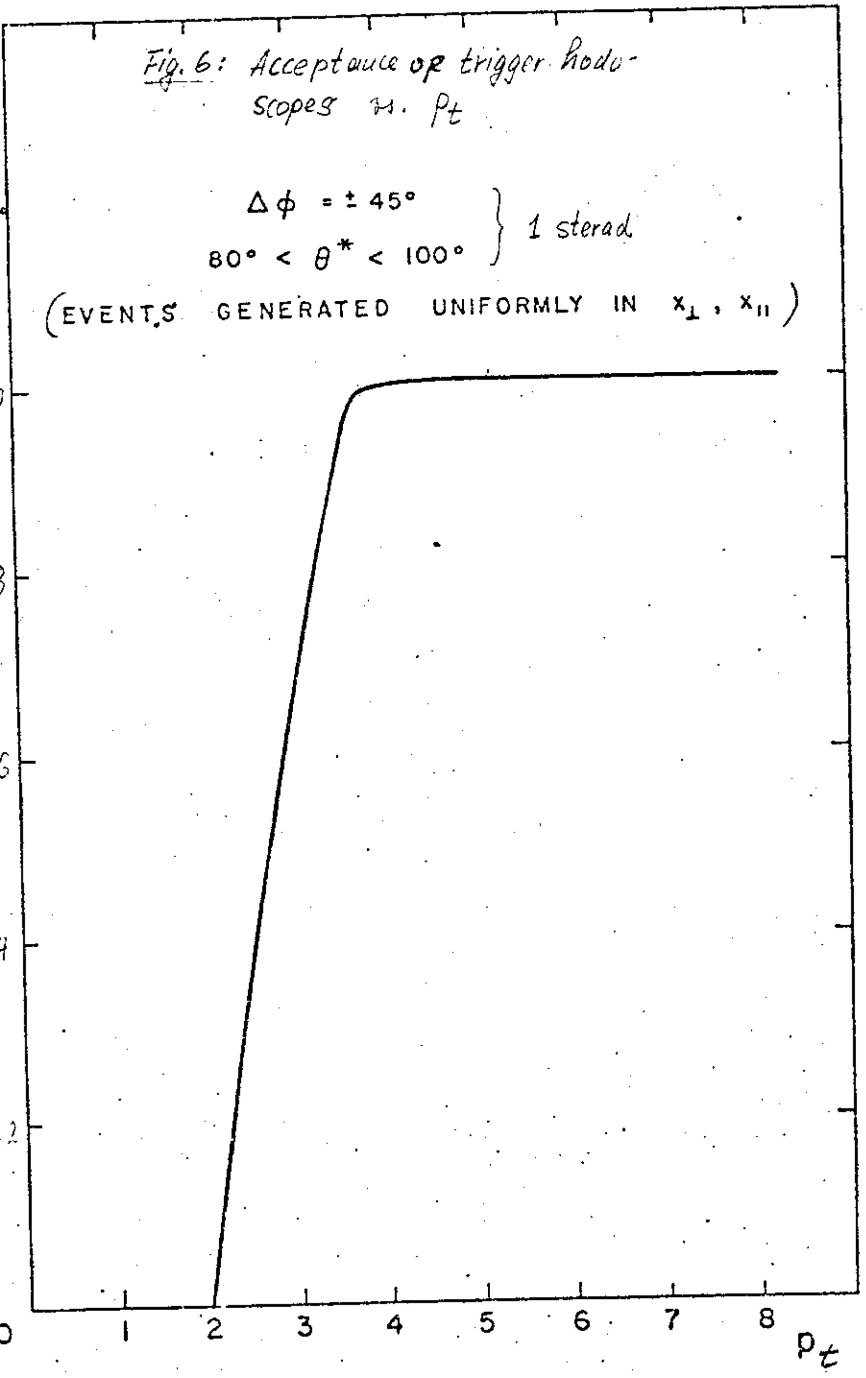

Fig. 6: Acceptance of trigger hodoscopes vs. p_t

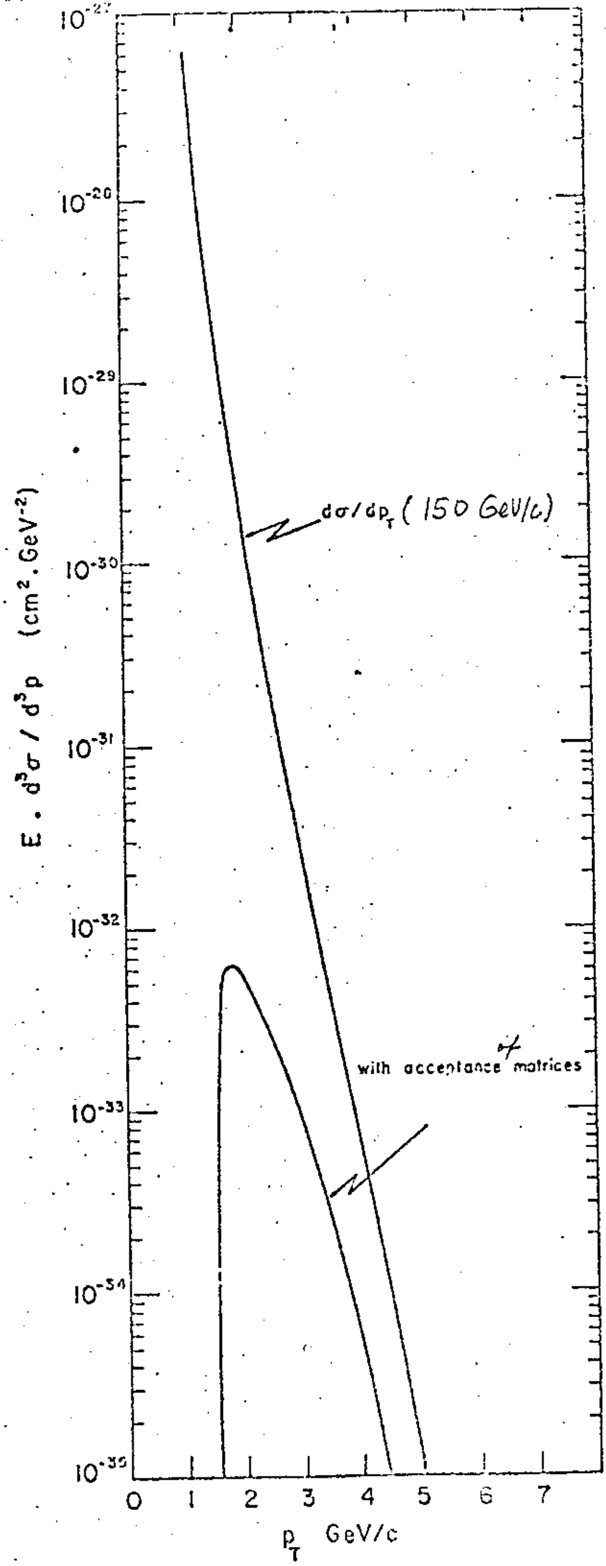

Fig. 7: Acceptance of MIPS trigger hodoscopes folded with physical $d\sigma/dp_t$ distribution

21/5 '74 WK

Fig. 9
Calorimeter Module

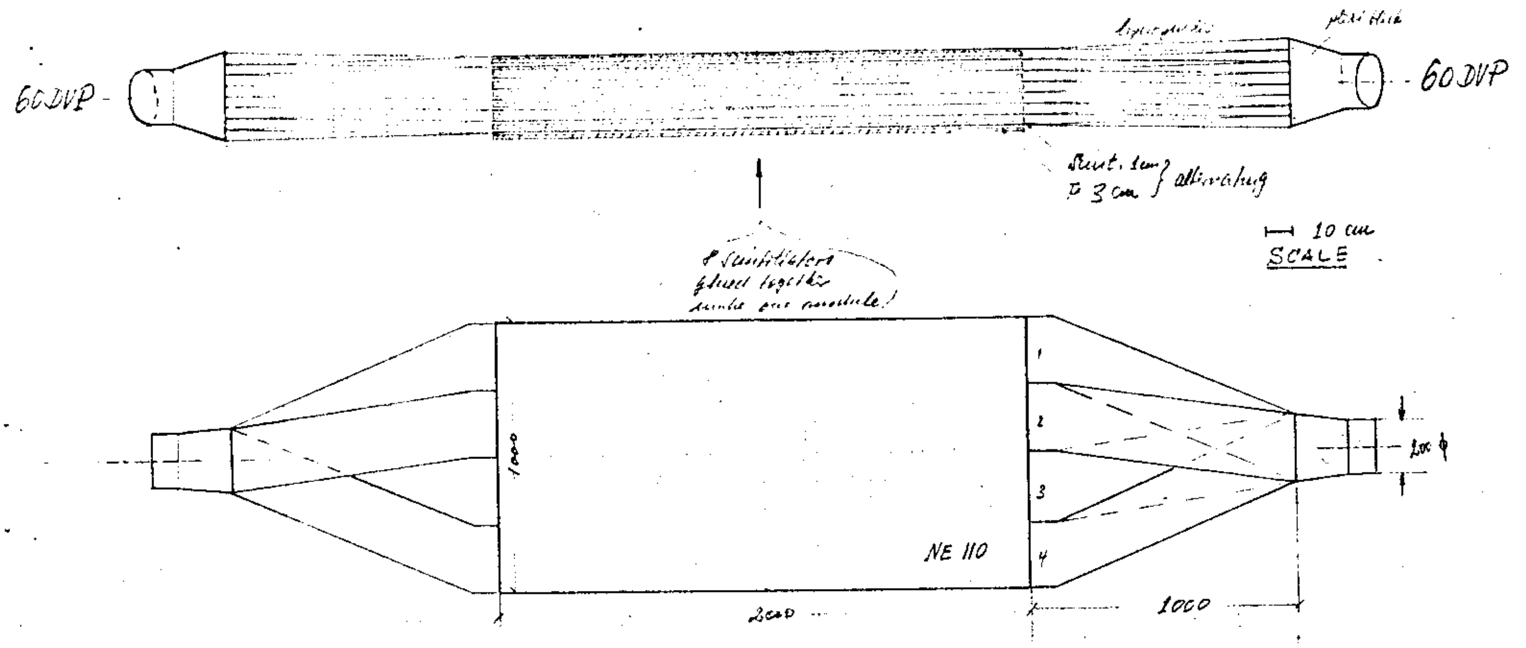

Sequence of Fe-Scintillator Sheets (scale 1:2):

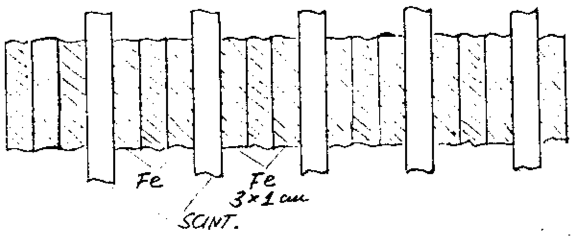

etc. 8x

total = 200 gr/cm²

≈ 1.5 int. length

plexiglass light guides:

each scintill. sheet seen by 4 lamellas of 250×10 mm² section, from both ends (uniform light collection + fast timing).

22/5/74
WK

Fig. 8
Calorimeter Unit (=6 modules)

total depth = 3 λ_{int} (mod. 1+2) + 6 $\lambda_{int.}$ (mod. 3-6) = $\underline{9\ \lambda_i}$

overall dim. ≈ 2 × 1 × 2.5 m

weight ≈ 25 tons

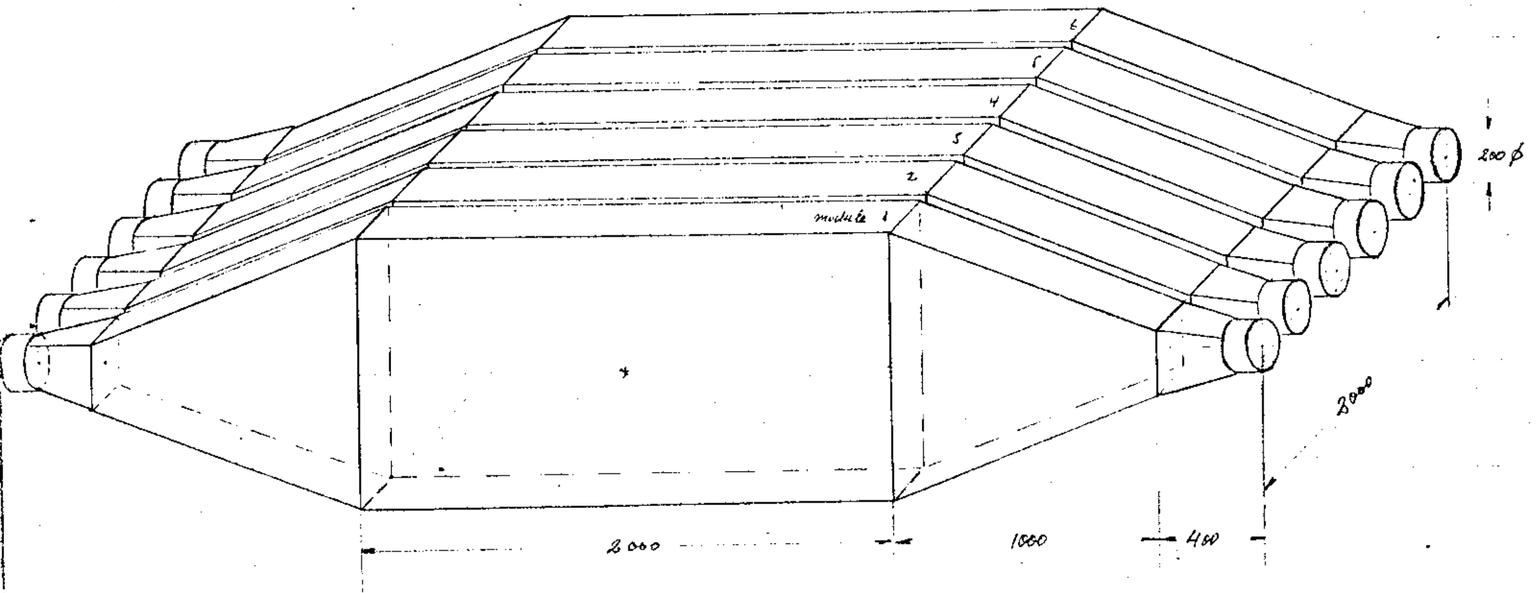

with STEEL frame)

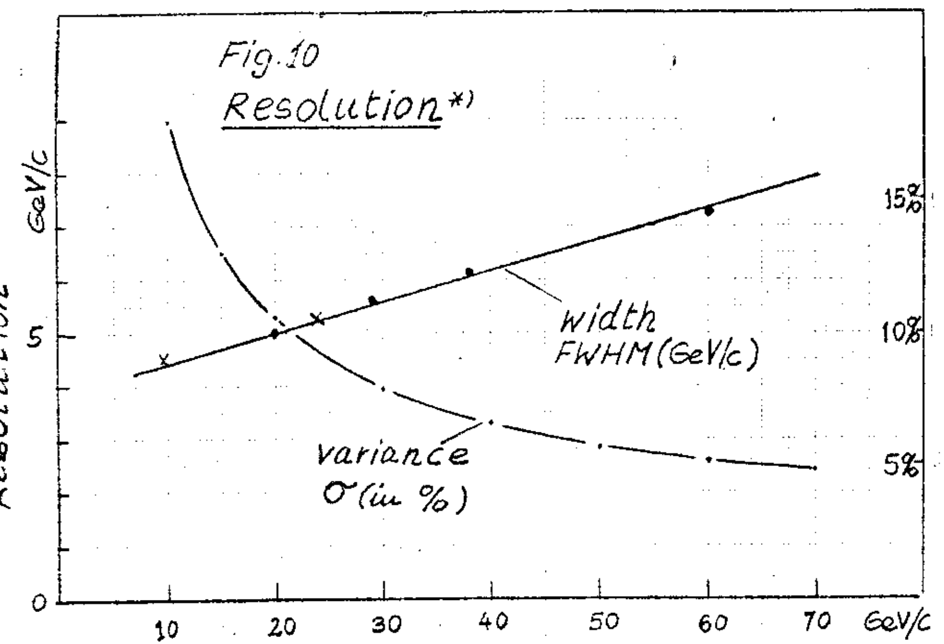

Fig. 10

Resolution*)

*) from J. Engler et al.

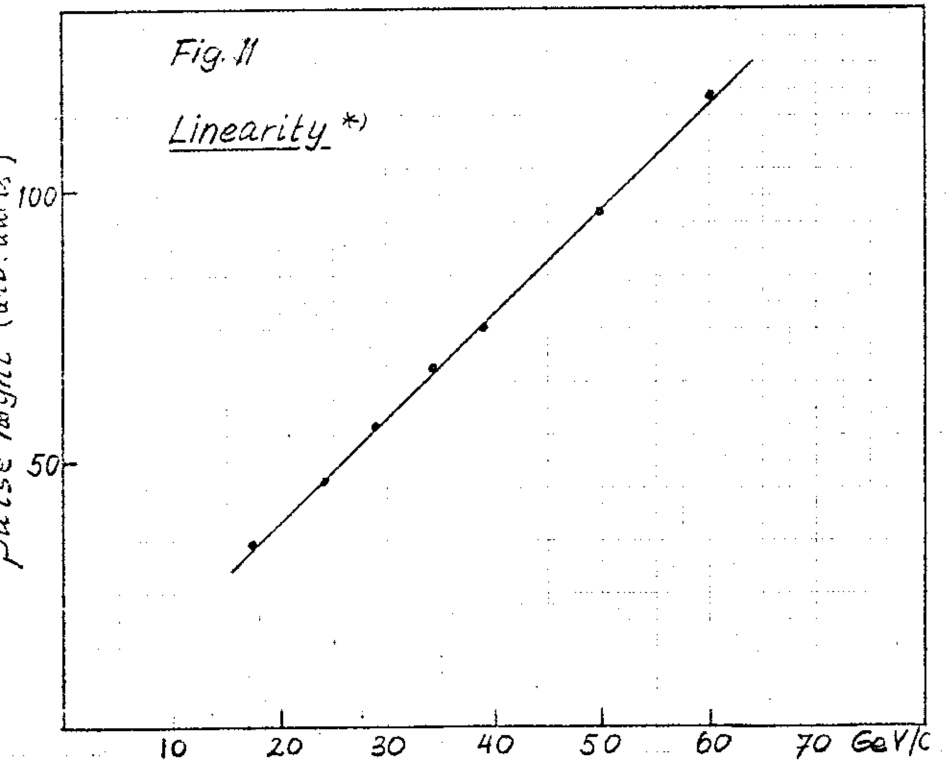

Fig. 11

Linearity *)

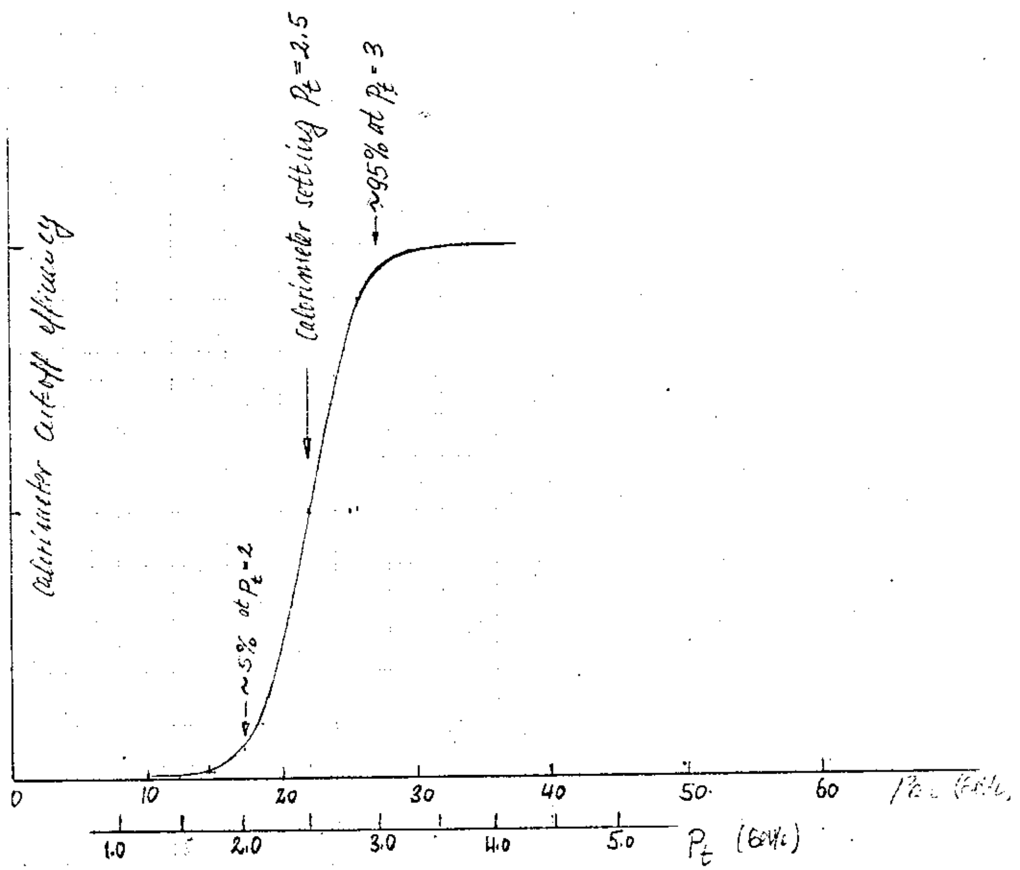

Fig. 12: Expected cut-off function of the calorimeters (p_{inc} = 150 GeV/c)

Fig. 14 : Shower containment (we have 6 λ_{int})

FROM B.C. BARISH et al., NAL TEST OF A STAC. at 200 GeV/c

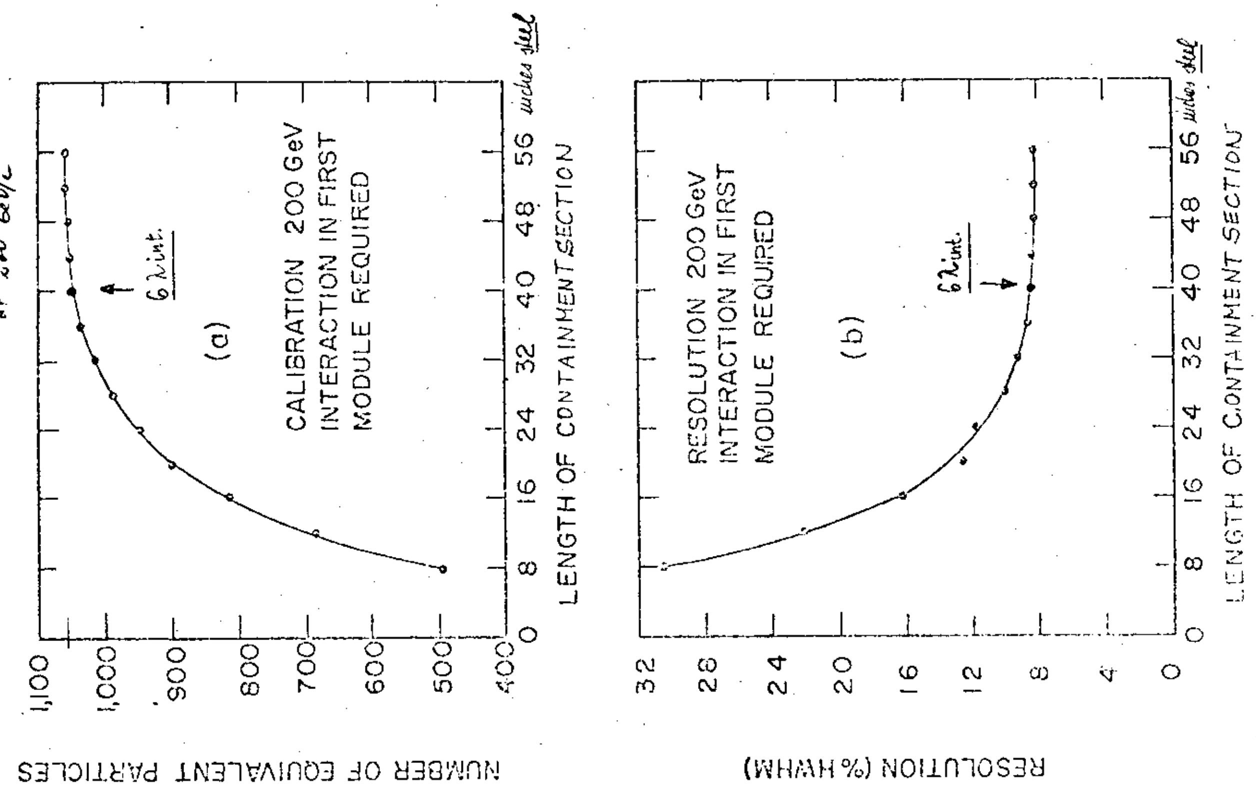

Fig. 13 : Response of STAC for 30 GeV Protons

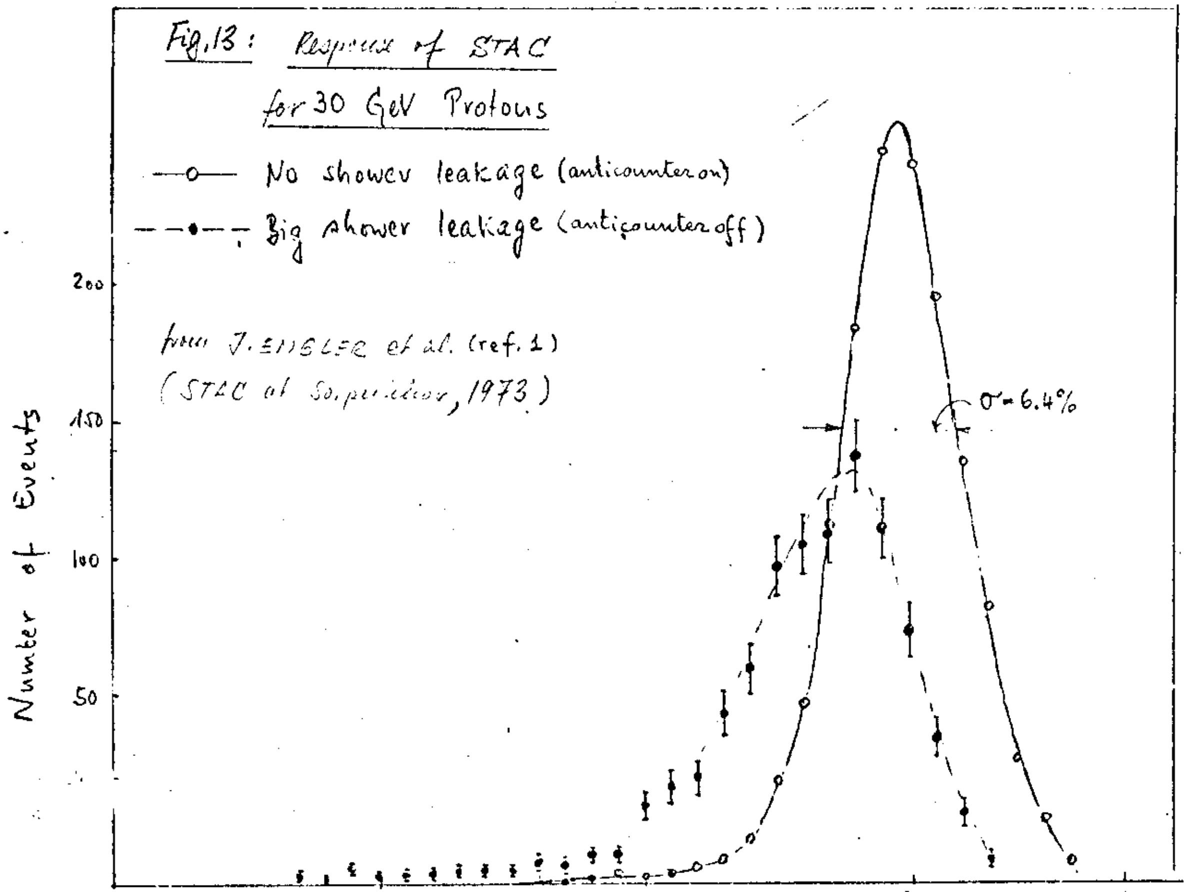

OMEGA MATRIX CORRELATION
FOR EVENTS WIT.. TRACK
IN THE SPARK CHAMBERS

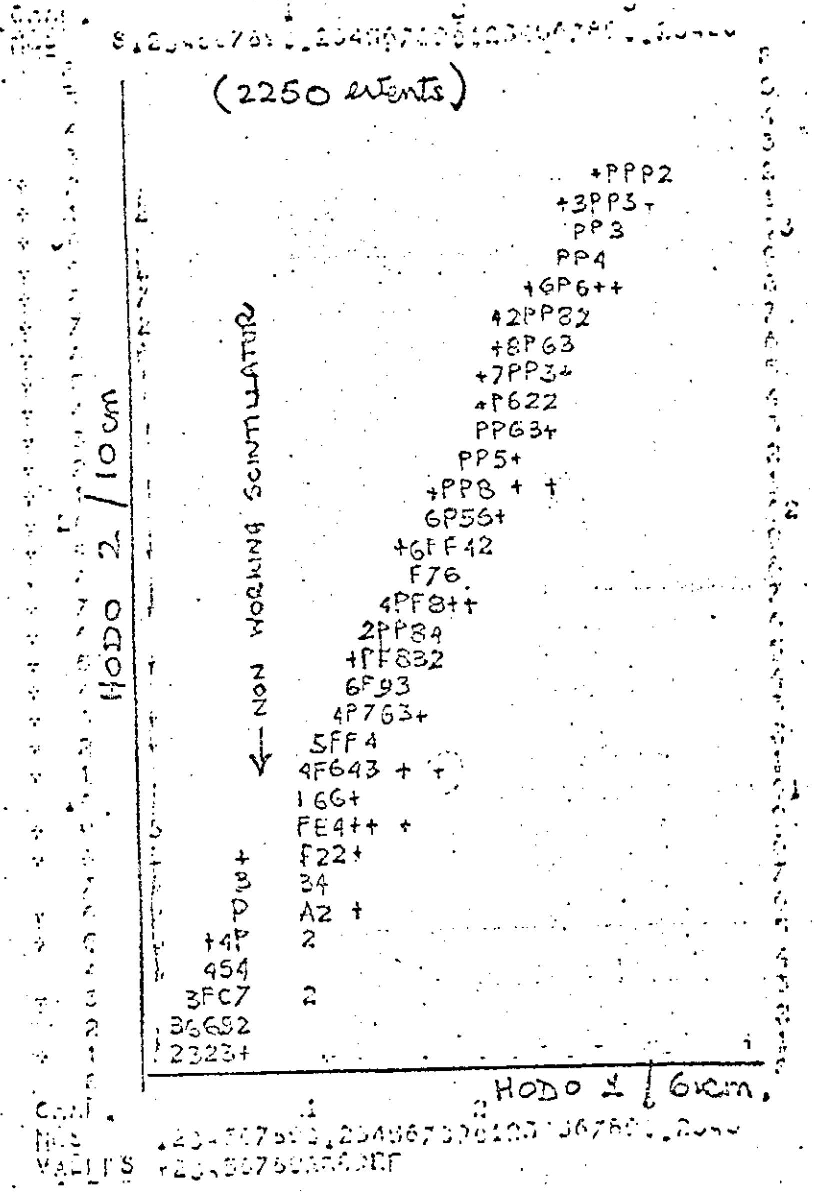

Fig 15a

OMEGA MATRIX · CORRELATION
FOR BACKGROUND EVENTS

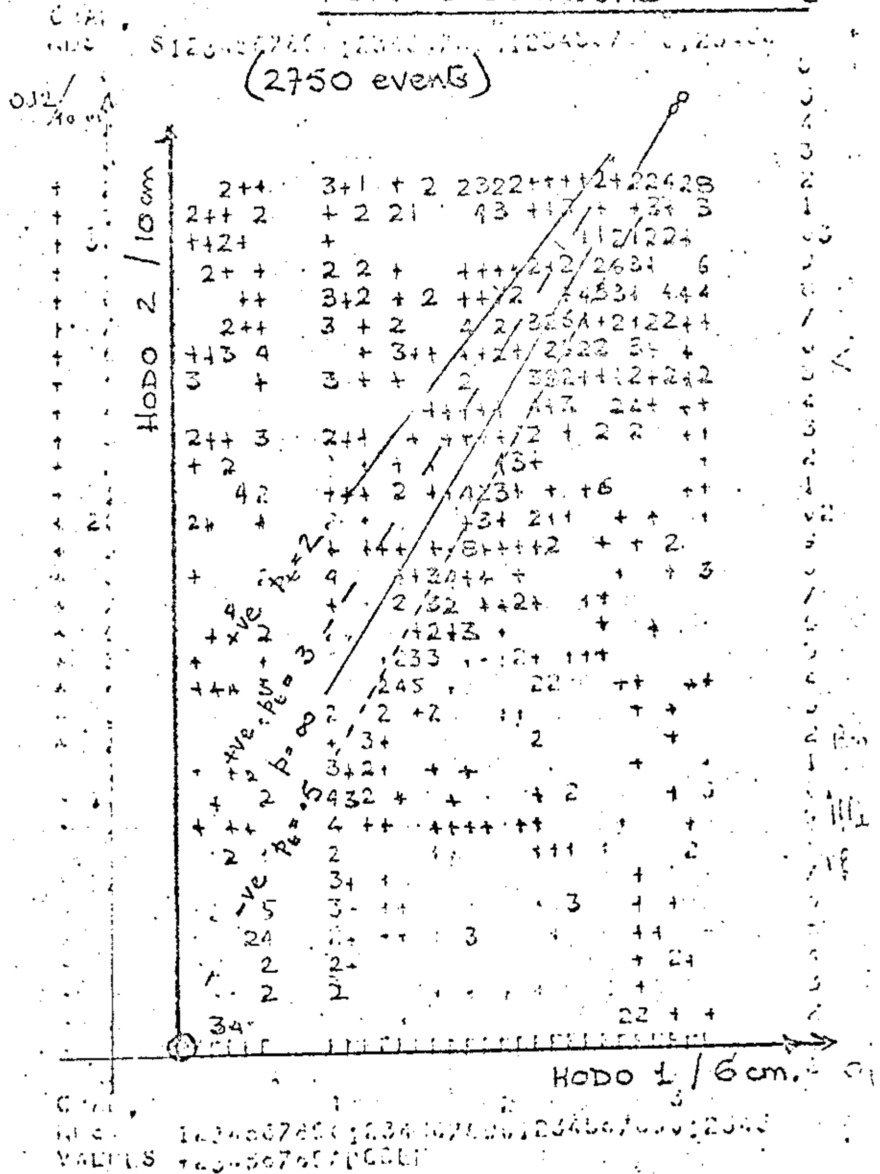

FIGURE 15b

IV. CERENKOV COUNTERS

1. Capability and performance

Our Cerenkov counters have been designed in order to provide good particle identification together with minimum length. The Cerenkov radiation formula gives the number of photons (dN_γ) emitted in a medium with index of refraction n over a given wave length interval dλ as

$$dN_\gamma = \frac{2\pi}{137} L \sin^2\theta \frac{d\lambda}{\lambda^2}$$

where L is the counter length and θ is the Cerenkov angle ($\cos\theta = 1/n\beta$). In the limit $\beta = 1$, $\sin^2\theta = 2(n-1)$ and

$$dN = \frac{2\pi}{137} L \; 2 \; \alpha \frac{d\lambda}{\lambda^2} \varepsilon_{PC} (\lambda)$$

where $\alpha = n-1$, $\varepsilon_{PC} (\lambda)$ is the photocathode conversion efficiency and dN is the number of produced photo electrons. Upon integrating one gets

$$N = N_o \; L \; 2 \; \alpha$$

where

$$N_o = \frac{2\pi}{137} \int_{\lambda_2}^{\lambda_1} \varepsilon_{PC} (\lambda) \frac{d\lambda}{\lambda^2}$$

In a given counter, L and 2α are fixed by the length and nature of the gas, so N is maximum when N_o is maximum. The value of N_o is governed by three factors

a) gas transmittivity $\varepsilon_T(\lambda)$

b) mirror reflectivity $\varepsilon_R(\lambda)$

c) photo cathode conversion efficiency $\varepsilon_{PC}(\lambda)$ of photomultiplier (PM)

In the sections which follow each of these factors will be considered. In terms of these factors we have

$$N_o = \frac{2\pi}{137} \int_{\lambda_2}^{\lambda_1} \varepsilon_T(\lambda) \; \varepsilon_R(\lambda) \; \varepsilon_{PC}(\lambda) \frac{d\lambda}{\lambda^2}$$

and for λ in units of 10^3 Å (i.e. 10^{-5} cm)

$$N_o = 4586 \int_{\lambda_2}^{\lambda_1} \varepsilon_T(\lambda)\ \varepsilon_R(\lambda)\ \varepsilon_{PC}(\lambda)\ \frac{d\lambda}{\lambda^2}$$

If for example one takes $\varepsilon_T = 0.9$, $\varepsilon_R = 0.8$ and $\varepsilon_{PC} = 0.25$ for the interval $\lambda_2 = 5.5$ (5500 A°) and $\lambda_1 = 2.0$ (2000 A°) we get

$$N_o = (4586)(0.9)(0.8)(0.25)\left(\frac{1}{2} - \frac{1}{5.5}\right) = 263\ \text{cm}^{-1}$$

Thus, for light collection through a quartz window PM ($\lambda \gtrsim 2000$ A°) and reasonably good reflectivity and good transmissivity gases (He, Ne, A, CO_2, H_2, CH_4 and others) one might expect N_o values $\approx 260\ \text{cm}^{-1}$. In actual practice most Cerenkov systems have values of N_o of 100 cm^{-1} or less because one or several of these factors have not been optimized. One experiment is reported(1) where N_o of 160 cm^{-1} was obtained. In this measurement they used a Quartz window PM (RCA 31000 M), He gas radiator and Al mirror coated with 250 A° thick protective layer of Mg F_2.
It will be the purpose of a test run (in a PS test beam starting at end April) to pinpoint those factors which limit the performance of Cerenkov counters so as, hopefully, to use such an improved system for the proposed exerpiment. Our presently proposed system is summarized in table 1 and N versus momentum is plotted in fig. 1.

TABLE 1

COUNTER	GAS	α	L(cm)	$N_o(\text{cm}^{-1})$	N (p.e, $\beta = 1$)
✓C1	N-pentane	18.10^{-4}	50	100	17.95
✓C2	CO_2 or CH_4	$4.5\ 10^{-4}$	110	160	15.80
✓C3	H2	$1.38\ 10^{-4}$	180	160	7.95
✓C4	Ne	$0.67\ 10^{-4}$	300	160	6.43

It is clear that our proposed system is well within the optimal limits given above and represents simply an attempt to build a Cerenkov system up to the presently achieved levels. In fact, from the discussion which follows, we have good reasons to believe that values of N even higher

a) Mirror Reflectivity.

In this domain advances in vacuum evaporation methods$^{(2)}$ for deposition and protection of Al mirrors with Mg F_2 or LiF films show that $\varepsilon_R = 0.8$ can be achieved from infrared to far ultra violet (i.e. from 6000 Å to 1100 Å). The reflectivity curves for Al (Mg F2) and unprotected Al mirrors are shown in figure 2. It was found that such protected mirrors Al (Mg F2) did not deteriorate with age. A mirror stored in a air filled box for up to two years lost 1-2% in reflectance even though no dessicant was present during storage. We have found that such mirrors can be obtained commercially in Europe at reasonable prices ($\sim$ 130 DM/ 50 x 40 cm^2 mirror) so we envision no problem here. From figure 2 one sees that even down to 1200 A^o $\varepsilon_R = .80$ and falls to 20% at 1000 A^o so one may take the effective lower limit at about 1100 A^o. Above this value, $\varepsilon_R = 0.8$ and constant seems a reasonable representation of the data. Figure 3 shows Al mirrors with Li F protective films. They have a lower low wave length limit but the average reflectivity seems to be worse in the above 1200 A^o region. It seems unlikely that any gain can be had by using Li F protected mirrors.

b) Transmission of U.V. in gases.

In this area we have rather fragmentary data $^{(3),(4)}$ which is summarized in Table 2. In most cases the transmission ε_T (through 1 meter of gas) is not known directly but can be inferred from the position of the absorption edge.

TABLE 2

HEMICAL NAME	GAS	(10^{-4}) $\alpha = n-1$	ABSORPTION EDGE (A^o)	$\varepsilon_T(\lambda)$
	He	.35	584	
	Ne	.67	744	
	H_2	1.38	1215	
	O_2	2.72	1971	
	A	2.84	1066	
	N_2	2.97	1400	.95(1875 Å)

Table 2 (Cont'd)

NAME	GAS	$\alpha = n-1$ (10^{-4})	ABSORPTION EDGE (Å)	$\varepsilon_T(\lambda)$
	Kr	4.27	1236	
Methane	CH_4	4.40	1640	
	CO_2	4.50	1920	.47(1860), .81(1930), .91(2000)
Methyl Alcohol	CH_3 OH	5.86		
Sulfur dioxide	SO_2	6.86		.67(3200)
Ethylene	C_2 H_4	6.96		
	X_e	7.02	1470	
Ethane	C_2 H_6	7.06		
	SF_6	7.85	1473	.95(1875 Å)
Freon 13	CCl F_3	7.99	1970	
Propane	C_3 H_8	10.05	1850	
Freon 13 B1	CBr F_3	10.07	2600	
Freon 12	CCl_2 F_2	11.52	2220	
Butane	C_4 H_{10}	14.37	1960	
Chloroform	$CHCl_3$	14.55		
Ethyl Ether	$(C_2H_5)_2$ OH	15.20		
Carbon Tetrachloride	CCl_4	17.70		
N-pentane	$(CH_3)_4C$	18.0		

One may infer from Table 2 that He, Ne, A, should be essentially transperent down to 1100 Å , H_2 down to about 1250 Å and Kr down to about 1300 Å . If one takes $\varepsilon_R = 0.8$ and $\varepsilon_T = 0.9$ for the wave length limits given above we find

TABLE 3

GAS	$N_o/\bar{\varepsilon}_{PC}$	N_o ($\bar{\varepsilon}_{PC} = .25$)
He	2400	600
Ne	2400	600
A	2400	600
H2	2040	510
Kr	1940	485

So we see that if photocathode efficiencies average 25% over the whole wave length interval (1100 Å to 5500 Å) then values of N_o between 485 and 600 should be possible.

c) Photomultipliers and photocathode efficiencies.

We have investigated existing P.M's on the market and find that EMI 9821Q *) 5" diameter (110 mm effective) seems to be the tube best suited to our needs. It has a spectrosil window (fused SiO_2) whose transmission is 50% at 1700 Å, 80% at 1730 Å and 90% at longer wave lengths as shown in Fig. 4a. The various photocathode efficiencies (which include window transmission) $\varepsilon_{PC}(\lambda)$ are shown in Fig. 4b. We will use the tube with bialkali (K-Cs) or possibly the S-20 photocathode. Taking $\varepsilon_T = 0.9$ and $\varepsilon_R = 0.8$ one gets

$$N_o = (4586)(0.9)(0.8)\int_{\lambda_1}^{\lambda_2} \varepsilon_{PC}(\lambda)\,\frac{d\lambda}{\lambda^2} = 3302\int_{\lambda_1}^{\lambda_2} \varepsilon_{PC}\,\frac{d\lambda}{\lambda^2}$$

which for the (K-Cs) photocathode integrates to

$$N_o = 300 \text{ cm}^{-1}$$

This value should obtain for all gases whose absorption edge is below about 1650 Å. With this tube and using good reflecting mirrors and proper transmitting gases we can certainly achieve the conservative design values given in Table 1.

Another possible way of achieving the largest $\bar{\varepsilon}_{PC}$ over the largest wave length interval is to utilize wave length shifters$^{(4)}$ as is common in the field of U.V. spectroscopy$^{(5)}$. The most commonly used material is a thin film of $\sim$ 3 $mg/_{cm}^2$ of Sodium Salicylate deposited on the PM entrance window. This material has the unique property of absorbing all U.V. photons between 600 A° and 3600 A° and emitting an equal number of photons at 4300 A° which is near the peak of the P.M. response. It emits half the photons forward (with cosθ distribution) and half backward so assuming none of the backward photons are utilized one can expect values of N_o exactly half of that listed in table 3 (i.e. $N_o = 300 \text{ cm}^{-1}$ for He, Ne, A 255 for H_2 and 240 for Kr). These values could probably be increased even further by constructing proper reflectors about the P.M. which allow detection of some fraction of the backward emitted is that it has a 10 ns decay time. Other wave length shifters are available (with shorter decay times) such as p-terphenyl, p-quaterphenyl, diphenylstilbene PPO, POPOP and perhaps most interesting Ca WO_4: 7% Pb which has been reported(6) to give more than one visible photon for each U.V. photon absorbed.

2. Test Program.

We are constructing apparatus for a run in a PS test beam (electrons) to measure N_o for various gases, photomultipliers (with and without wave length shifters) and mirrors. The method which we will use to measure N_o follows closely the technique used Yovanovitch et al(1) with a slight variation. From the relation $N = N_o L 2 \alpha$ we can write $\alpha = \alpha_o P$ where $\alpha_o = (n - 1)_{P=1}$ and P is the pressure in atmospheres. Thus

$$N = N_o L 2 \alpha_o P$$

The inefficiency of a counter is $e^{-N} = 1-\varepsilon$ where ε = efficiency. The method of Yovanovitch et al(1) was to plot $- \ln (1-\varepsilon)$ vs P and determine the slope $N_o L 2 \alpha_o$. Since L and $\alpha_o=(n-1)_{P=1}$ were known then N_o was determined. In the measurements the plot of $- \ln(1-\varepsilon)$ vs P was linear over several decades indicating that the above formulation is reasonable. In our case we wish to determine N_o without varying the gas pressure so we will vary the effective length L by moving a baffle in the $\check{C}$ gas region.

REFERENCES

[1] Yovanovitch et al., Nucl. Instr. and Methods 94, 477 (1971).

[2] G. Hass and R. Tousey. J. Opt. Soc. Cim. 49 , 593 (1959).

[3] Garwin and Roder. Nucl. Instr. and Methods 93, 593 (1971)

[4] Garwin, Tomkiewicz and Trines Nucl. Instr. and Methods 107, 365 (1973).

[5] Allison, Barnes and Tuzzolino J. Opt. Soc. Am 54, 747 (1964).

[6] Saxona, Rinse and Bruner J. Opt. Soc.Am. 60, 865 (1970).

FIGURE CAPTIONS

1 Number of photoelectrons versus momentum (P_K, P_π, P_P). Threshold of $\check{C}1$ set at 6 photoelectrons to avoid counting π's as K's because of $\check{C}1$ inefficiency.

2 Reflectivity of Al (Mg F_2) mirrors vs wave length.

3a Reflectivity of Al (Li F) mirrors vs wave length.

b Reflectivity of Al (Mg F_2) mirrors vs angle of incidence.

4a Transmission of various photomultiplier window materials vs wave length.

b Photocathode efficiencies ε_{PC} for various photocathodes vs wave length.

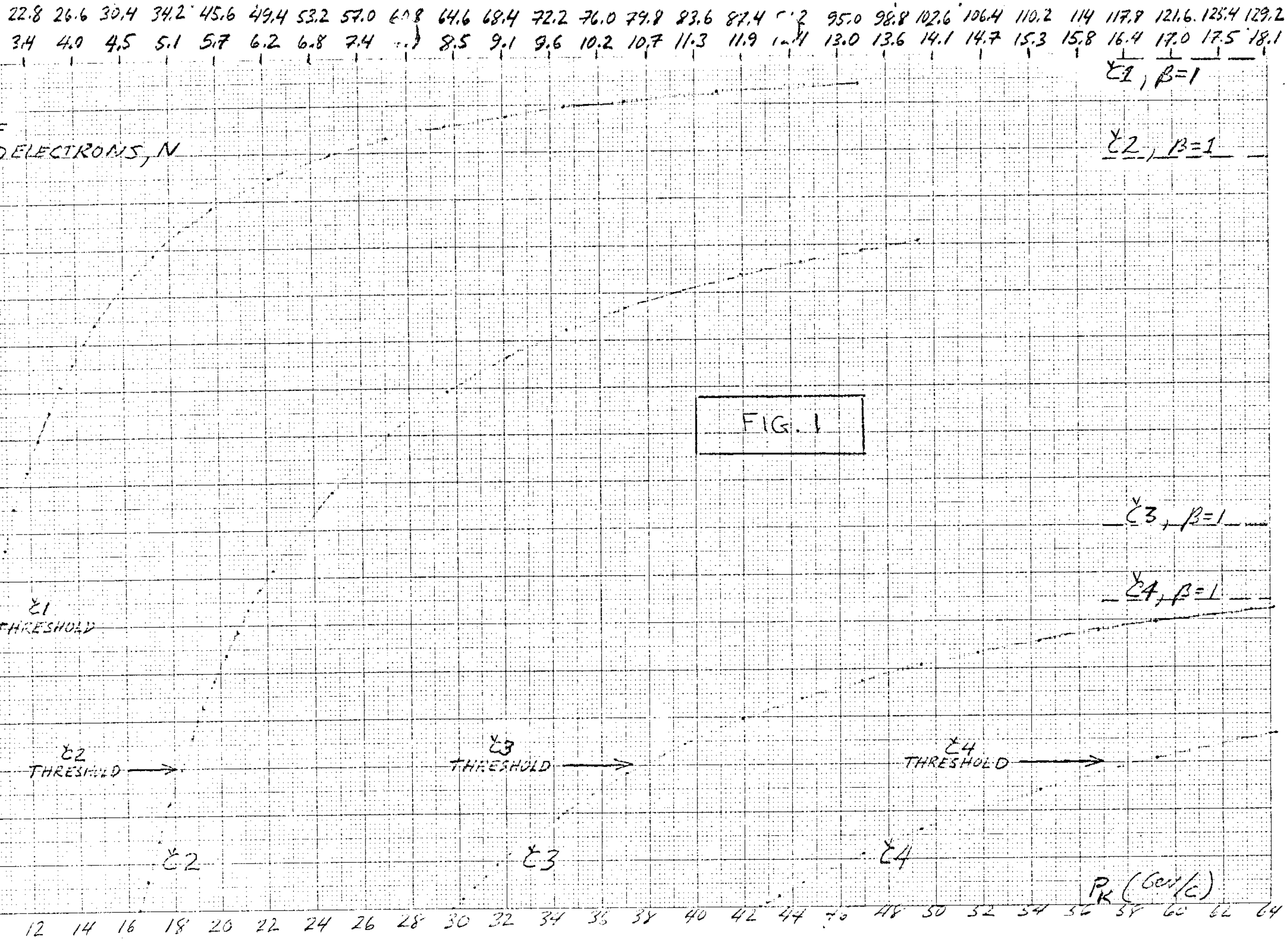

FIG. 1

22.8 26.6 30.4 34.2 45.6 49.4 53.2 57.0 64.6 68.4 72.2 76.0 79.8 83.6 87.4 95.0 98.8 102.6 106.4 110.2 114 117.8 121.6 125.4 129.2
3.4 4.0 4.5 5.1 5.7 6.2 6.8 7.4 8.5 9.1 9.6 10.2 10.7 11.3 11.9 13.0 13.6 14.1 14.7 15.3 15.8 16.4 17.0 17.5 18.1
Č1, β=1
Č2, β=1
Č3, β=1
Č4, β=1
ELECTRONS, N
Č1
THRESHOLD
Č2
THRESHOLD
Č3
THRESHOLD
Č4
THRESHOLD
Č2
Č3
Č4
P_K (Gev/c)
12 14 16 18 20 22 24 26 28 30 32 34 36 38 40 42 44 46 48 50 52 54 56 58 60 62 64

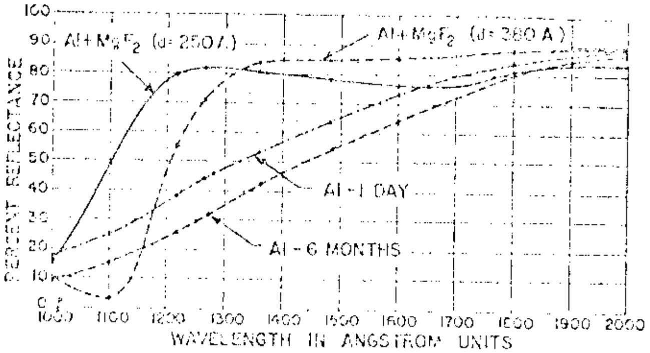

FIG. 2 Vacuum ultraviolet reflectance of evaporated aluminum with and without protective layers of MgF_2 of two different thicknesses (250 and 380 A). The reflectance of unprotected aluminum films is shown after 1 day and after 6 months of normal aging.

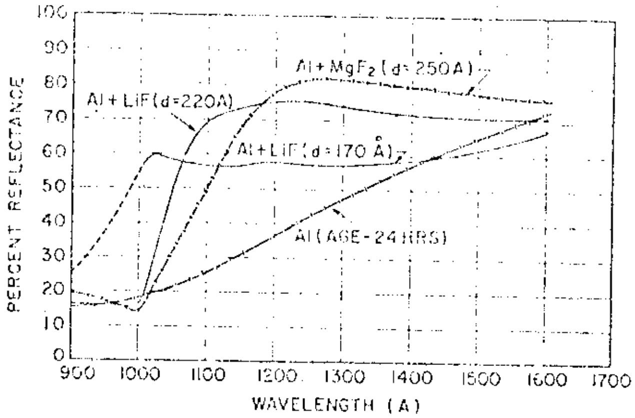

FIG 3 a. Vacuum ultraviolet reflectance of evaporated aluminum with and without protective layers of LiF of two different thicknesses (170 and 220 A). The reflectance of aluminum protected with 250 A of MgF_2 is also shown.

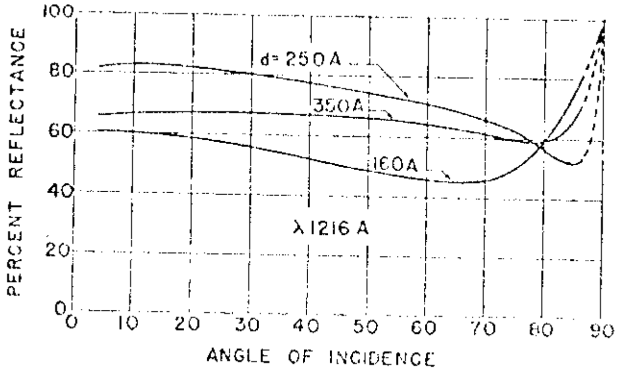

FIG. 3,b. Reflectance of MgF_2 protected aluminum films as a function of incidence angle for various thicknesses of MgF_2. (Wavelength: λ1216 A.)

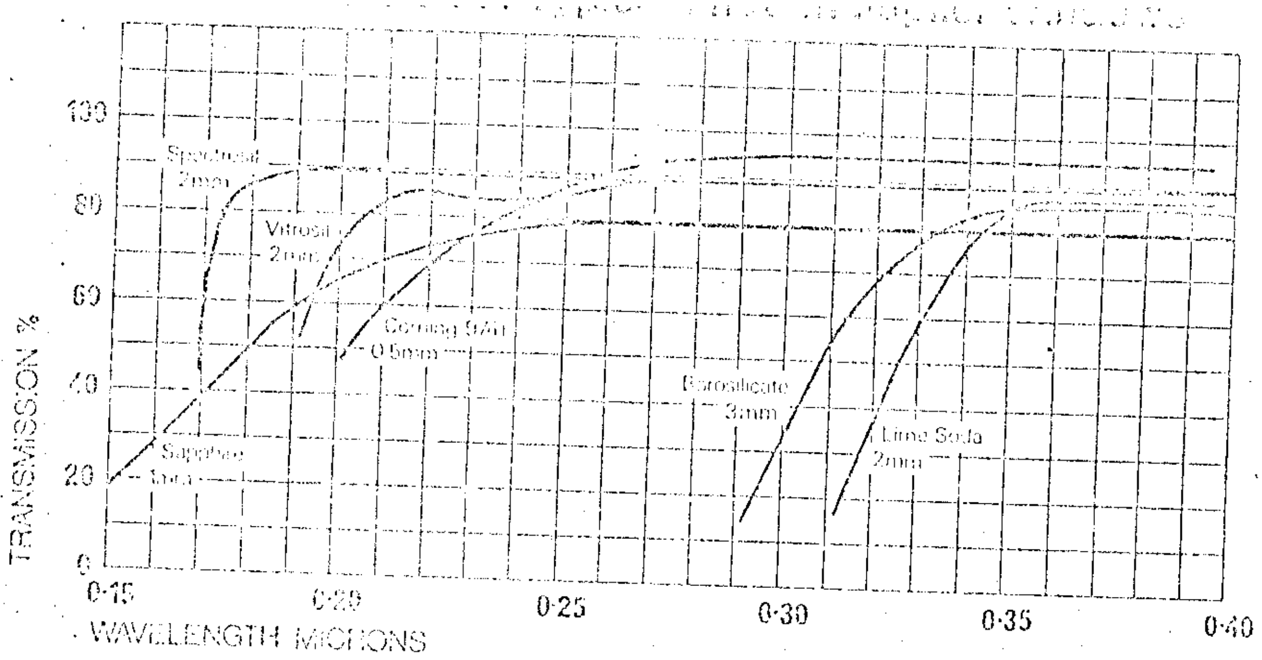

FIG. 4a

Typical Spectral Response Curves for EMI Photocathodes (50 and 30 mm diameter tubes)

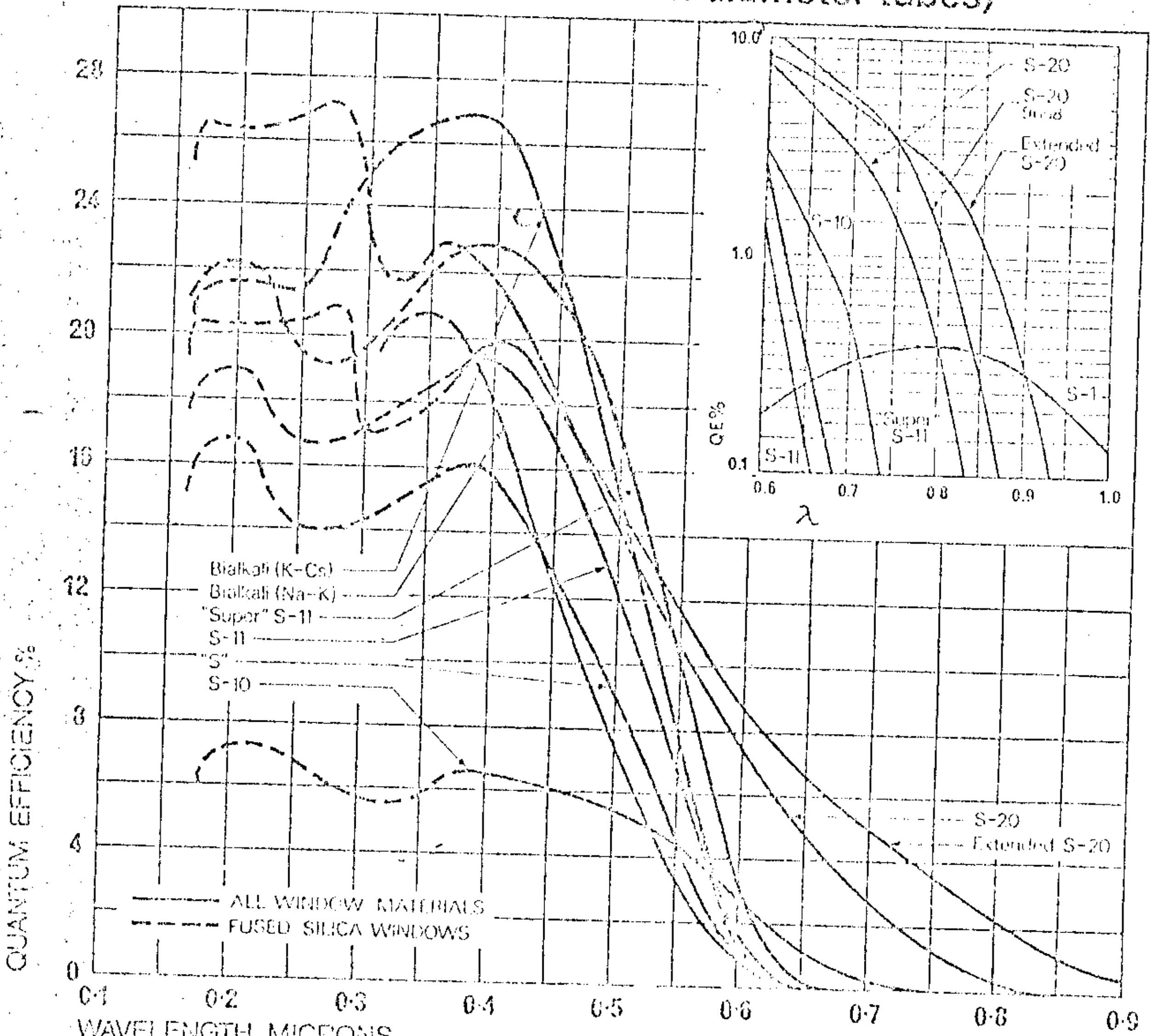

V. VERTEX DETECTOR

The vertex detector is made up of modules of MWPC's with three planes per module. The chambers are positioned inside the gap of a magnet such as "GOLIATH" of Saclay (Fig. 1) which has 2 m diameter pole pieces, 1.2 m gap and consumes 2.7 MW at 17 K gauss.

The number of modules and their disposition has been specifically designed to optimize the pattern recognition programs discussed in section VIII.

We distinguish forward and side modules, the former being perpendicular and the latter parallel to the beam direction. Each forward module (area 1.0 x 0.8 m^2) consists of one plane of vertical wires and two planes of inclined wires (± 25^o with respect to the vertical). Each side module (area 0.6 x 0.8 m^2) consists of one vertical plane, one horizontal and one plane of wires inclined at 5^o. The sense wires are made of tungsten (gold plated), 20 µm diameter and stretched at 35 gm. The wire spacing is 2 mm at a distance of 3 mm from the high voltage planes (50 µ diameter Cu-Be wires at a tension of 100 gm). The total number of wires in the vertex detector is of the order of 16000.

The mechanical conception of the ensemble has been studied in detail to satisfy the following conditions:

a) To obtain a precision of 0.2 mm or better in the positioning of wires within the same module and in the relative positioning of the modules.

b) To guarantee good precision and stability of the ensemble relative to the SPS floor and to insure interchangeability amongst modules.

c) To limit the amount of material per module so as to minimize the multiple scattering for low energies particles, to reduce the δ-ray production (which limits the detection efficiency and complicates the pattern recognition by multiplying the number of wires hit) and to limit the conversion of γ rays from π^o's (which contribute to the background of the experiment).

The present design achieves the figure of 1 radiation length per 100 m of particle path.

The frame which supports the modules is made of stainless steel and will be fixed such as to minimize the displacement of the system when the magnet is energised. The standardised modules are positioned on the frame, with the precision mentioned above, by ball bearing rollers which provide guidance when setting the modules in place (Fig. 2). In fig. 3 we show the prototype of a side module partially wired. The frame has the form of a C with the horizontal wires being attached at the open end to a 3 mm diameter Cu-Be wire under a tension of 60 Kg. This method of frameless support of the horizontal wires has been tested with success. The lower part of the frame is hinged so that when transfering the module from inside the magnet to an external frame any slight difference in the two supporting frames can be adjusted. The forward modules will be desensitised in the region of the primary beam ("beam-killers" technique). Fig. 4 shows details of the wire mounting. The wires are clamped, not soldered, in copper tubes at their ends. If a wire breaks in a given module it can be replaced without disassembling the module in a relatively short time (∿ 1/2 hour). The new wire is introduced through the outside frame by a stainless steel needle and guided to the corresponding hole by means of a magnetized shaft.

Various solutions are under study for the associated electronics and the final choice depends on how much real time pre-treatment of the data is required in order to reduce the rate of data taking to a manageable level.

The amplifiers, placed outside the magnet, are connected to the wires by "twisted pairs" of 3 to 4 meters length. The prototype, now under test, has a threshold of 1 μA (which is necessary for a chamber functioning with a classical gas mixture of Argon-Isobutane). It has a 40 MHz band-width and the dead-time of a wire is 150 ns. Two or three stages of buffer memory will be available in order to be able to make logical decisions on data retention without increasing the dead-time of the system.

A side module will be completely tested in a particle beam by the end of the summer. During this period a forward module will be completed; testing of this module will go on to the end of the year (1974). The serial production of both side and forward modules could then start at the beginning of 1975.

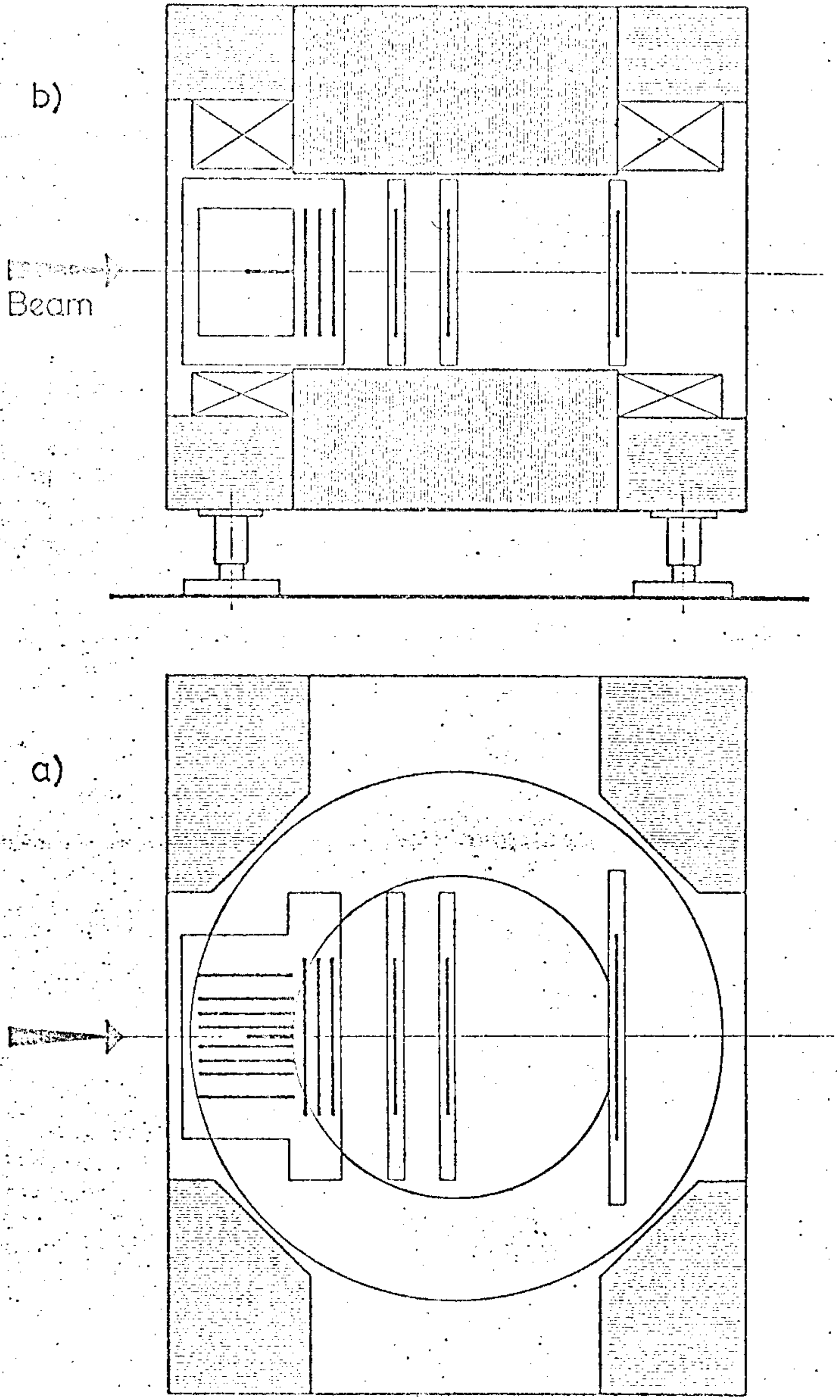

FIG.1

VERTEX DETECTOR
a) plan view
b) elevation

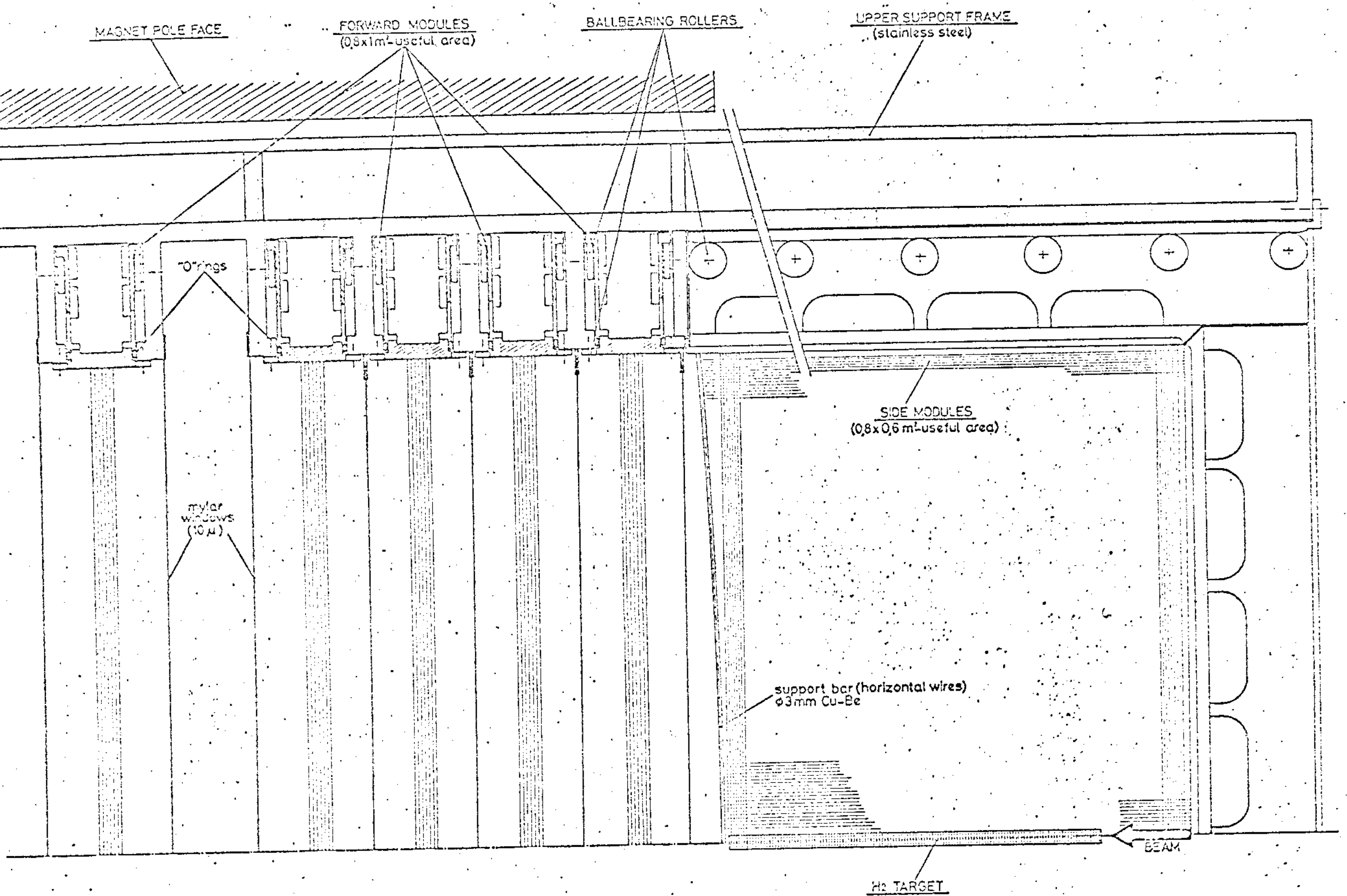

FIG.2

VERTEX DETECTOR (ASSEMBLY OF UPPER HALF)

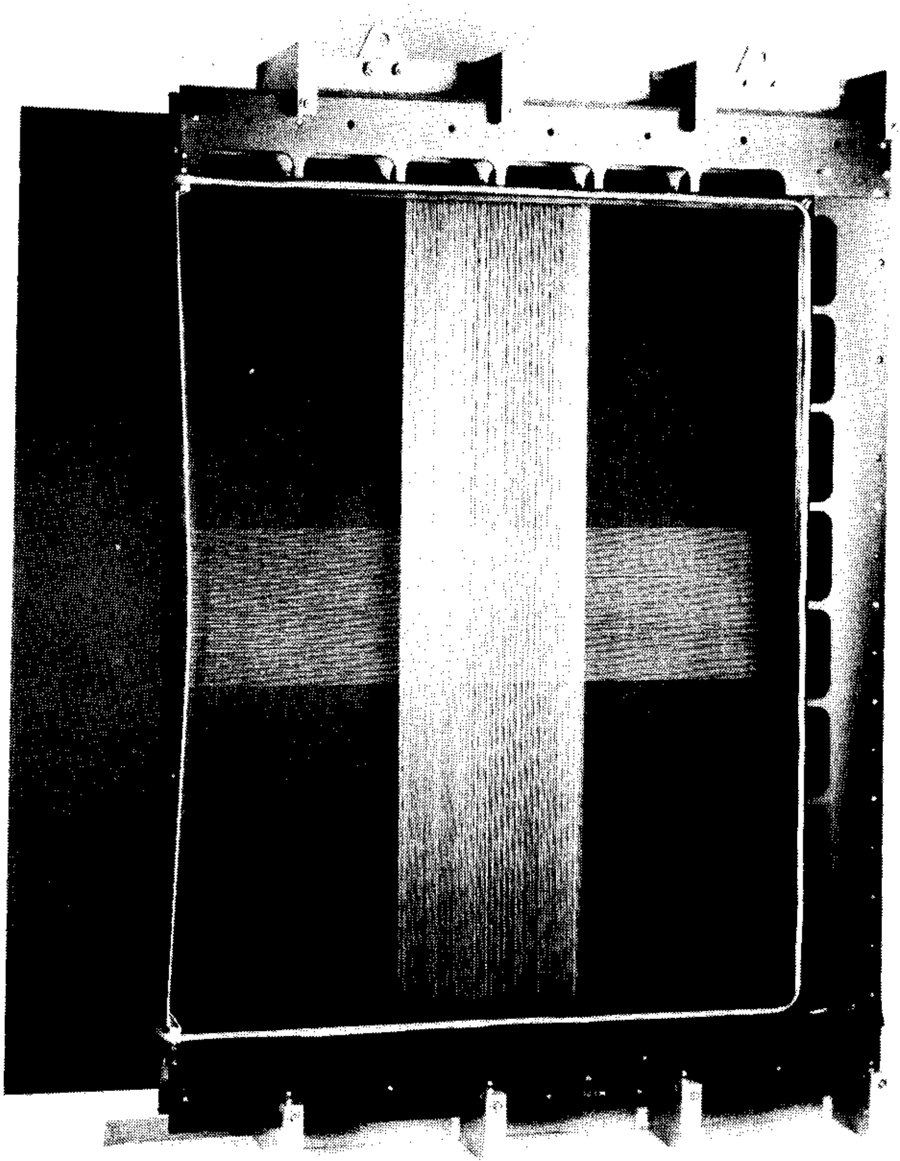

FIG. 3 SIDE MODULE

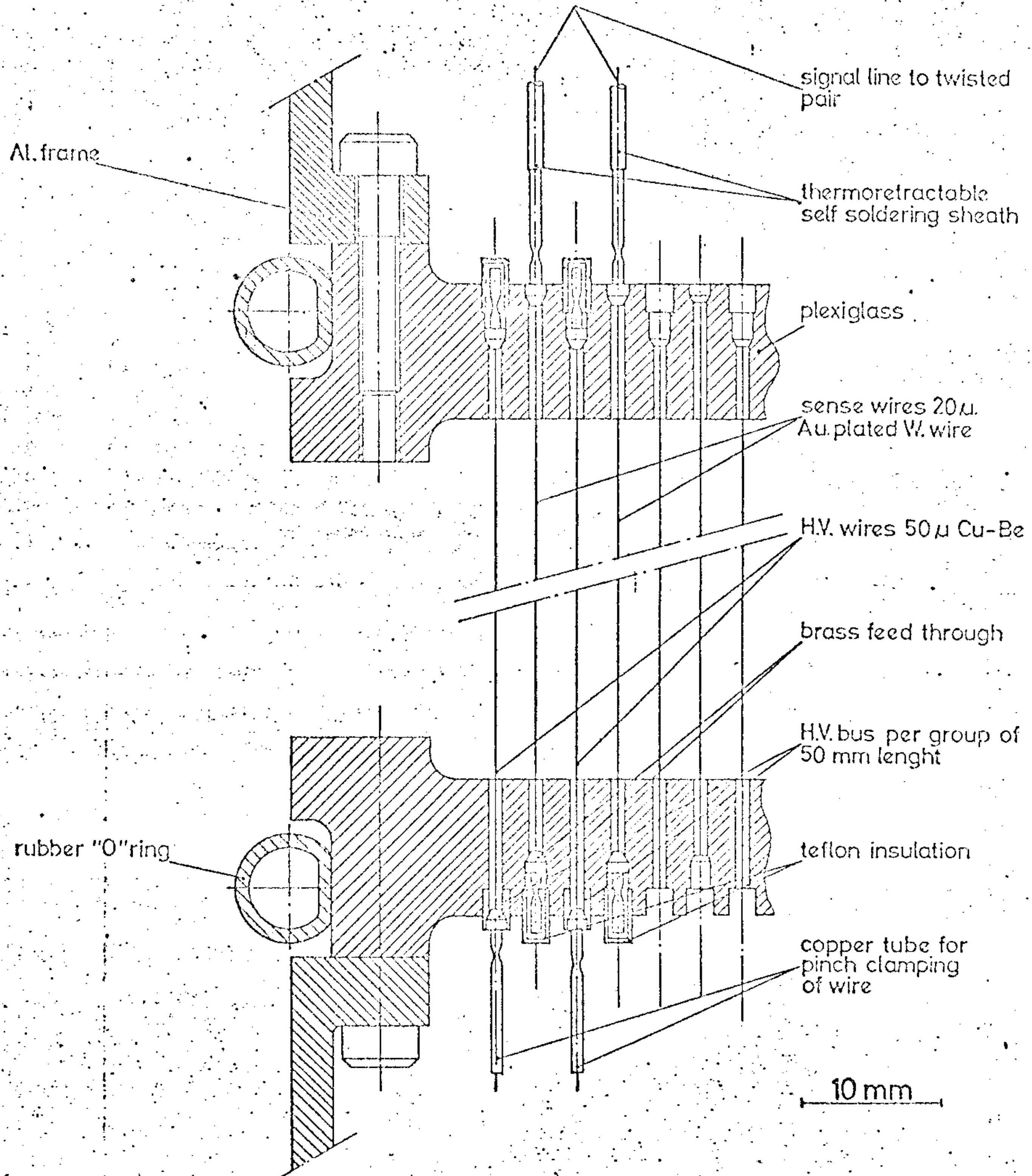

- FIG.4 -

DETAILS: WIRES FIXATION AND ELECTRIC CONNECTION

VI. FORWARD DETECTOR

The choice of drift chambers for the lever arm situated outside the magnetic field appears the only realistic possibility to obtain the necessary experimental space precision of ± 0.3 mm and ± 0.6 mm over the required dimensions of 2 x 2 m^2 and 4 x 4 m^2 respectively.

The wire separation is fixed at 2 cm due to considerations of cost, resolution time (300 nsec) and multitrack resolution necessary within the forward diffraction cone. We are also studying a MWPC design to cover the central region in an angular interval $\Delta\theta = \pm 3^o$ with respect to the beam.

The rate of accidental tracks coming from interactions occuring during the resolution time of the chambers will be eliminated by paralysing the trigger during an equivalent time after each detected interaction. This procedure reduces the effective beam intensity by 20% for a beam flux of 10^7 particles/second. The number of background tracks per event due to beam-halo muons is estimated to be $\sim 0.3/m^2$.

In order to overcome the left-right ambiguity in locating the particle position with respect to the sensitive wire we use two planes displayed by 1/2 of the sensitive wire spacing. The sensitive wires are of gold plated tungsten, 50 μm in diameter spaced 2 cm apart and at positive HV. Field wires, at negative HV are placed regularly in between the sensitive wires in order to linearise to a good degree the drift speed. These wires are of Cu-Be and have a 100 μm diameter.

The cathode planes are at ground potential and are made of mylar strips, 10 cm wide, 25 μm thick aluminised on both sides. The strips are stretched by means of springs (see figure 6). An anode-cathode distance of 1 cm. establishes a near radial structure for the electric field.

The position measurement is achieved by measuring the difference in the collection time of the two sensitive wires touched. The correction due to the incident angle of the track is relatively easy, and the linearity of the drift velocity is sufficient for the required spatial accuracy. No ambiguities in reconstruction occur since the angle of incidence is $< \pm 15^{o}$. The method of measuring the difference in the drift time has the advantage of reducing the errors coming from uncertainties of the drift velocity (the time difference is zero when the two collection times are equal).

Each chamber (see figures 1 and 2) consists of 2 modules (each module having 2 displaced planes) with horizontal and vertical co-ordinates and 1 plane of wires at 30^{o} in order to resolve point ambiguities (2 cm spacing between wires). In order to reduce the effects of thermal expansion the points of support are placed on the axes of symmetry (Figure 1). The study of the mechanical construction is well advanced and a prototype of 2×2 m^2 can be constructed, following the planning, for the end of the year.

The chamber electronics does not pose any serious technical problem and is more one of choosing the cheapest method capable of giving the accuracy required. The amplifiers attached to each wire have been designed and tested. The sensitivity is 2 μA for a maximum slewing time of 3.5 nsec. They contain two fast transistors (BSX27) and an amplifier (MC 10116).

The time coding system is not yet frozen. Several solutions are possible (time-stretcher or analogue system associated to each wire). Within the limits of precision desired, counting frequencies of 100 and 50 MHz are in principle sufficient for the chambers of 2×2 m^2 and 4×4 m^2 respectively and pose no problems. We have developed a method which consists in passing the signals of the wires onto a delay line. The delay of each cell, coupling 2 sensitive wires relative to the next, is 360 nsec. This is achieved by means of 3 monostables of

120 nsec each placed in series in order to reduce the dead-time; it will assure a precision on the propagation time of the cell of $\sqrt{3}$ x (0.02 x 120) = 4 nsec. The pulses are synchronised in phase at the end of each cell by a 100 MHz voltage. The accuracy of the time between two successive pulses (taken as a multiple of the period) becomes, in this way, independent of the delay line length; this is a gain over the quadratic sum of the fluctuations of each cell. Such a system is the fast equivalent of the magneto-strictive delay lines attached to wire spark chambers. In this way we need only a number of counters equal to twice the maximum number of particles expected if the measurement is done with respect to an external time reference. The method reduces to a minimum the number of counters. By dividing the chambers into lengths of 1 meter, the dead-time due to the propagation of the line will be 36 μsec; this is acceptable if we compare it with the total decoding time of 400-500 μsec.

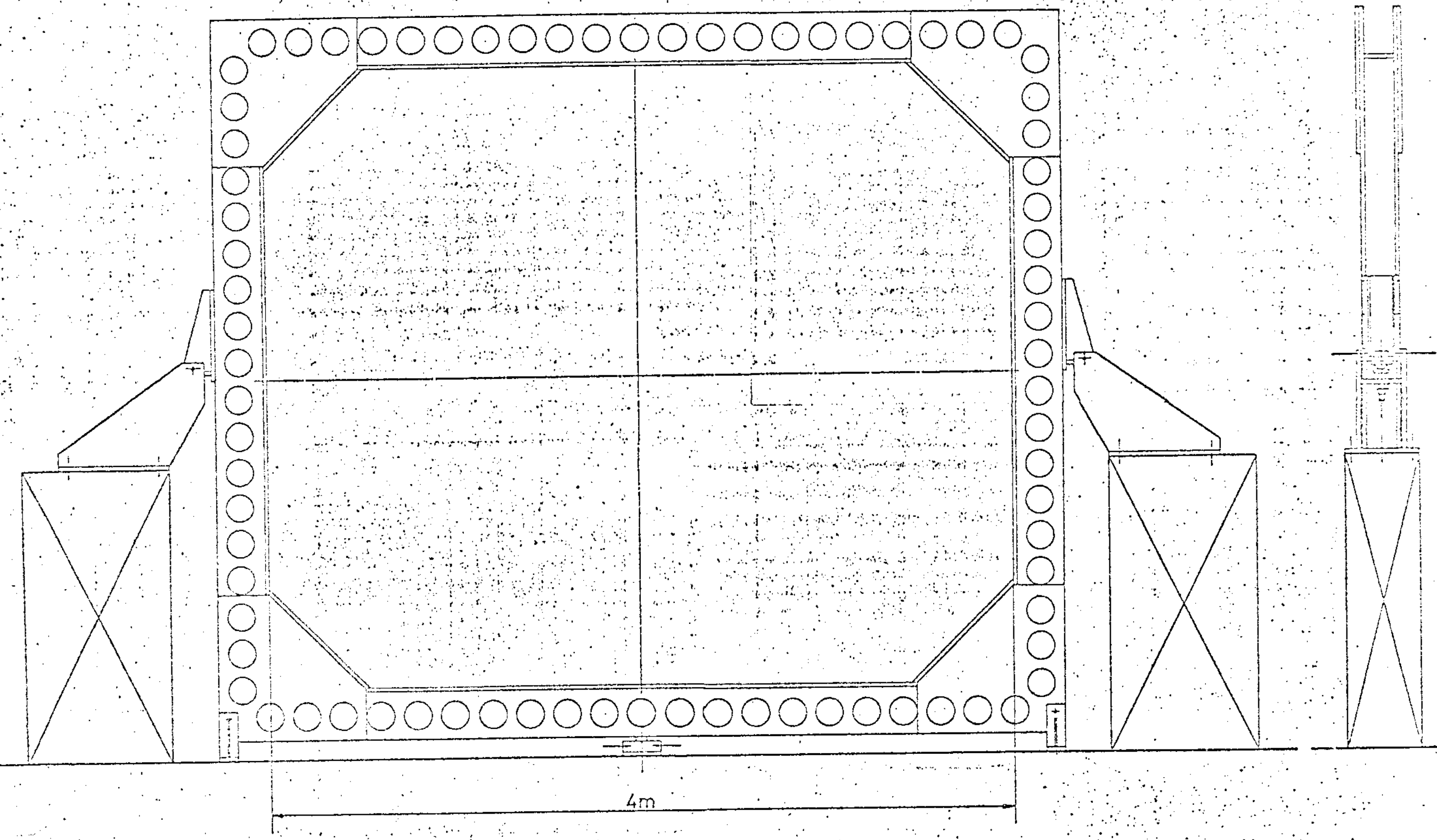

FIG.1
DRIFT CHAMBER –
General construction principle.

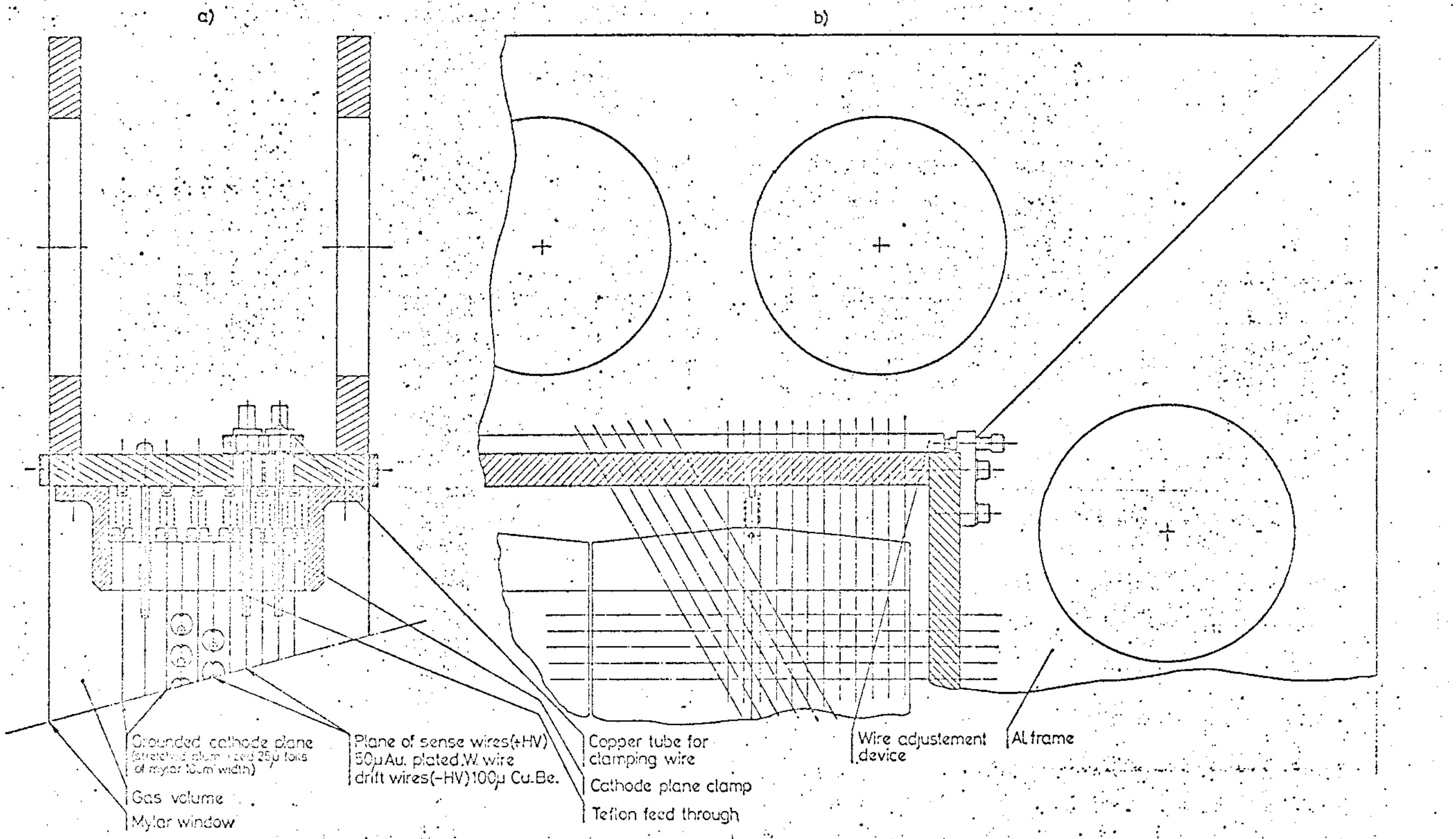

FIG.2
DRIFT CHAMBER DETAILS
a) side view
b) front view

VII. DATA ACQUISITION

The information coming from the apparatus is read, decoded and stored by the system described below.

The number of events to be recorded per accelerator cycle is ∿ 100. Each event consists of 800 words of 16 bits for a charged particle multiplicity of 8. The duration of the data acquisition is ∿ 0.5 seconds every 4 or 8 seconds. If we wish to reduce the loss of events due to the system dead-time to less than 20%, the recording speed must be at least 10^6 words/second. The storing of this information must then be done at a speed of 20000 words/second; these must then be written onto magnetic tape at 5×10^7 words/hour (i.e. 3 tapes per hour).

The computer needed for these operations must have a minimum memory of 64000 words. The computer will control the data acquisition, memorise the information during the bursts and perform a certain number of technical controls. The following peripheral equipment will be needed:

(i) A CAMAC interface adapted to the 0.8 μsec fast memory access time; it should have direct access to the computer memory.

(ii) A high performance tape unit: it should be capable of working at a speed of 75 inches/sec with a density of 1600 bytes/inch.

Two types of control will be performed by the computer. First, an efficiency check of all the detectors for each event. Second, a stability check of the detectors (e.g. voltages, multiplier amplifications, magnet currents and fields, gas flows, etc..) to be done between bursts.

In addition to this computer, it would be an advantage to be connected to a more powerful computer. This would allow a detailed study of the operation of each detector, the calibration of the geometry with straight tracks and all the operations usually performed during the debugging stage of the apparatus. During data-taking it would allow the complete analysis of a sample of events. An IBM 360-40 would be suitable for this role. Alternatively, one could have a data link to one of the larger CERN computers.

Much of the equipment mentioned above is already available to the collaborating laboratories, viz:

- PDP 11/40 computer with 8K memory and basic peripherals.
- Fast electronics.
- CAMAC chassis and CAMAC modules, scalers, pattern units, digital voltmeter, display and its interface.

The missing equipment is:

- 4 blocks of 16K words.
- 2 magnetic tape units (1600 bpi, 75 ips).
- 1 magnetic tape controller.
- 1 CAMAC interface for PDP 11.
- 1 read-out logic for digital MWPC.

VIII. PATTERN RECOGNITION

As described in the original proposal we have chosen a disposition for the MWPC's and drift chambers which should enable us to attack the problem of reconstructing high multiplicity events. The philosophy which we arrived at, after some study, is as follows.

The lever arm, which comprises four drift chambers, is in a field free region. At 150 GeV/c about 60% of all charged secondaries, be it a peripheral or high p_t type of event, go into the lever arm. The ambiguities in the pattern recognition of these tracks (as shown below) is essentially zero. They have been well spread out by the magnetic field and the track points lie on a straight line. All pattern recognition is done in space. This means, for example, that in a 10-charged-track event 6 have been already identified.

Then, by knowing the origin (which is well determined by the beam direction and the high-p_t track or a single wide angle track), the points in the MWPC system inside the magnet can be associated to these tracks by back-tracking. Ambiguities of association there will be, as we show below, but this does not matter as the momenta and angles are determined by the lever arm and the origin alone.

We are then left with the problem of recognising the 40% (or 4) charged tracks of momenta < 10 GeV/c in the MWPC vertex system in the magnetic field. Now we know from the OMEGA spectrometer, where pattern recognition is done in projection, that 4 tracks of < 10 GeV/c present no problems. We believe pattern recognition in space, which is much emptier than its projection, will allow us to go to higher multiplicities than 4 (in principle one might guess at $4^2 = 16$ tracks as a possibility, due to another dimension).

Our choice of vertex detector layout was arrived at by our wish to obtain, as a minimum, the possibility of measuring a good fraction of the events containing tracks over the entire region of phase space (momentum and angle) in the c.m. For example, among the 4 remaining tracks to be identified,we found that only 5% of high-p_t type generated events have a track with momentum < 1 GeV/c and < 3 points (hence non identifiable) in the geometry of fig. 1a. In the case of peripheral-type generated events this figure becomes 72%, and is worse (see Table 6) if we do not add the chambers on each side of the target.

Below we describe :

1) The acceptance and track recognition properties of the vertex-detector shown in fig. 1a.

2) The track recognition capabilities of the complete set-up for peripheral and high-p_t type of events.

3) Characteristics of the lost particles.

As a result of this work we reduced the number of MWPC's in the vertex detector to those indicated by an arrow in fig. 1a. The total complement of MWPC's of fig. 1a will be constructed but will only be equiped with read-out electronics depending on the experience gained during initial running.

1. Low momentum tracks in the vertex detector

i) Simulation of low momenta.

We have studied acceptances and track recognition for simulated tracks with momenta less than 1 GeV/c. The chamber layout and the two target positions that are considered are shown in figs. 1b, c. The chamber dimensions and positions are summarised in table 1. For the simulation, uniform distributions in the track parameters (momentum, azimuth, dip as defined in fig. 2, and vertex position) have been used and the ranges of these parameters are given in table 2.

The particles are tracked in the two-coil magnetic field of the Omega spectrometer - but with the spatial dimensions scaled by a factor 2/3. Two target positions are considered: "back",positioned symmetrically with respect to the side chambers (fig. 1b) and "forward", with the front end of the target level with the front edge of the side chambers (fig. 1c). For the forward target position, the side chambers are decreased in width to give the same acceptance in the backward direction as for the target back configuration.

In the tracking, each chamber gives a space point with a random error of ± 0.7 mm. Tracks are followed from the side chambers into the forward chambers and vice versa, but with a cut-off on a turning angle of more than 180°.

ii) Acceptance for single tracks.

The minimum number of space points to define a track in a magnetic field is three. In table 3 we give the percentage of tracks with momentum greater than 100 MeV/c that fulfil this requirement in the forward and side cones for the two target positions. Extra points obtained by a track passing through the same plane twice are not included. In the following we give figures for the forward target position, which gave the best results.

The dip-azimuth and momentum-azimuth correlations of the tracks in the side cone which are lost (i.e. have less than 3 points) are shown in figs. 2 and 3. The dip-azimuth and momentum-dip correlation for the forward cone are shown in figs. 4 and 5a. We see that except for large dip angles the ϕ vs λ plot in fairly uniformly populated. The momentum projection (fig. 5b) shows no particular biases or loss, except that expected at lower momenta due to the small curvature.

As can be seen from table 3, the target position does not greatly affect the overall acceptance for tracks less than 1 GeV/c. However, the effect is more noticeable for the higher momenta (> 1 GeV/c) in the forward cone, where tracks of larger dip are accepted with the target forward than with the target back. Acceptances are given in table 3 for the forward cone in a momentum range of 1-10 GeV/c. The momentum-angle correlations for the tracks from this sample with less than 3 space points are shown in figs. 6 and 7.

iii) Track recognition.

For tracks with three points or more we have the problem of associating the points to tracks i.e. track recognition. This has been studied in detail for the side cone and the conclusions checked in the forward cone. The conclusions may be summarised as follows:

1) For 5 or more space points (in the same geometry) good linear constraints are obtained from the principal component method (see ref. 1). Thus tracks may be identified using certain linear combination of the measurements.

2) For 3 or 4-point tracks the number of measurements results in insufficient redundancy for the solution to become unique, so that track recognition by linear tests is very inefficient (many ambiguities). This also applies to tracks having 5 or 6 points, but with only 2 or 3 points in a given set of chambers i.e. the tracks linking the two geometries. For these tracks it is necessary to use a non-linear constraint for track recognition. We have used a quintic spline fit for each track (see ref. 2). This fit incorporates the non uniformity of the magnetic field and is therefore more time-consuming than the linear constraints - but it includes a better momentum estimate at the same time.

3) In order to test the track recognition procedures described above, two prong pseudo events were simulated by grouping tracks in the side cone. No kinematics or physics was included. Track recognition was done by the brute force approach-looking at all possible combinations of the track points in an "event", and using linear or spline constraints to identify track combination. The program was set up to find all true tracks, and in table 4 we give typical "contamination" figures for two-track events i.e. the percentage of extra tracks found. Similar figures were obtained for the low momentum tracks in the forward cone.

4) Typical times for track identification using linear and spline methods are given in table 5, both for single tracks and for the two-track pseudo-events where all combinations are tested for tracks.

References

1. H. Wind, Function Parametrisation, CERN 72-22.

2. H. Wind, Nuclear Inst. and Methods (submitted) NP-DHG 73/5.

2. Results on simulated peripheral and high p_t type of events.

i) Generation :- We have generated two kinds of events.

a) 100 "peripheral" Van-Hove longitudinal phase space type at 150 GeV/c, $\pi^- p \rightarrow p 3\pi^+ 4\pi^- \pi^o$.

b) 100 high p_t (so called "explosive") events in which two mass M_5^o of 5 GeV each, produced isotropically along with one π^o, $\pi^- p \rightarrow M_5^o M_5^o \pi^o$, are allowed to decay isotropically to 4 charged particles each, viz. $\pi^- p \rightarrow p 3\pi^+ 4\pi^- \pi^o$.

ii) Pattern recognition.

Each track point was randomised with an error of ± 0.7 mm as before, and we then went through a large number of exersises using existing pattern recognition programs. These are the "principal component" method and spline fit as mentioned above. We give here some results which give us a certain confidence that the pattern recognition problems associated with the higher multiplicity events occuring can be overcome in the proposed layout.

Thus fig. 8 shows the distribution of what is essentially a measure of the "mean residual" for the possible track combinations, using the linear test on the 5 points occuring in the chambers 1, 3, 5, 7 and 9 of fig. 1a for each "explosive" event. The full line histogram shows the distribution for the true tracks. In order to retain all true tracks we see we have also 16% extra spurious tracks. If we then take these candidates and repeat the spline fit on them the contamination falls to 12% (see fig. 9). This is not a very happy result. Fig. 10 and 11 display similar results for the peripheral events where track separation in space is smaller. Here a contamination factor of 3.88 falls to 2.77 by using the spline fit. The results clearly demonstrate the impossibility of pattern recognition of tracks with this spatial separation and point error over such a distance from the target. Figs. 12 and 13 which repeat the exercise on chambers 6 to 10, where the tracks are best separated in the vertex magnet, show a net amelioration for the "explosion" events but the situation for peripheral events (fig. 14 and 15) is still bad - 26% background tracks.

However, when we move further downstream from the target and consider the 3 lever arm chambers 11, 12 and 13 the track background has completely disappeared (fig. 16). Hence our insistence on first performing pattern recognition on the tracks in the lever arm chambers.

We then looked at all the tracks < 10 GeV/c having $\gtrsim 5$ points and find, after removing all points from the tracks > 10 GeV/c (assumed found in the lever arm), that the background tracks were reduced to 1% for explosive events (fig. 17 and 18) and 2% for peripheral events which we consider acceptable. (figs. 19 and 20).

For the tracks with less than 5 points which then remain and are mainly < 1 GeV/c we used the spline fit and found no contamination for these tracks. This is reasonable since there are less of them and they are well separated in space.

Figs. 21 - 25 show the spread in $\Delta p/p$ obtained from the spline fit along with the correlation lines calculated using the formula of Gluckstern,(1) with an R.M.S. error of ± 0.4 mms.

The results of this section are summarised briefly in table VI along with the timings (Table VI.3) which indicate about 0.5 sec. 6600 CP time/ event of 8 prongs. Note that the complete calculation is necessary only for those events in which a high p_t track occurs.

3. Characteristics of lost particles.

As we see from table 6 (1) there are 72 tracks from peripheral events with $P < 1$ GeV/c lost from the original 249. The P, ϕ correlation of these tracks is shown in figs. 26 and 27 and no obvious bias is seen. On the contrary figs. 28 and 29 showing the λ, ϕ correlation, show that tracks with large dip are preferentially lost, as expected for this geometry. If, as could be the case, there are few tracks of this peripheral nature < 1 GeV/c in the high p_t events then we have a good chance of obtaining a sample where all tracks are seen. In the regions above and below the target (large dip) we will place scintillation counters to know that a track passed in this region.

For the tracks > 1 GeV/c and < 10 GeV/c the P, λ of the actual tracks for the peripheral and explosion events is compared to the P, λ distribution for the lost tracks in the uniform simulation in figs. 30 to 32. No track lies in the lost region.

1) R.L. Gluckstern Nucl. Instr. and Meth. 24 (1963), 381.

TABLE 1

REGION	TARGET CENTRE (x)	CHAMBER DIMENSIONS WIDTH (y or x)	DEPTH (z)	CHAMBER POSITION (cm)
Side	-80.0	60.0	80.0	y = + 6,+12,+18,+24,+36,+48
Forward	-80.0	110.0	80.0	x = - 45,-39,-33,-27,-15,-3
Side	-65.0	45.0	80.0	y = + 6,+12,+18,+24,+36,+48
Forward	-65.0	110.0	80.0	x = - 45,-39,-33,-27,-15,-3

TABLE 2

REGION	P (GeV/c)	ϕ	λ	TARGET DIMENSIONS
Forward Cone	0 to 1	-60° to $+60^{\circ}$	-60° to $+60^{\circ}$	30 cm x 2 cm x 2 cm
Side Cone	0 to 1	$+30^{\circ}$ to $+150^{\circ}$	-60° to $+60^{\circ}$	30 cm x 2 cm x 2 cm
Forward Cone	1 to 10	-60 to $+60^{\circ}$	-60° to $+60^{\circ}$	30 cm x 2 cm x 2 cm

TABLE 3

REGION	MOMENTUM RANGE	TARGET CENTRE	ACCEPTANCE (%)
Forward	0.1 to 1 GeV/c	-80	81
		-65	87
Side	0.1 to 1 GeV/c	-80	85
		-65	83
Forward	1 to 10 GeV/c	-80	79
		-65	86
Forward + Side	0 to 1 GeV/c	-80	81
		-65	80

TABLE 4

No. of Tracks/"Event"	No. of Points per Track	No. of Extra Tracks (%)	Method Used
2	3	$\sim$ 12	Spline
2	4	$\sim$ 1	Spline
2	5	$\sim$ 3	Linear
2	6	$\sim$ 3	Linear

TABLE 5

Timings (in msec of CDC 7600)

No. of Points/Track	3	4	5	6	
Linear	.3	.4	.5	.7	1 Track/"Event"
Spline	2.4	2.8	3.5	4.3	
Linear	.7	1.2	3.3	7.0	2 Tracks/"Event"
Spline	5.0	13.5	-	-	

TABLE 6

SIMULATION RESULTS 150 GeV/c EXPLOSION + PERIPHERAL

All P Total No. Tracks	0 to 1 GeV/c Total	< 3 Pts.	1 < P < 10 Total	< 3 Pts.	> 10 GeV/c Total	< 3 pts.
Explosion : 800	36	4	360	0	404	0
Peripheral : 800	249	72	198	0	353	0

2. Track Recognition Results

a) 0 to 1 GeV/c. Peripheral (Worst Case)

Spline :	No contamination for 3, 4, 5 and 6 point tracks
Linear :	∼ 2% Contamination for 5 or 6 point tracks

b) 0 to 100 GeV/c.

No. of points in forward chambers	0	1	2	3	4	≥ 5 p > 10	≥ 5 p < 10 GeV/c
Explosion :	10	0	2	1	2	404	381
Peripheral :	122	16	12	13	21	353	263

Recognition : Linear tests; ≥ 5 PTS/TRK ; p < 10 GeV/c.

	No. of Tracks	Efficiency	Contamination	Lin + Spline	Time/Track (7600)
Explosion :	381	99.5%	∼ 2%	∼ 1%	∼ 3 msecs
Peripheral :	263	99.0%	∼ 6%	∼ 2%	∼ 3 msecs

3. Time/Event (8-Prongs) (7600 Time)

	Fraction > 10 GeV/c	Fraction 0 to 10 GeV/c ≥ 5 pts.	Fraction 0 to 10 GeV/c < 5 pts.	Total	
losion :	.50 (x 5 msecs)	.48 (x 3 msecs)	.02 (x 5 msecs)	∼30msecs	+ Point -fin ing + Over -hea
ipheral :					
ipheral :	.44 (x 5 msecs)	.33 (x 3 msecs)	.23 (x 20 msecs)	∼60msecs	

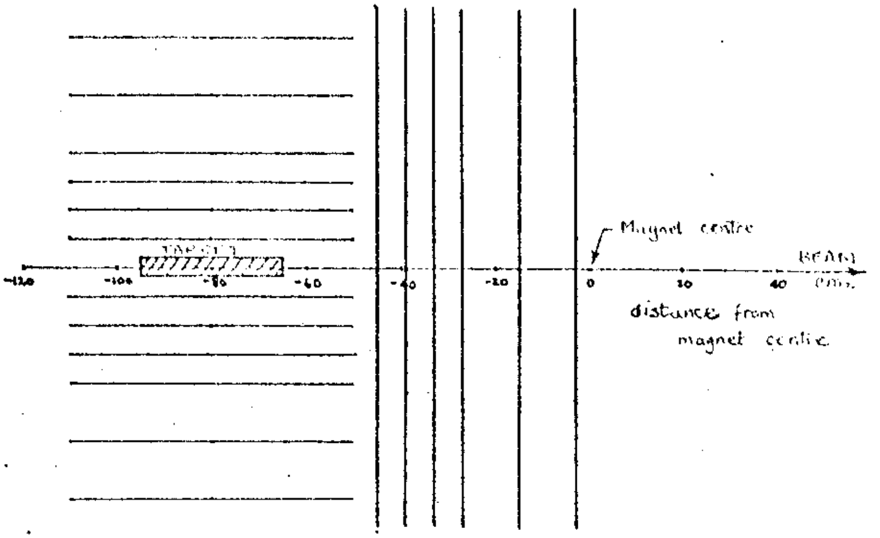

Fig. 1b : TARGET BACK

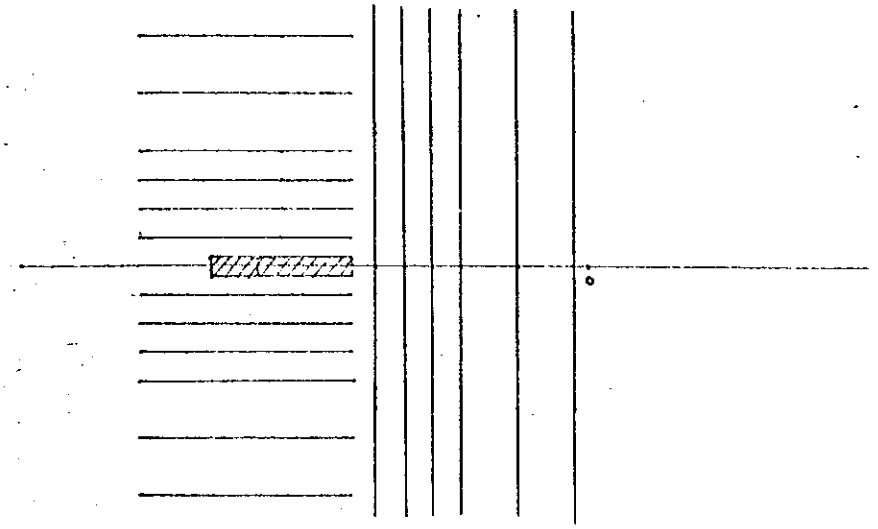

Fig 1c : TARGET FORWARD.

Scale : 1 mm = 1 cm.

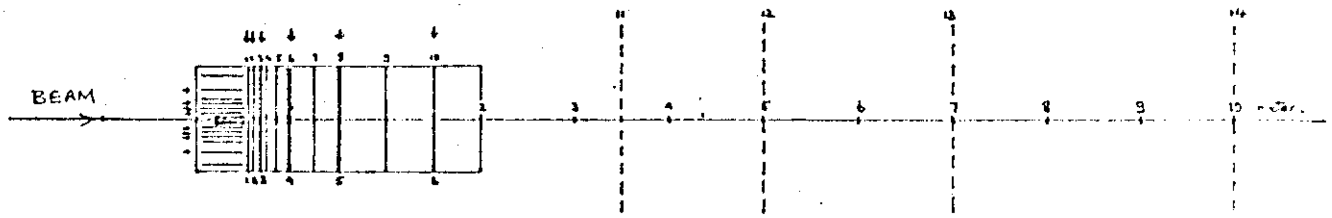

FIGURE 1a (PLAN VIEW)

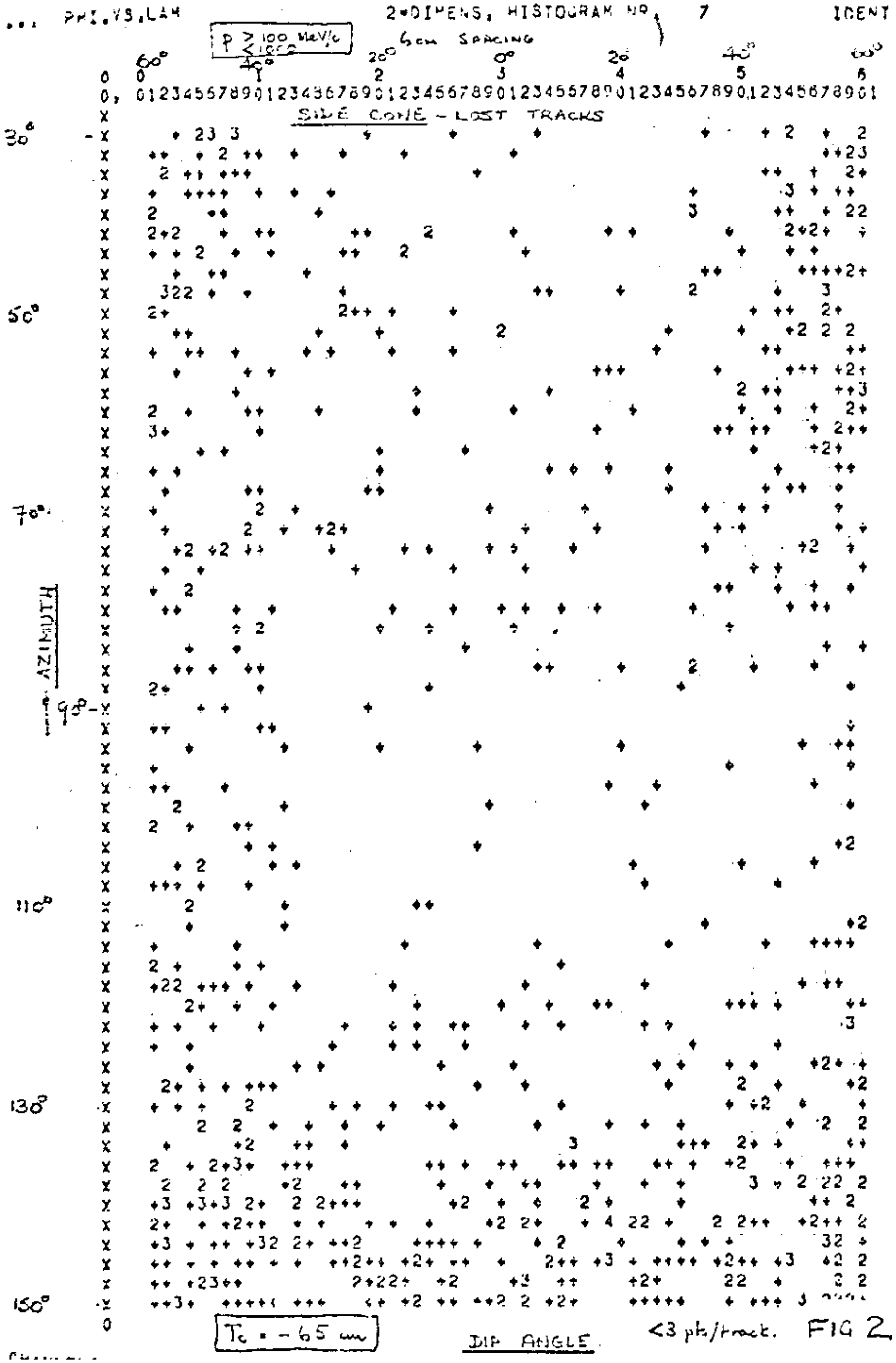
PHI.VS.LAM
2-DIMENS, HISTOGRAM NO. 7
IDENT
P ≥ 100 MeV/c
≤ 1000
6cm SPACING
60°
40°
20°
0°
20
40°
60°
SIDE CONE - LOST TRACKS
30°
50°
70°
AZIMUTH
90°
110°
130°
150°
Tc = - 65 cm
DIP ANGLE
<3 pts/track.

FIG 2

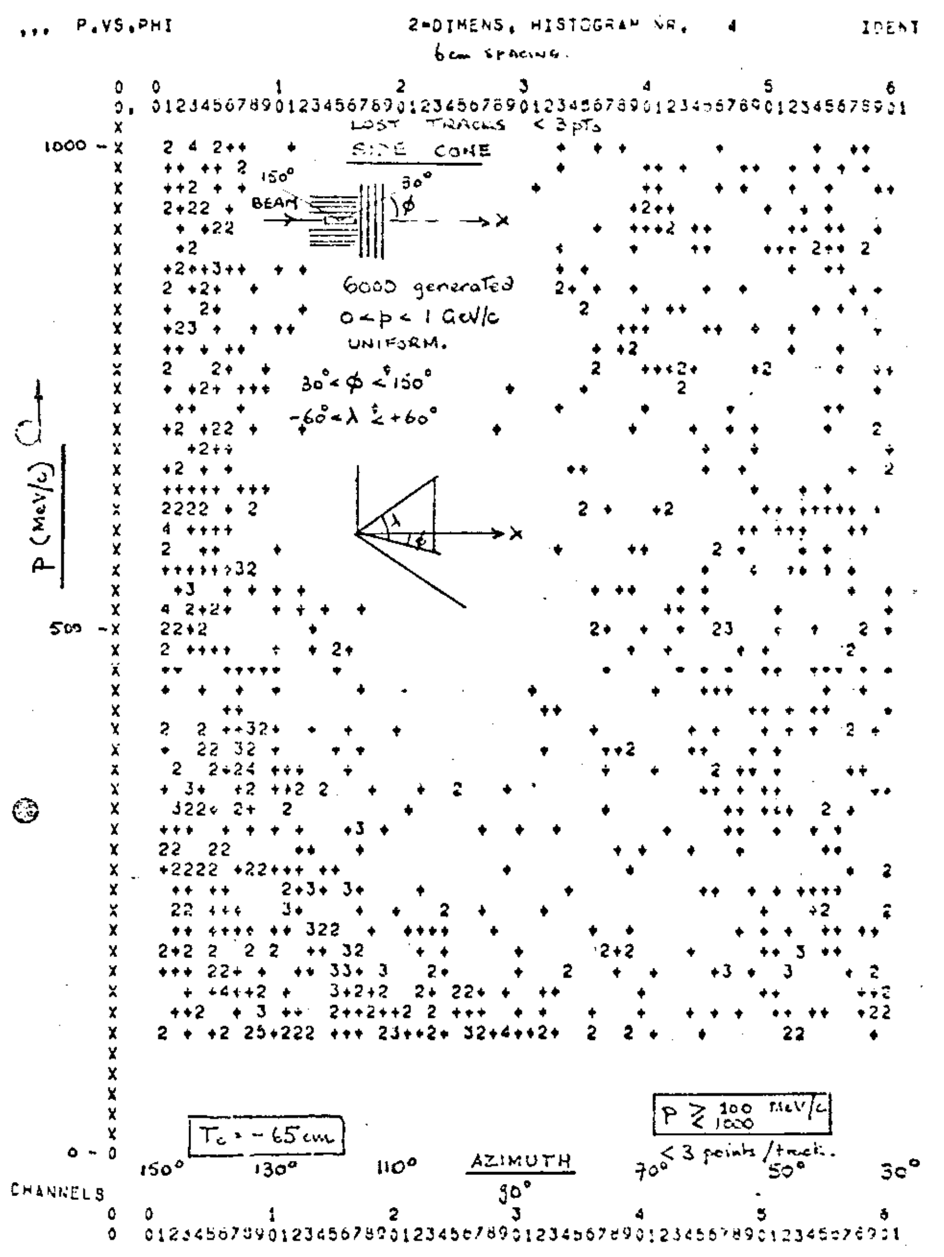
P.VS.PHI
2-DIMENS, HISTOGRAM NR. 4
IDENT
6cm SPACING.
LOST TRACKS < 3pts
SIDE CONE
1000
500
0
P (MeV/c)
150°
30°
BEAM
φ
x
6000 generated
0 < p < 1 GeV/c
UNIFORM.
30° < φ < 150°
-60° < λ < +60°
λ
φ
x
Tc = - 65 cm
P ≥ 100 MeV/c
≤ 1000
< 3 points / track.
150°
130°
110°
AZIMUTH
90°
70°
50°
30°
CHANNELS

Fic 3.

7.

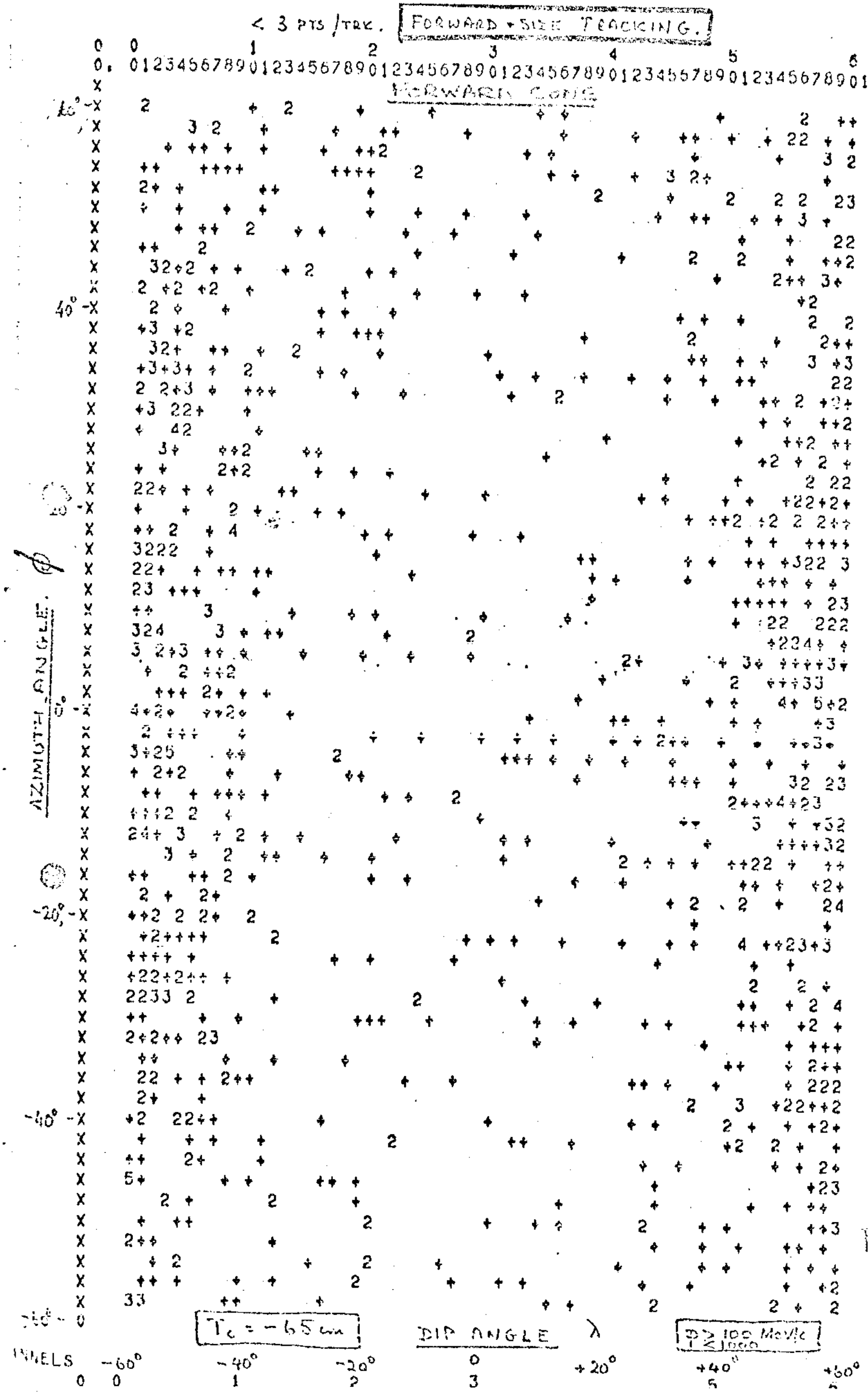

< 3 PTS / TRK.
FORWARD + SIDE TRACKING.
0 0 1 2 3 4 5 6
0. 0123456789012345678901234567890123456789012345678901234567890 1
FORWARD CONE
60°
40°
20°
0°
-20°
-40°
-60°
AZIMUTH ANGLE φ
Tc = -65 cm
DIP ANGLE λ
P > 100 MeV/c
T < 1000
NNELS
-60°
-40°
-20°
0
+20°
+40°
+60°
0 0 1 2 3 5 6

FIG 4.

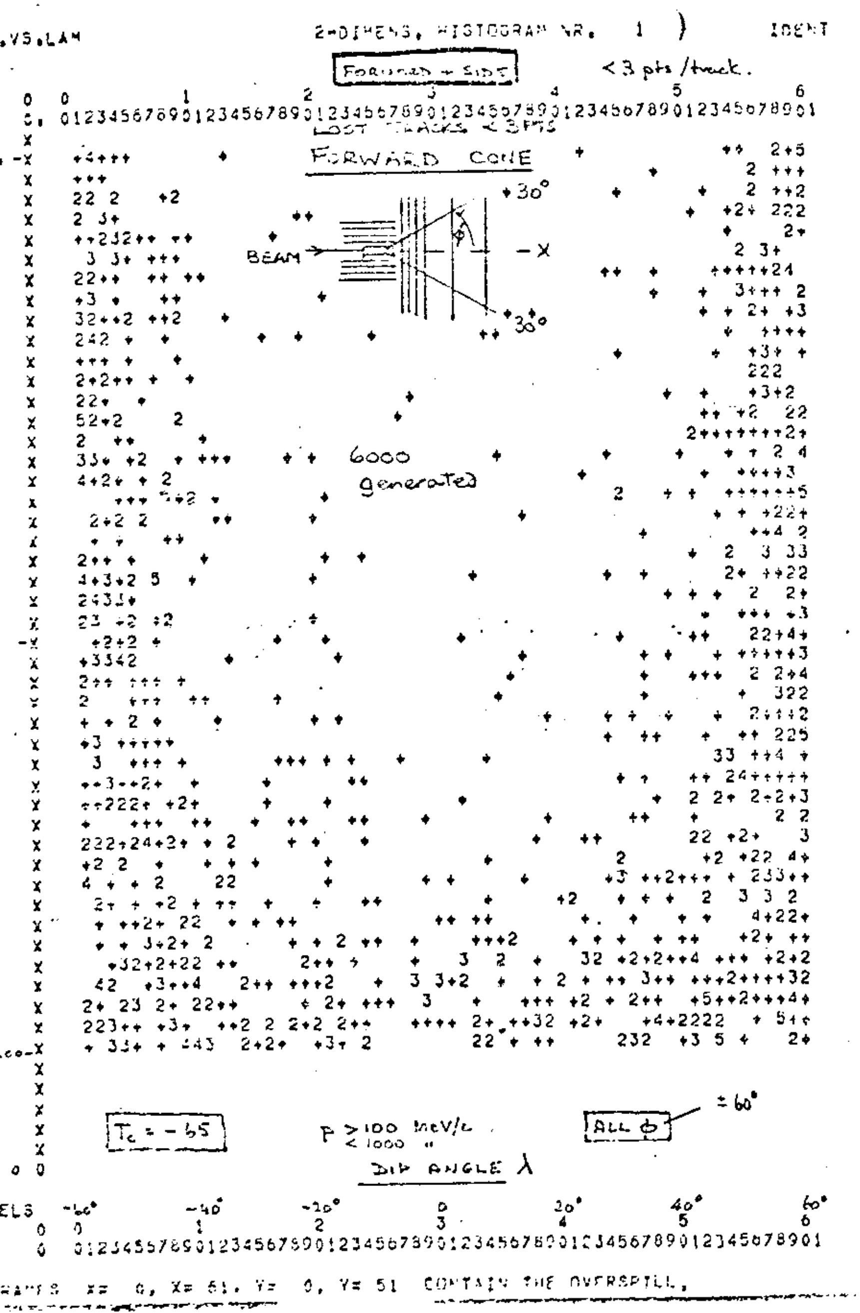
.VS.LAM
2-DIMENS, HISTOGRAM NR. 1
IDENT
FORWARD + SIDE
< 3 pts / track.
LOST TRACKS < 3PTS
FORWARD CONE
+30°
BEAM
φ
- X
-30°
6000 generated
Tc = - 65
P ≥ 100 MeV/c < 1000
DIP ANGLE λ
ALL φ
± 60°
-60°
-40°
-20°
0
20°
40°
60°
ELS
0 0 01234567890123456789012345678901234567890123456789012345678901
...ANNELS X= 0, X= 61, Y= 0, Y= 51 CONTAIN THE OVERSPILL,

FIG 5a

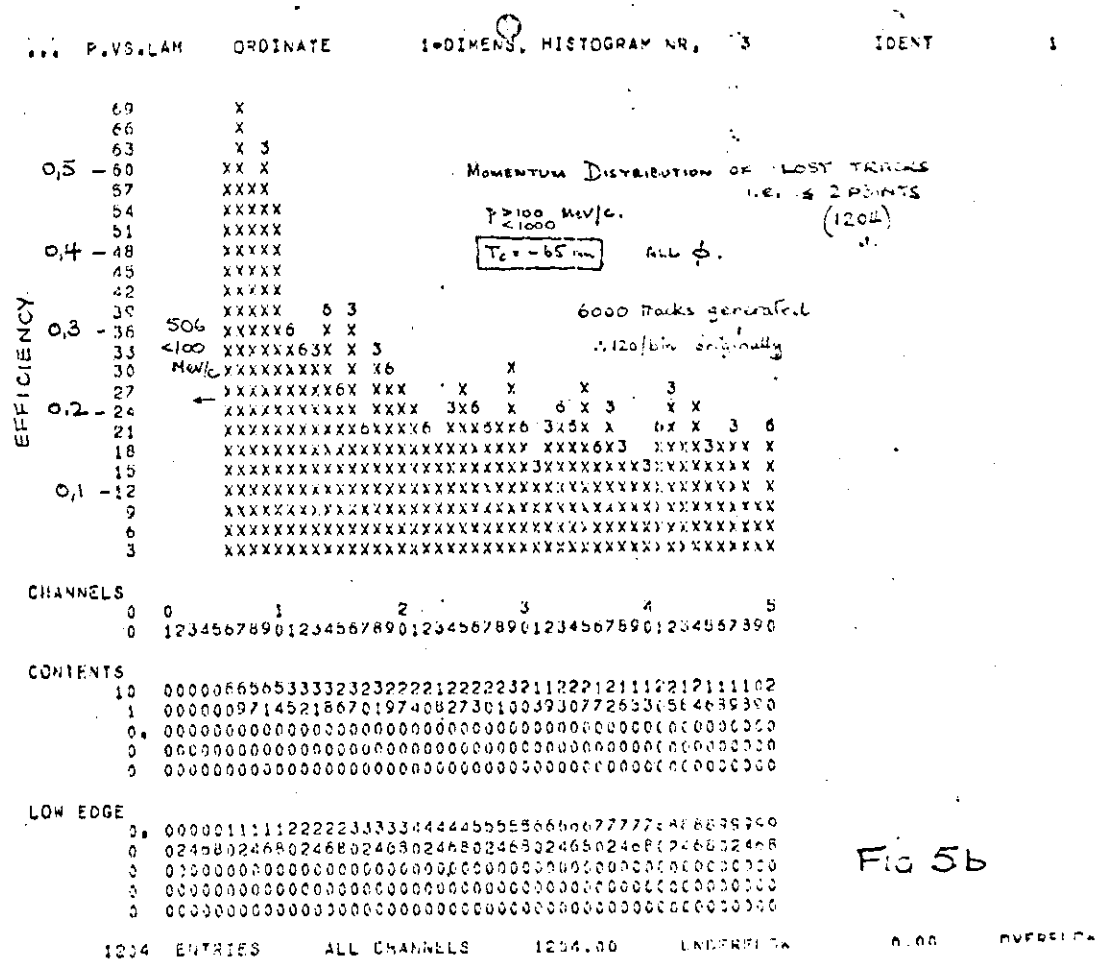
... P.VS.LAM
ORDINATE
1-DIMENS, HISTOGRAM NR, 3
IDENT 1
EFFICIENCY
0,5
0,4
0,3
0,2
0,1
506 <100 MeV/c
MOMENTUM DISTRIBUTION OF LOST TRACKS i.e. ≤ 2 POINTS (1204)
P ≥ 100 MeV/c < 1000
Tc = -65 mm
ALL φ.
6000 tracks generated
∴ 120/bin originally
CHANNELS
CONTENTS
LOW EDGE
1204 ENTRIES
ALL CHANNELS 1204.00
UNDERFLOW 0.00
OVERFLOW

Fig 5b

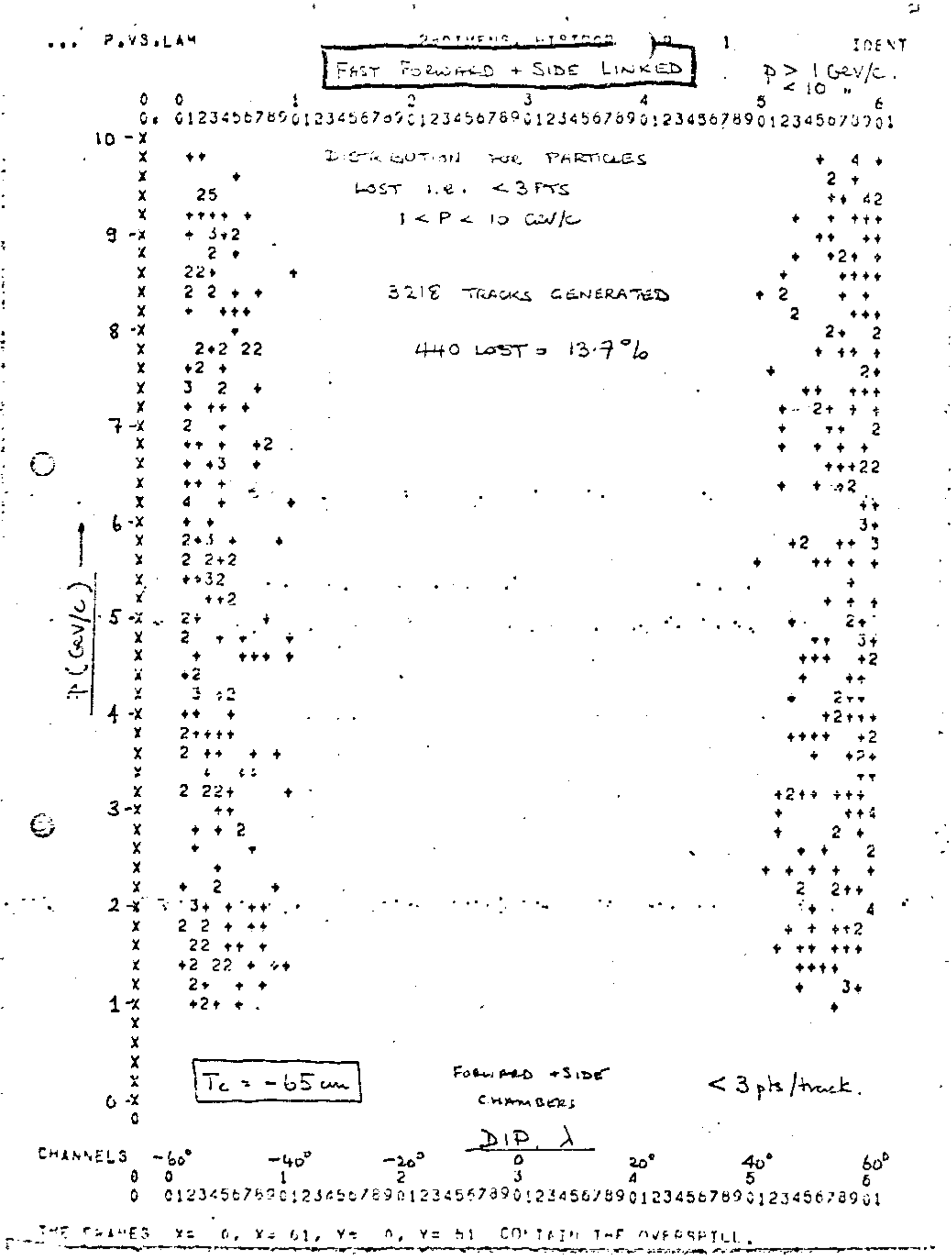

FIG 6

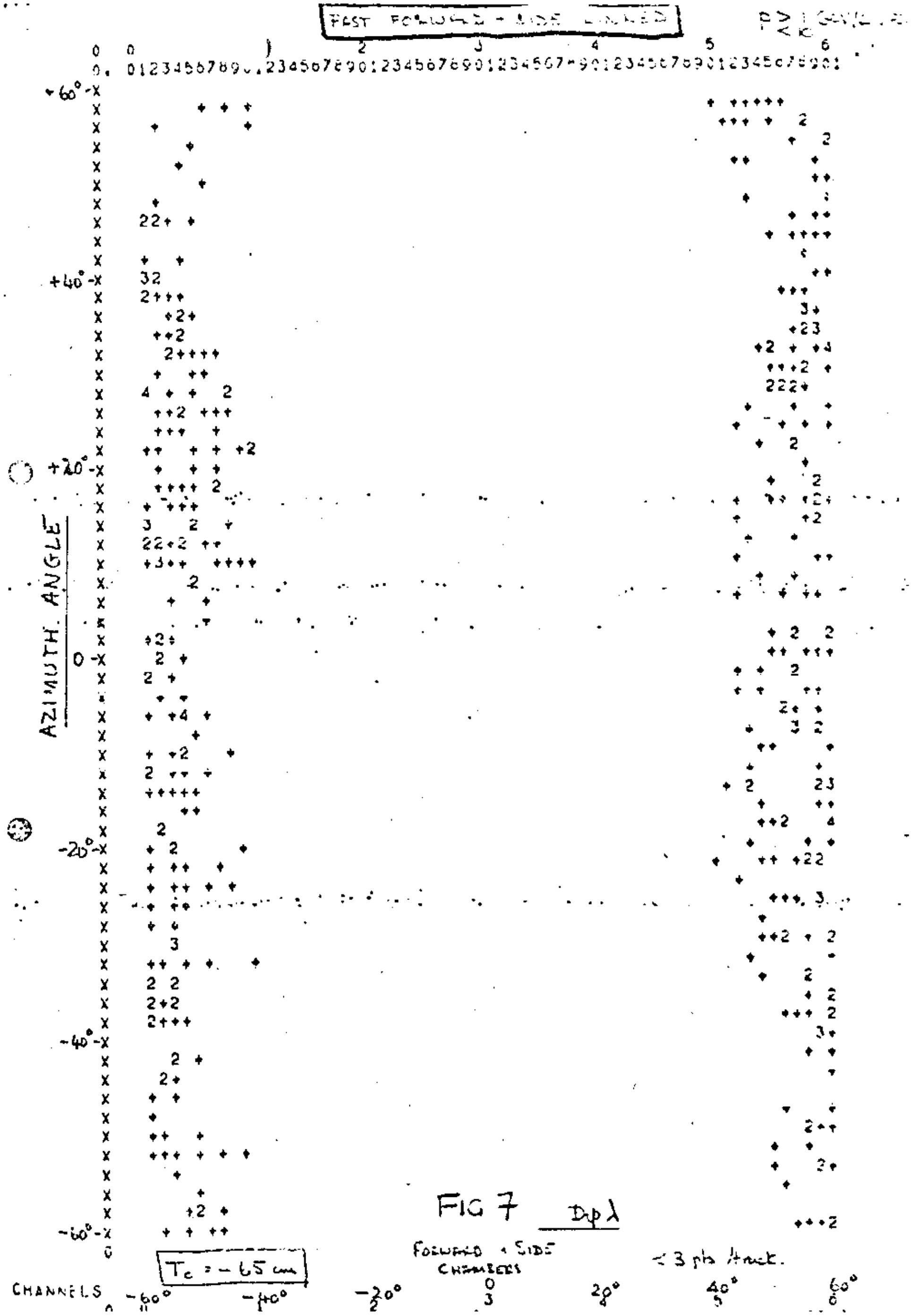

FIG 7 Dip λ

```
D5          1-DIMENS, HISTOGRAM NR,   5          IDENT          5          DATE   07/02/74
```

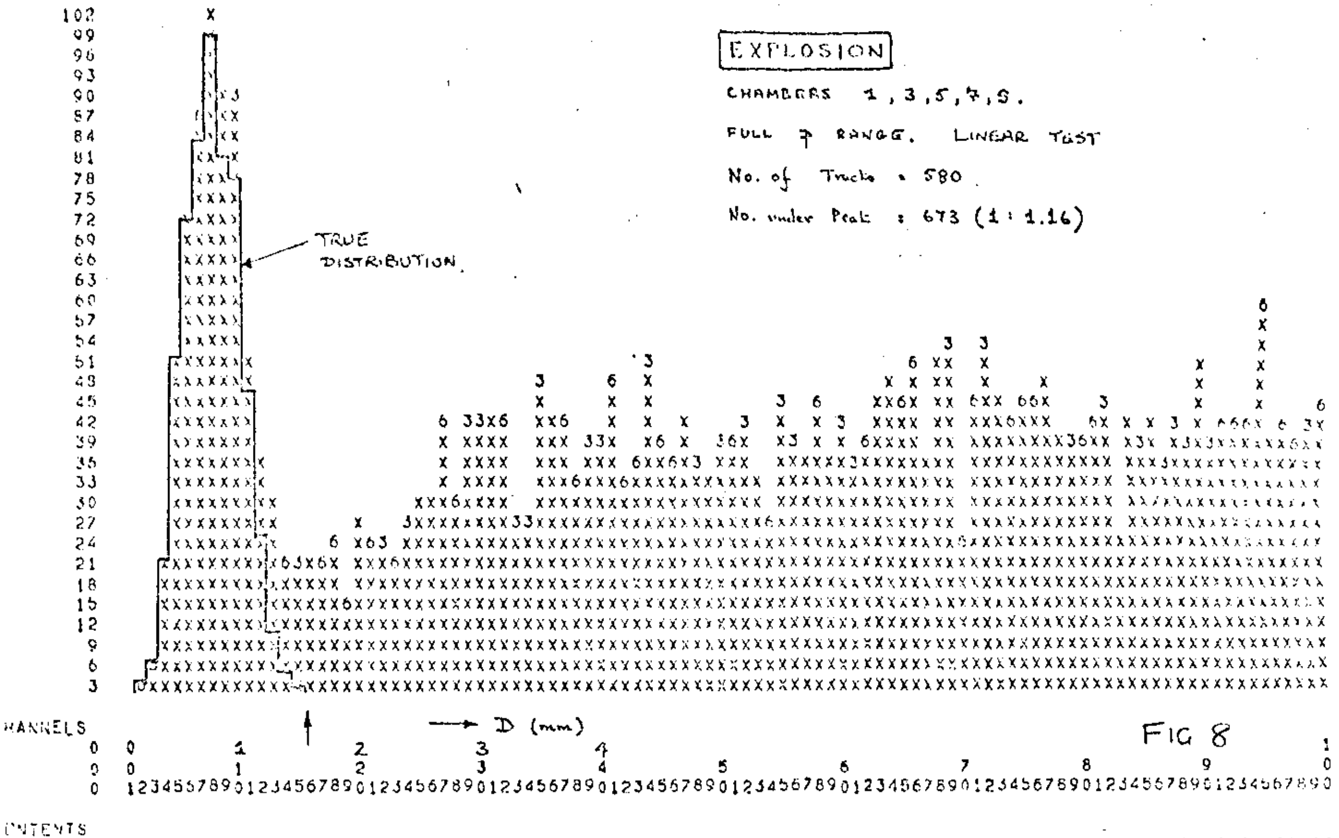

EXPLOSION

CHAMBERS 1, 3, 5, 7, 9.

FULL p RANGE. LINEAR TEST

No. of Tracks : 580

No. under Peak : 673 (1 : 1.16)

FIG 8

```
D1          1-DIMENS, HISTOGRAM NR,   1          IDENT          1          DATE   11/02/74
```

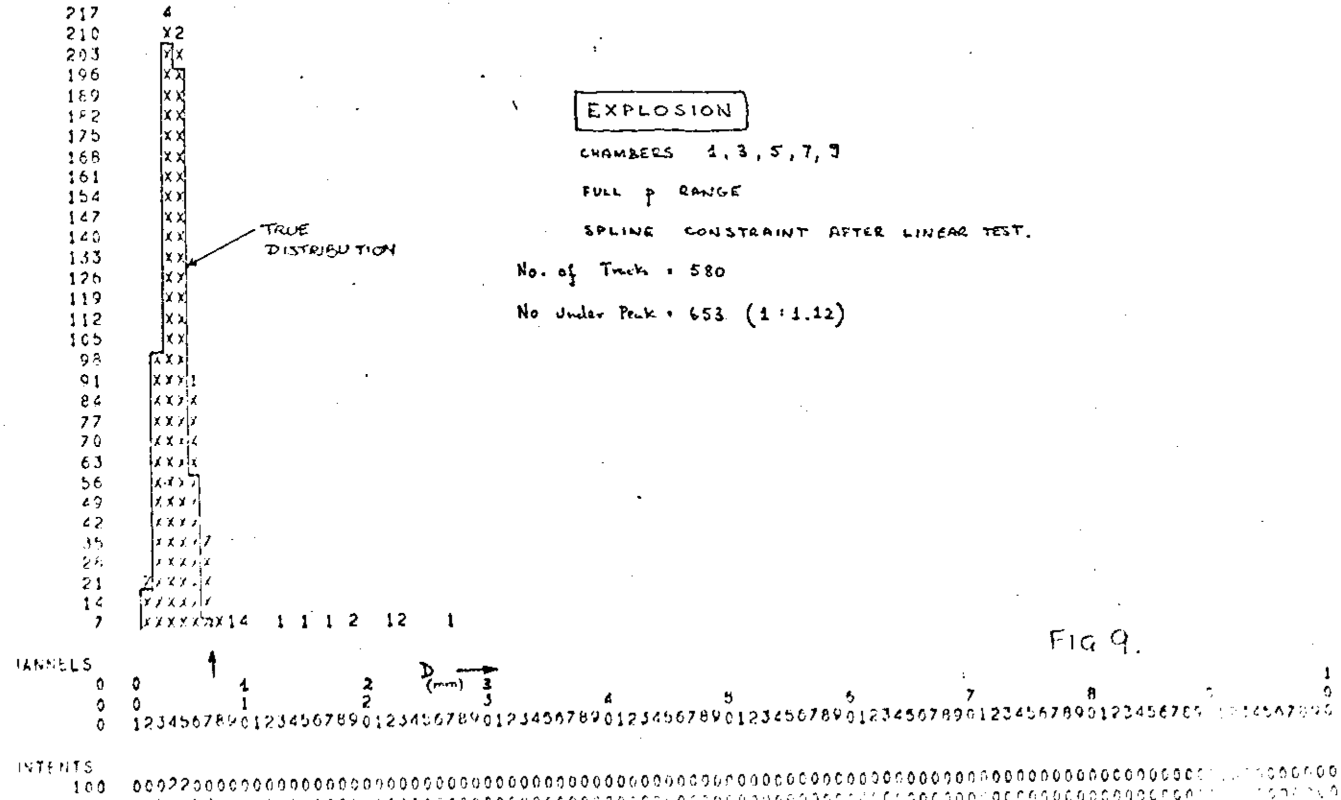

EXPLOSION

CHAMBERS 1, 3, 5, 7, 9

FULL p RANGE

SPLINE CONSTRAINT AFTER LINEAR TEST.

No. of Tracks : 580

No Under Peak : 653 (1 : 1.12)

FIG 9.

```
05            1-DIMENS HISTOGRAM NR.  5         IDENT   )  6          DATE  07/02/74
```

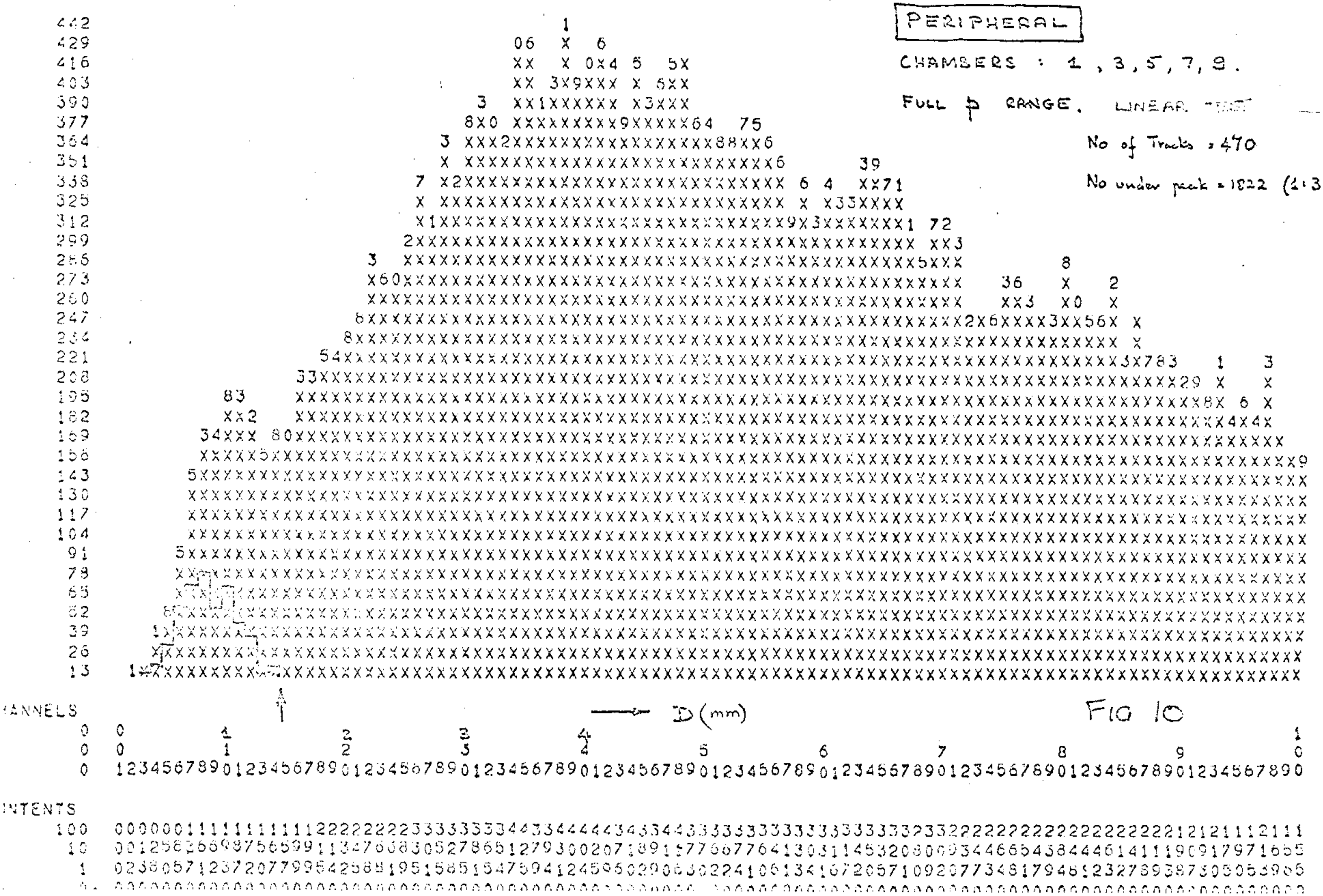

PERIPHERAL

CHAMBERS : 1, 3, 5, 7, 9.

FULL p RANGE. LINEAR

No of Tracks = 470

No under peak = 1822 (1:3.88)

FIG 10

```
,,   04          1-DIMENS, HISTOGRAM NR,   4          IDENT        4          DATE   11/02/74
```

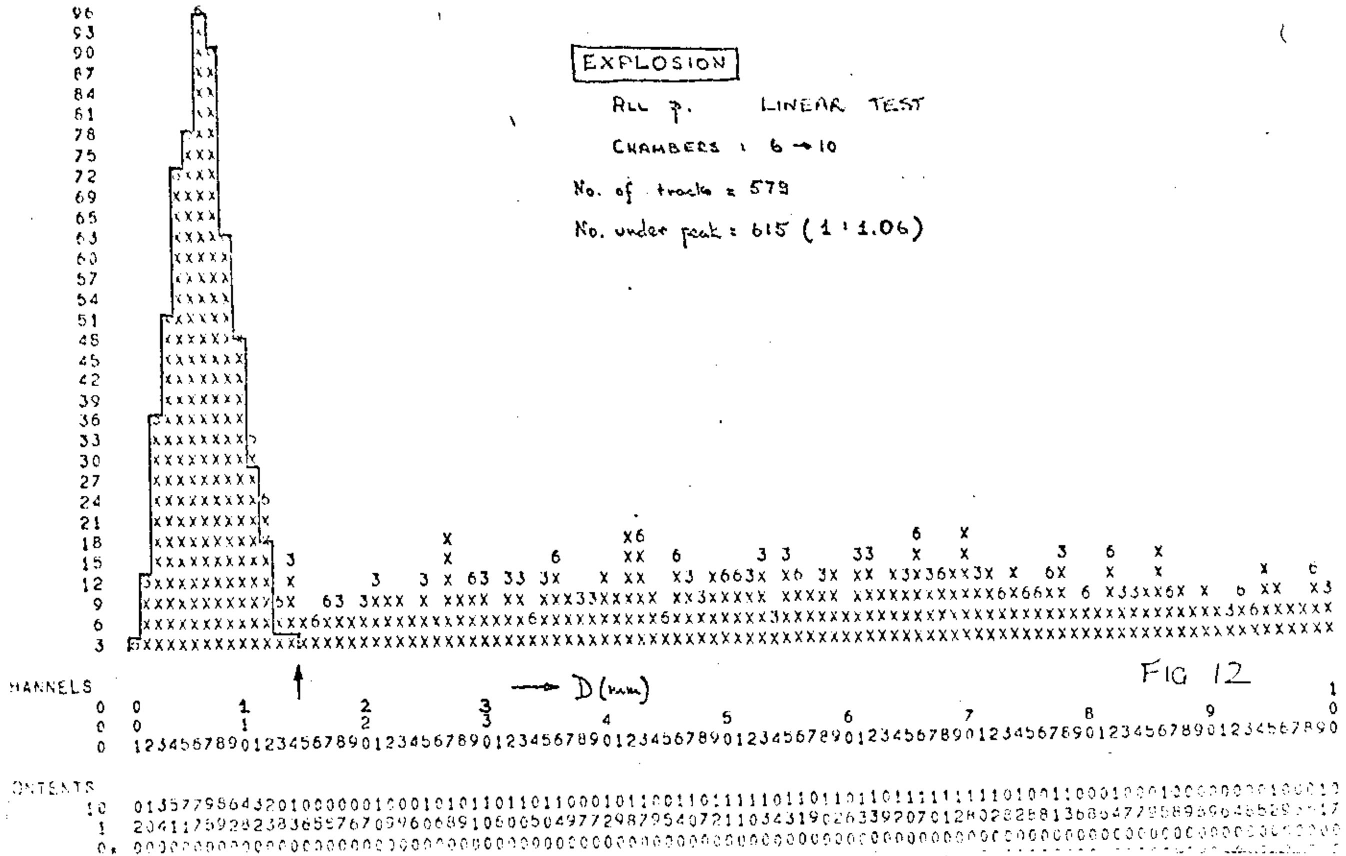

EXPLOSION

ALL p.   LINEAR TEST

CHAMBERS : 6 → 10

No. of tracks = 579

No. under peak = 615 (1 : 1.06)

FIG 12

```
,,   D1          1-DIMENS, HISTOGRAM NR,   1          IDENT        1          DATE   11/02/74
```

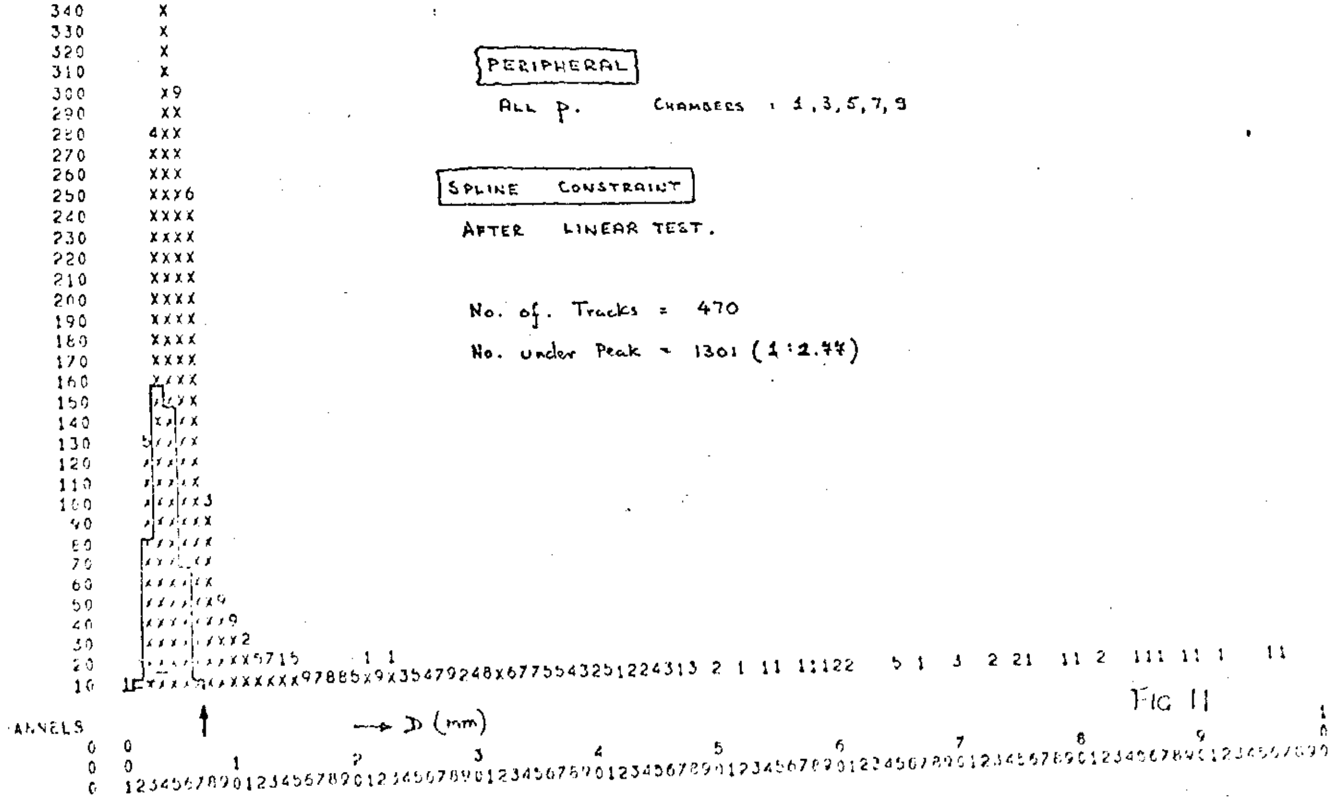

PERIPHERAL

ALL p.   CHAMBERS : 1, 3, 5, 7, 9

SPLINE CONSTRAINT

AFTER LINEAR TEST.

No. of. Tracks = 470

No. under Peak = 1301 (1 : 2.77)

FIG 11

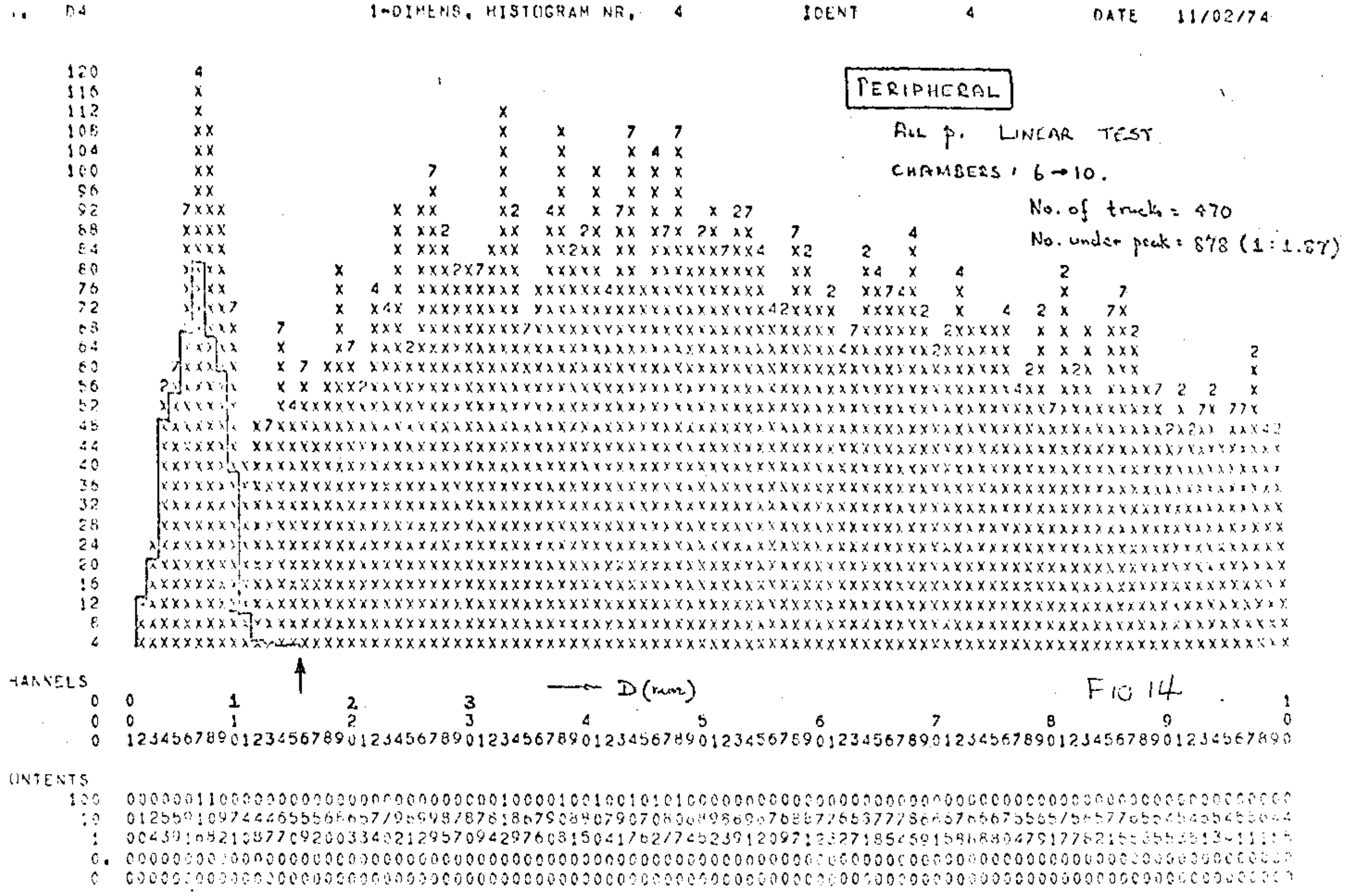

PERIPHERAL

All p. LINEAR TEST

CHAMBERS : 6 → 10.

No. of tracks = 470

No. under peak = 878 (1 : 1.87)

FIG 14

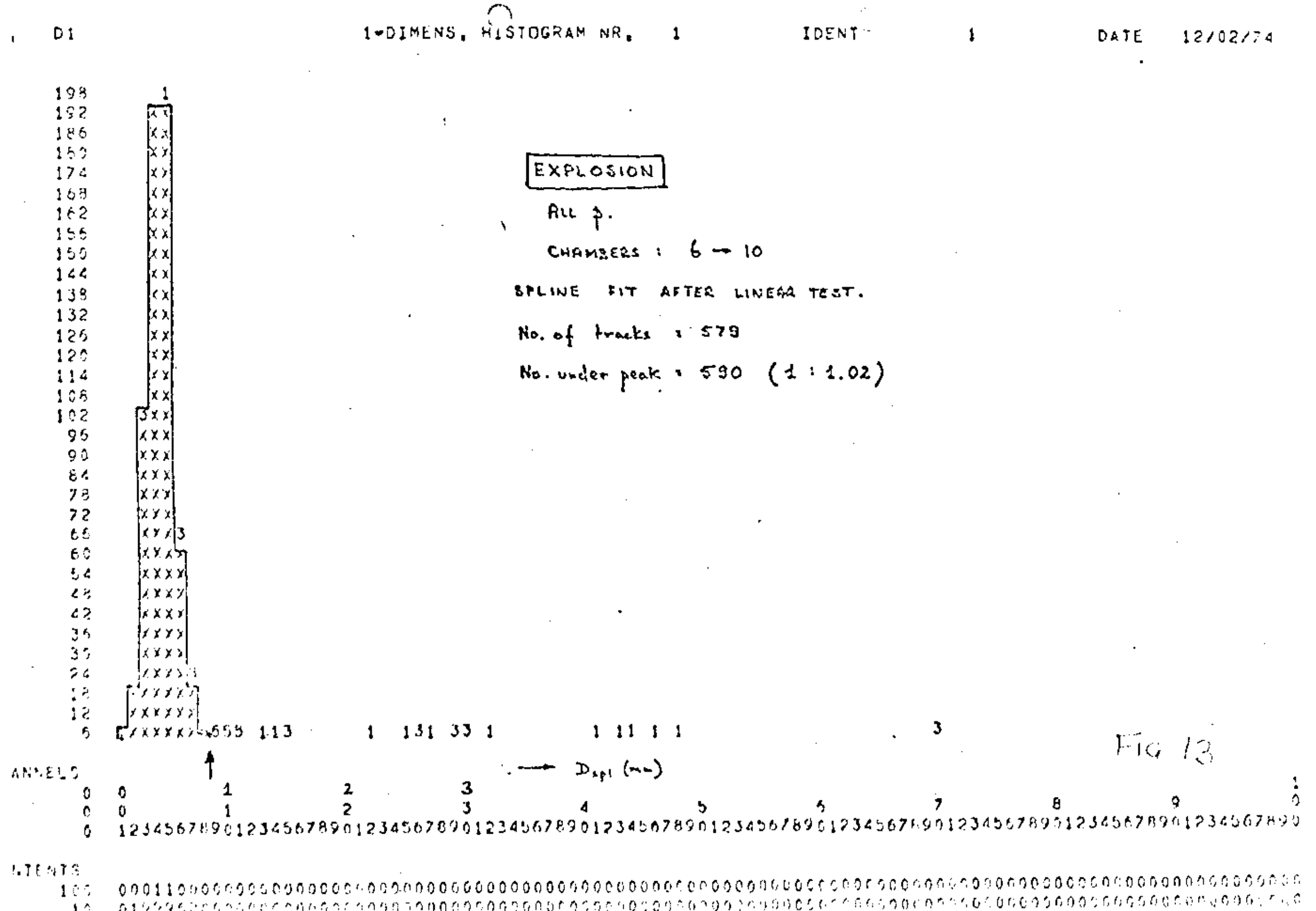

EXPLOSION

All p.

CHAMBERS : 6 → 10

SPLINE FIT AFTER LINEAR TEST.

No. of tracks : 579

No. under peak : 590 (1 : 1.02)

Fig 13

D3 1-DIMENS. HISTOGRAM NR. 3 IDENT 3 DATE 20/02/74

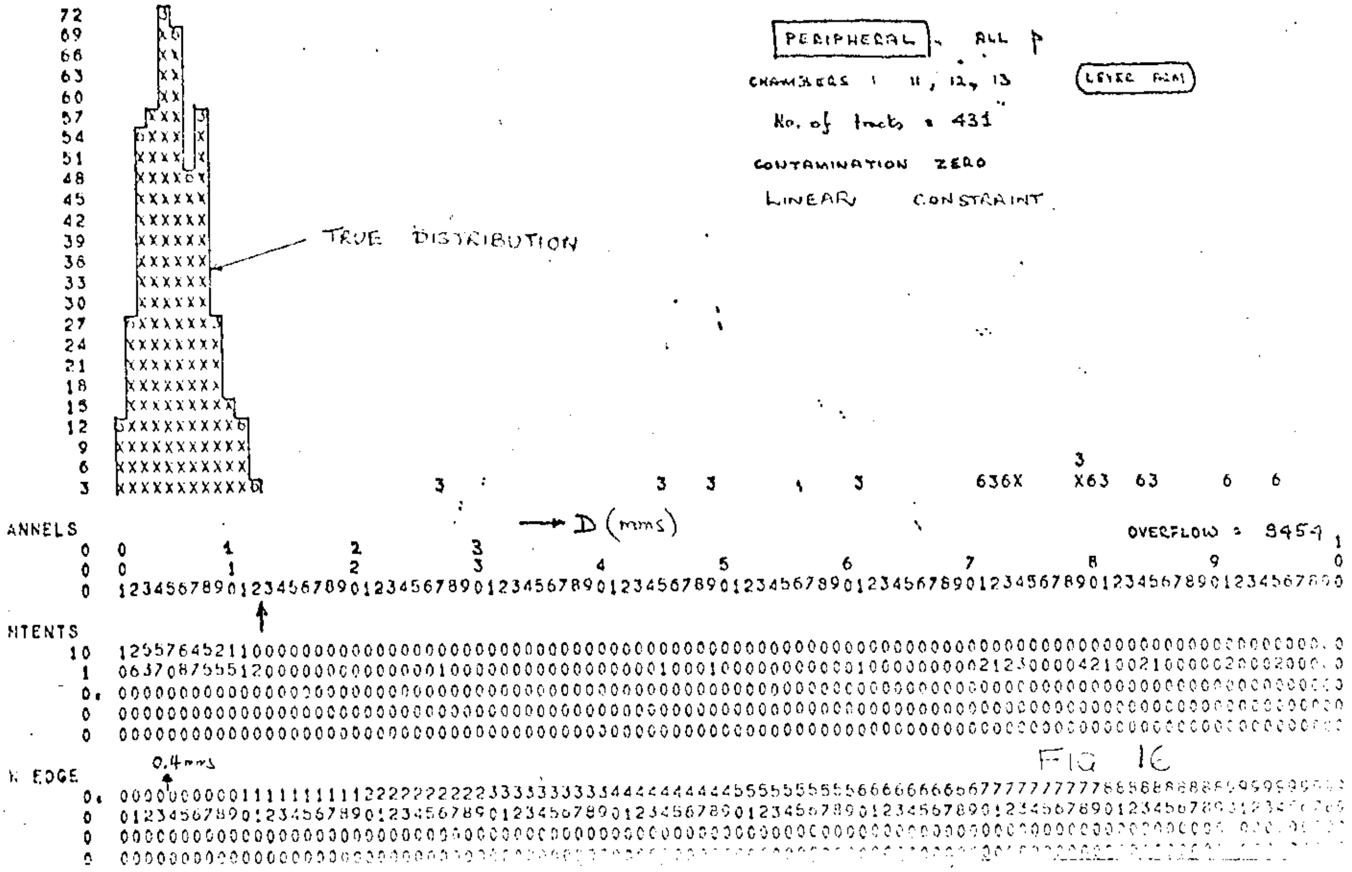

PERIPHERAL, ALL p

CHAMBERS : 11, 12, 13

LEVER ARM

No. of tracks = 431

CONTAMINATION ZERO

LINEAR CONSTRAINT

FIG 16

D1 1-DIMENS. HISTOGRAM NR. 1 IDENT 1 DATE 12/02/74

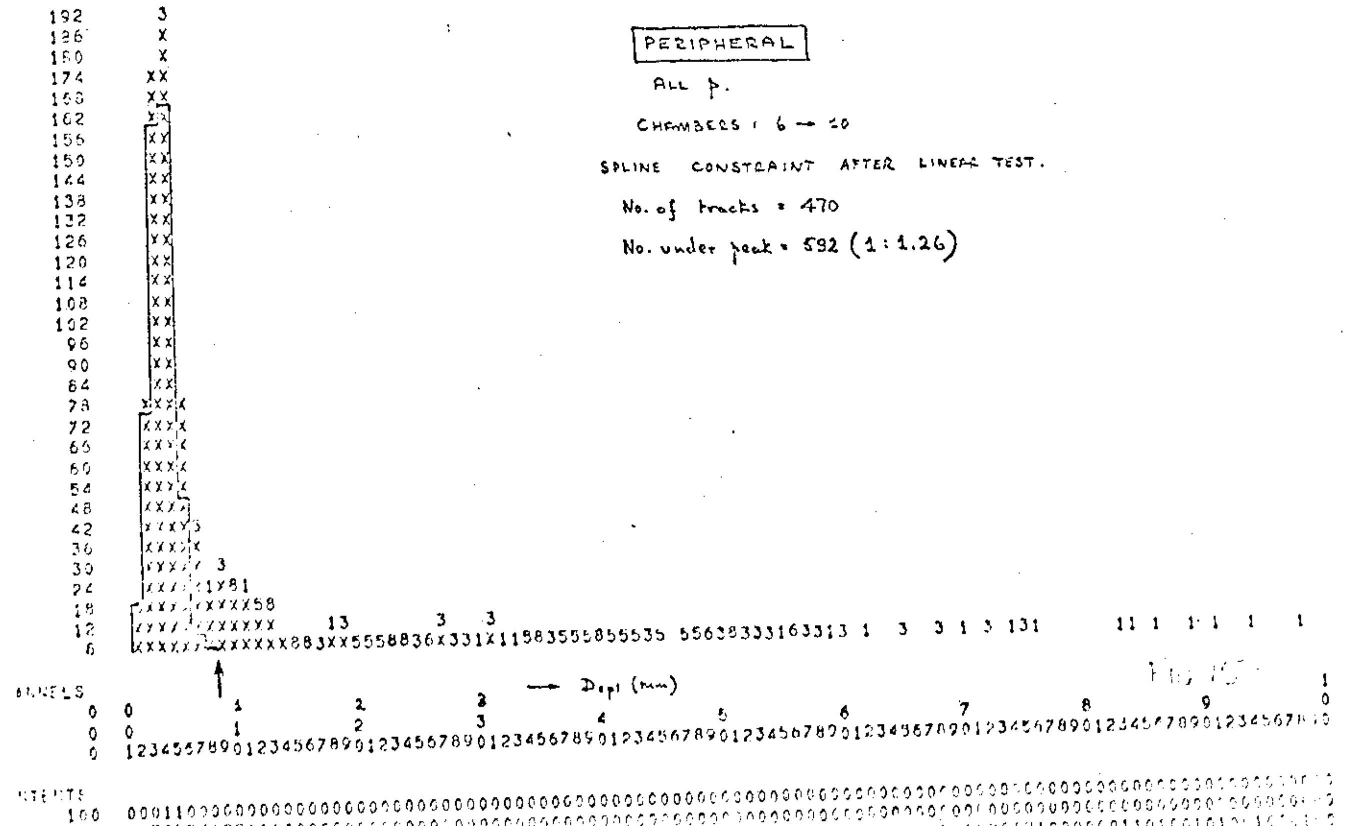

PERIPHERAL

ALL p.

CHAMBERS : 6 → 10

SPLINE CONSTRAINT AFTER LINEAR TEST.

No. of tracks = 470

No. under peak = 592 (1:1.26)

Fig 15

```
,  D5                    1-DIMENS, HISTOGRAM NR,   5          IDENT          5            DATE   05/02/74

   62        4
   60        X
   58        XXX
   56        XXX
   54        XXX
   52        XXX
   50        XXX
   48       XXXX
   46       XXXX
   44       XXXX
   42       XXXX
   40      XXXXXX
   38      XXXXXX
   36      XXXXXX
   34      XXXXXX
   32      XXXXXX
   30      XXXXXX4
   28      XXXXXXX
   26     4XXXXXXX
   24     XXXXXXXX
   22     XXXXXXXX
   20     XXXXXXXX
   18     XXXXXXXX
   16     XXXXXXXX
   14     XXXXXXXX
   12     XXXXXXXX
   10    XXXXXXXXXX
    8   4XXXXXXXXXX         X         44                X                                         4
    6   XXXXXXXXXXX         X4 4 44   XX XXX      4     X               4   4                 4 4     XX
    4   XXXXXXXXXXX   444 XX X XXXXXX XXXXXX4 XXX   X XXX44XX4    XX   X X             4  XXXXXX4   XX X 4X
    2   XXXXXXXXXXXXXXXXX XXXXXXXXXX4XXXXXXX XXX44X4XXXXXXXXX4 4XXXXXXXXXXX4X4X44X44XXXXXXXX44XXXX XXX4X444
ANNELS
    0   0         1         2         3         4                                                       1
    0   0         1         2         3         4         5         6         7         8         9         0
    0   1234567890123456789012345678901234567890123456789012345678901234567890123456789012345678901234567890
NTENTS
   10   0001244655421000000000000000000000000000000000000000000000000000000000000000000000000000000000000000
    1   0070500158090222333065252554477156644430456411014443344310154225242222121211311454544311762[illegible]
   0.   0000000000000000000000000000000000000000000000000000000000000000000000000000000000000000000[illegible]
    0   0000000000000000000000000000000000000000000000000000000000000000000000000000000000000000000[illegible]
```

EXPLOSION

0 ≤ p ≤ 10 GeV/c ; ≥ 5 pts/track.

ALL PTS ON TRACKS > 10 GeV/c REMOVED

No. of tracks = 381

No. under peak = 390 (1 : 1.02)

→ D₄ (mm)

↑ limit of true tracks

Fig 17

```
,  D1                    1-DIMENS, HISTOGRAM NR,   1          IDENT          1            DATE   06/02/74

  124      2
  120      X
  116     7X
  112     XX
  108     XX
  104     XX
  100     XX
   96     XX
   92     XX
   88     XX
   84     XX
   80     XX
   76     XX
   72     XX
   68     XX
   64     XX
   60    2XX
   56    XXXX
   52    XXXX
   48    XXXX
   44    XXXX
   40    XXXX
   36    XXXX
   32    XXXX
   28    XXXX
   24    XXXX
   20    XXXX
   16    XXXX
   12   7XXXX7
    8   XXXXXX2
    4   XXXXXXX2 24     22 2        2                   2 2  2                                        2
ANNELS
    0   0         1         2         3         4                                                       1
    0   0         1         2         3         4         5         6         7         8         9         0
    0   1234567890123456789012345678901234567890123456789012345678901234567890123456789012345678901234567890
NTENTS
  100   0001100000000000000000000000000000000000000000000000000000000000000000000000000000000000000000000000
   10   0151251000000000000000000000000000000000000000000000000000000000000000000000000000[illegible]
```

EXPLOSION

0 ≤ p ≤ 10 GeV/c ; ≥ 5 pts/trk.

SPLINE AFTER LINEAR TEST

1% BACKGROUND

→ D (mm)

↑ limit of true tracks

Fig 18

```
D1                     1-DIMENS, HISTOGRAM NR,    1          IDENT          1          DATE   06/02/74
```

PERIPHERAL   0 ≤ p ≤ 10 Gev/c.   ≥5 PTS/TRACK.

SPLINE CONSTRAINT AFTER LINEAR TEST

2% BACKGROUND

```
  90       3
  87       X
  84       X
  81       X
  78       X
  75       XX
  72       XX
  69       XX
  66       XX
  63       XX
  60       XX
  57       XX
  54       XX
  51       XX
  48      6XX
  45      XXX
  42      XXX
  39      XXX
  36      XXX
  33      XXX
  30      XXX3
  27      XXXX
  24      XXXX
  21      XXXX
  18      XXXX
  15      XXXX
  12     6XXXX
   9     XXXXX
   6     XXXXXX     3
   3     XXXXXX6 36 X36 3 3 6 363333           3     3    3
```

D →

```
ANNELS
   0    0        1         2         3                                                                     1
   0    0        1         2         3         4         5         6         7         8         9         0
   0    1234567890123456789012345678901234567890123456789012345678901234567890123456789012345678901234567890

NTENTS
  10    0148720000000000000000000000000000000000000000000000000000000000000000000000000000000000000000000000
   1    0179556201204120101020121111000000000000100000100001000000000000000000000000000000000000000000000000
  0.    0000000000000000000000000000000000000000000000000000000000000000000000000000000000000000000000000000
   0    0000000000000000000000000000000000000000000000000000000000000000000000000000000000000000000000000000
   0    0000000000000000000000000000000000000000000000000000000000000000000000000000000000000000000000000000
```

Fig 20

```
D4                     1-DIMENS, HISTOGRAM NR,    4          IDENT          4          DATE   05/02/74
```

PERIPHERAL

0 ≤ p ≤ 10 Gev/c ; ≥5 pts/track.

No. of tracks = 263

No. under peak = 280 (1 : 1.06)

```
  44          4
  42          X
  40          X
  38          X
  36         XXX4
  34         XXXX
  32         XXXX
  30        XXXXX
  28        XXXXX4
  26        XXXXXX
  24        XXXXXX
  22        XXXXXX
  20       4XXXXXX
  18       XXXXXXX
  16       XXXXXXXX
  14       XXXXXXXX
  12       XXXXXXXX4                         4
  10      4XXXXXXXXX              4X X X     X                                     4
   8      XXXXXXXXXX 4 X     4  4 XX X X     X           4 4                       X
   6      XXXXXXXXXX X X   44X4 XXXX X XX    X X X 4    XX X  X4 4X4     X4 X      X X  4       X4  4  4  4
   4     XXXXXXXXXXXXX4XX  XXXX XXXXXXXXXX 44X XXXXXXX4XXX XXXXX XXX 4XXXXX X44 4XXX X4 X 444 4XXX 4X  X 4XX
   2     XXXXXXXXXXXXXXXXX4XXXXXXXXXXXXXXX4XXXXXXXXXXXXXXX4XXXXXXXXXXXXXXXXXXXXXXXXXXXXXX XXXXXXXXXXXXXX4XXX
```

→ D (mm)

```
ANNELS
   0    0        1         2         3         4                                                           1
   0    0        1         2         3         4         5         6         7         8         9         0
   0    1234567890123456789012345678901234567890123456789012345678901234567890123456789012345678901234567890

NTENTS
  10    0001334332110000000000000000010101000001000000000000000000000000000000000000000000000000000000000000
   1    0499063657614738421557527699404064133126464544346717446525652344465263323449263256333534652152251354
  0.    0000000000000000000000000000000000000000000000000000000000000000000000000000000000000000000000000000
   0    0000000000000000000000000000000000000000000000000000000000000000000000000000000000000000000000000000
   0    0000000000000000000000000000000000000000000000000000000000000000000000000000000000000000000000000000
```

Fig 19

```
W EDGE
  0.    0000000000111111111122222222223333333333444444444455555555556666666666777777777788888888889999999999
   0    0123456789012345678901234567890123456789012345678901234567890123456789012345678901234567890123456789
   0    0000000000000000000000000000000000000000000000000000000000000000000000000000000000000000000000000000
   0    0000000000000000000000000000000000000000000000000000000000000000000000000000000000000000000000000000
   0    0000000000000000000000000000000000000000000000000000000000000000000000000000000000000000000000000000
```

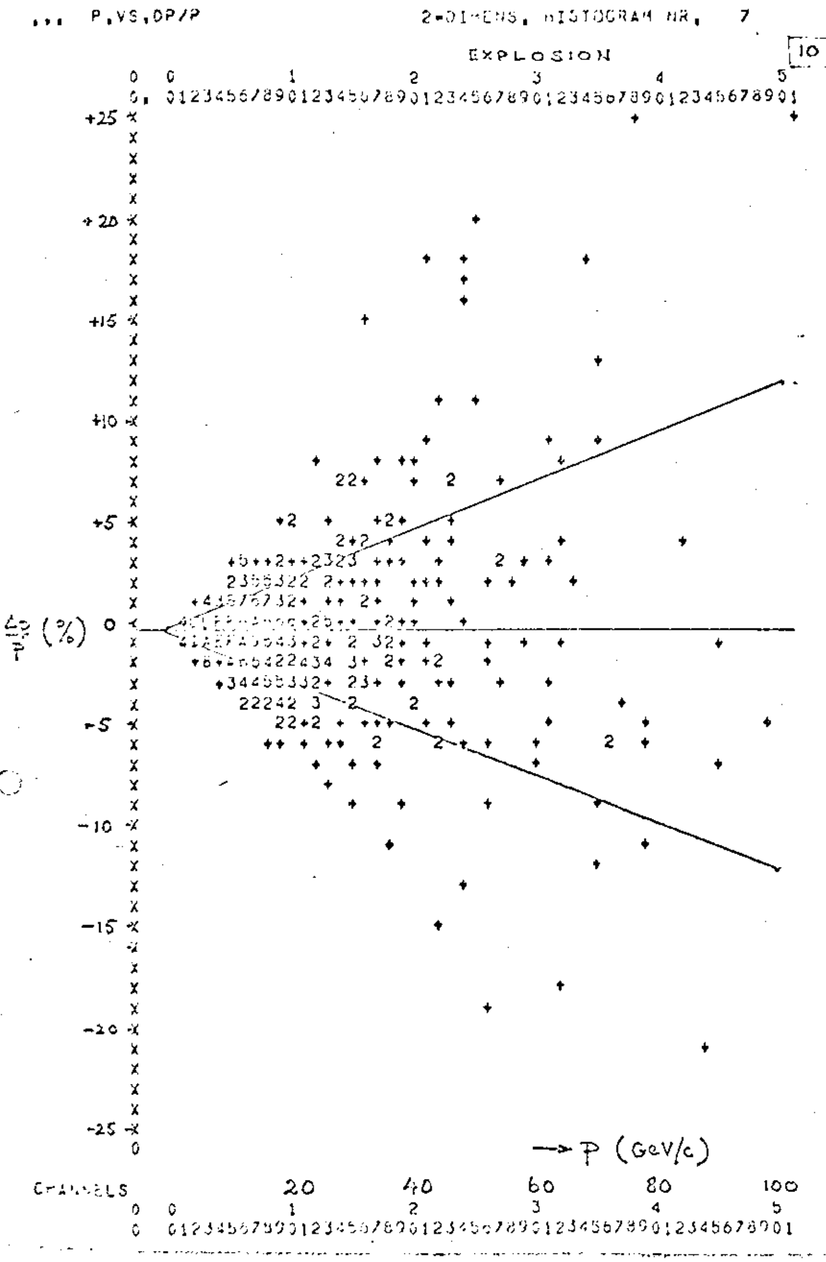
... P,VS,DP/P
2-DIMENS, HISTOGRAM NR, 7
IDENT
EXPLOSION
10 PLANES
$\frac{\Delta p}{p}$ (%)
+25
+20
+15
+10
+5
0
-5
-10
-15
-20
-25
CHANNELS
→ P (GeV/c)
20
40
60
80
100

FIG 21

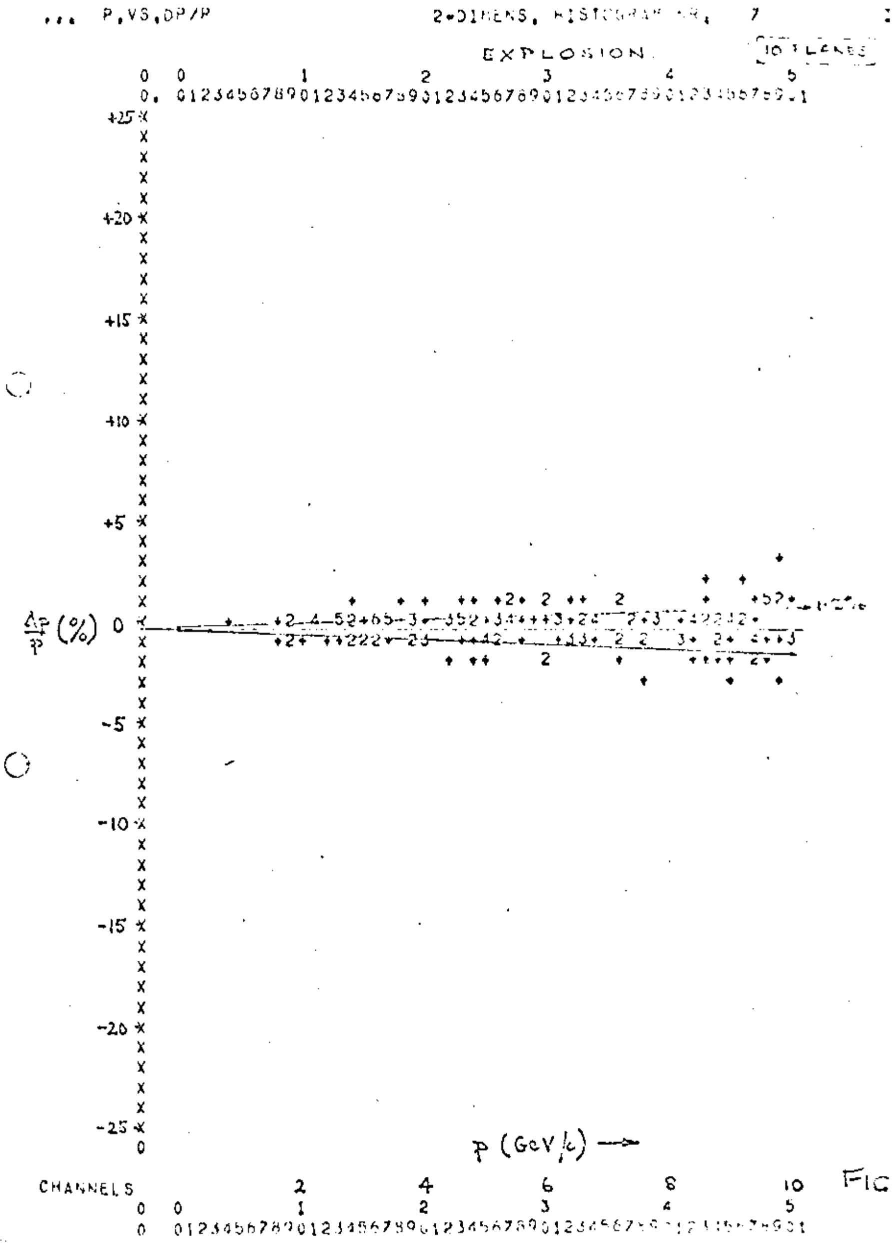
... P,VS,DP/P
2-DIMENS, HISTOGRAM NR, 7
IDENT
EXPLOSION
10 PLANES
$\frac{\Delta p}{p}$ (%)
+25
+20
+15
+10
+5
0
-5
-10
-15
-20
-25
CHANNELS
P (GeV/c) →
2
4
6
8
10

FIG 22

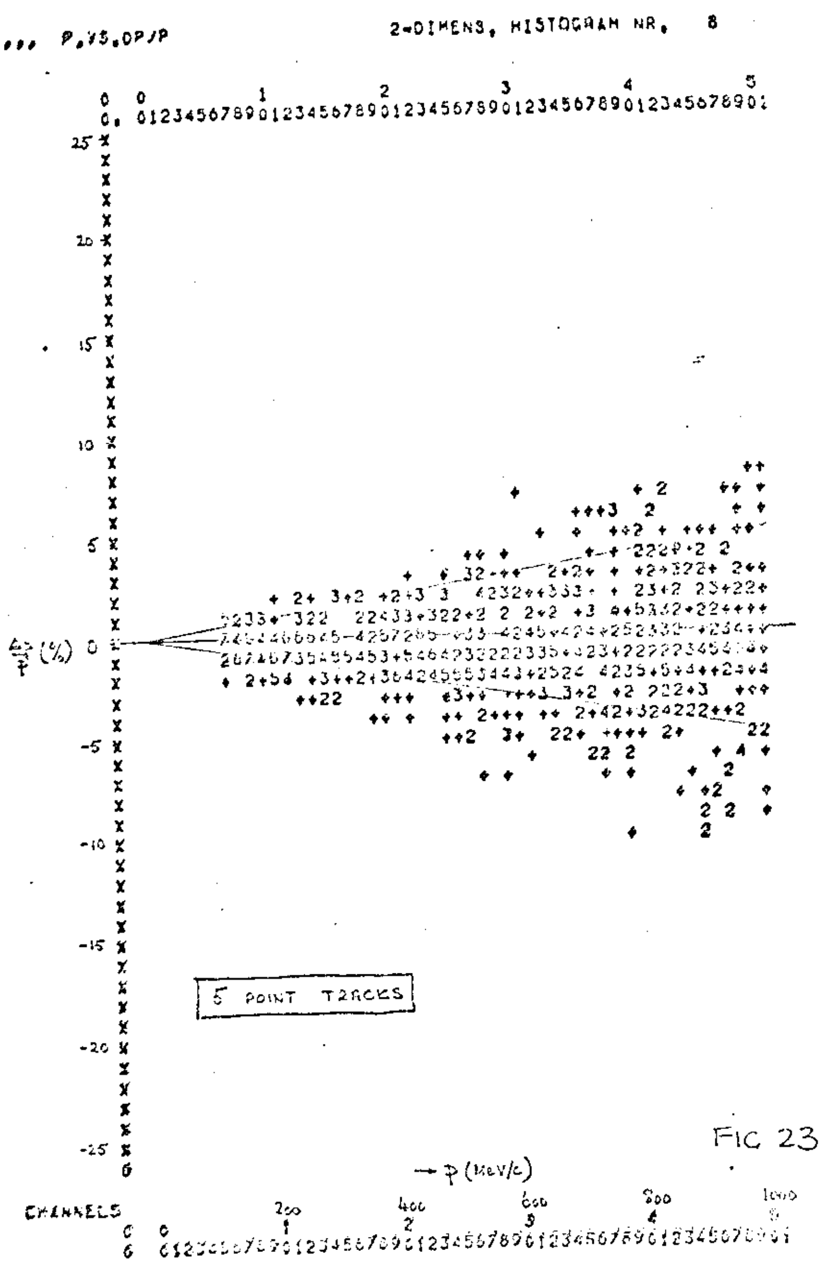
*** P,VS,DP/P
2-DIMENS, HISTOGRAM NR. 8
Δp/p (%)
25
20
15
10
5
0
-5
-10
-15
-20
-25
5 POINT TRACKS
→ p (MeV/c)
CHANNELS
200
400
600
800
1000

FIG 23

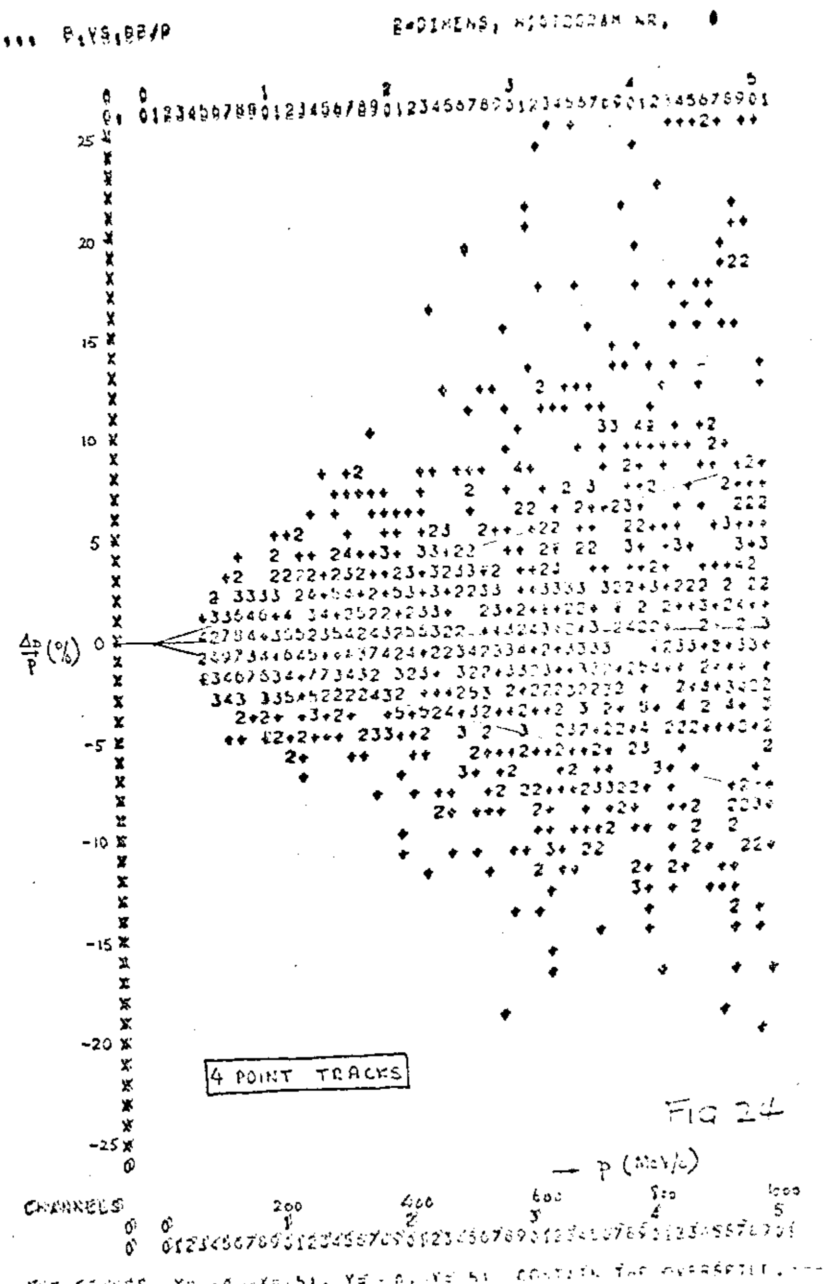
*** P,VS,DP/P
2-DIMENS, HISTOGRAM NR.
Δp/p (%)
25
20
15
10
5
0
-5
-10
-15
-20
-25
4 POINT TRACKS
→ p (MeV/c)
CHANNELS
200
400
600
800
1000

FIG 24

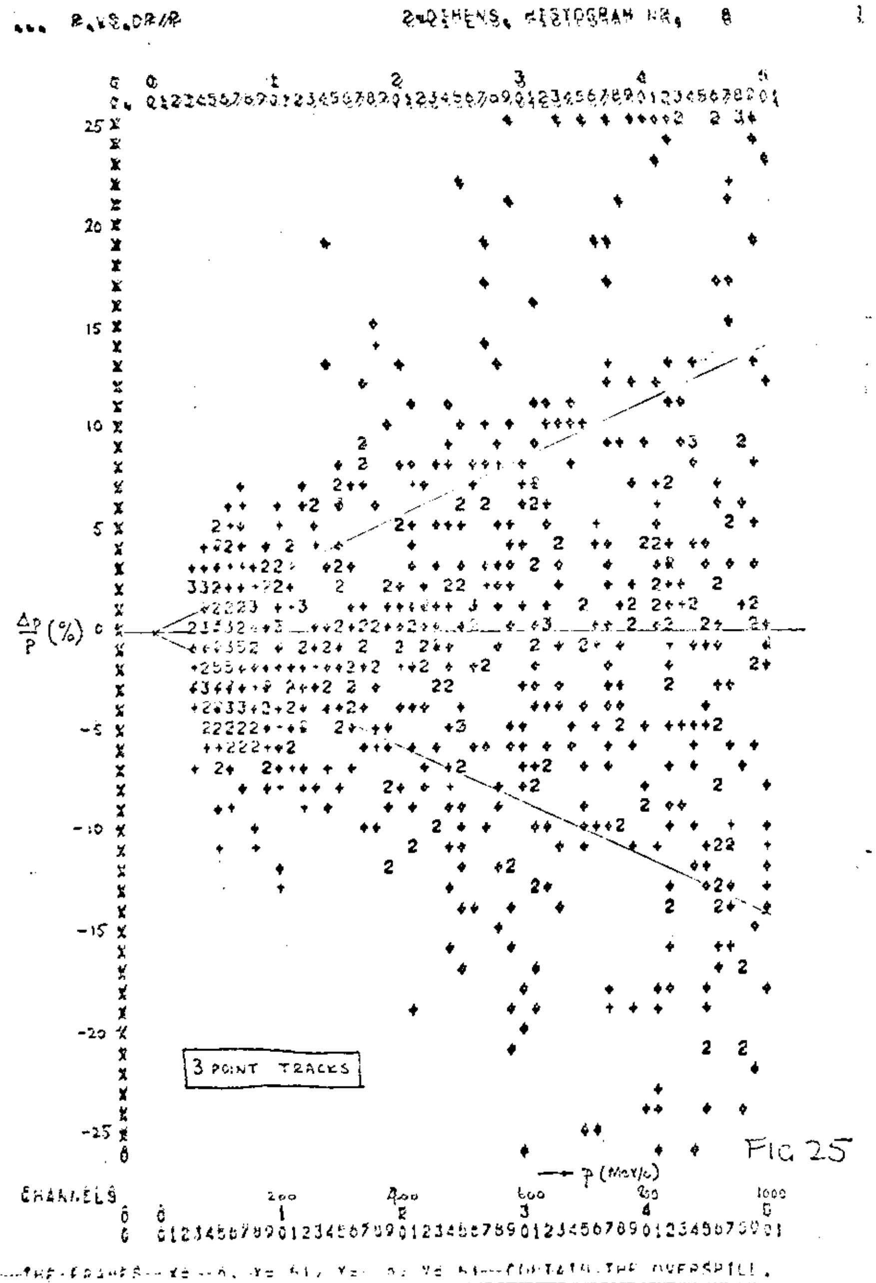
*** P,VS,DP/P
2-DIMENS, HISTOGRAM NR, 8
$\frac{\Delta p}{p}$ (%)
25
20
15
10
5
0
-5
-10
-15
-20
-25
3 POINT TRACKS
CHANNELS
200
400
600
800
1000
→ p (MeV/c)
THE FRAMES X= 0, X= 61, Y= 0, Y= 61 CONTAIN THE OVERSPILL.

FIG 25

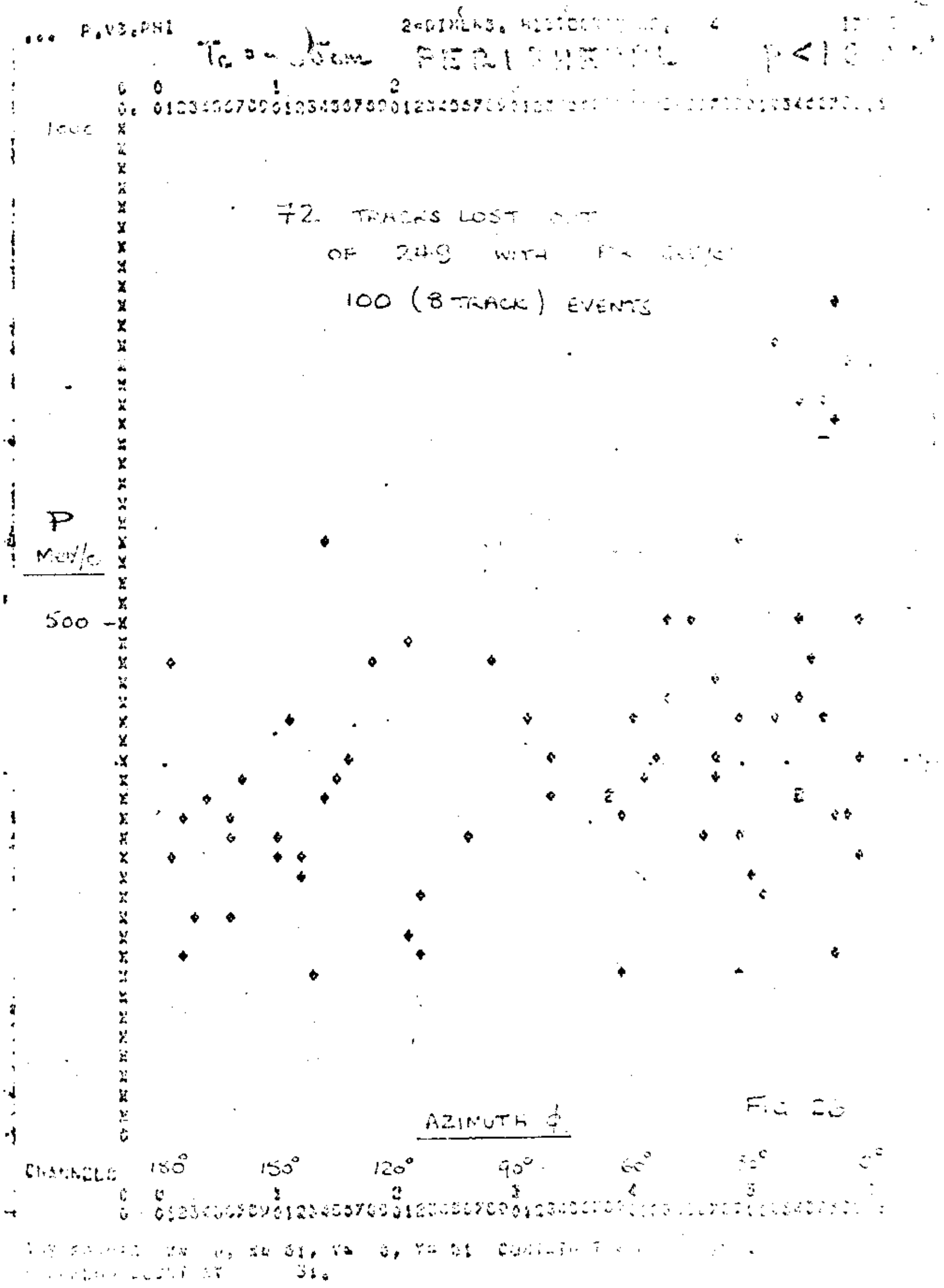
*** P,VS,PHI
2-DIMENS, HISTOGRAM NR, 4
PERIPHERAL
p < 1
1000
P MeV/c
500
#2. TRACKS LOST
OF 289 WITH
100 (8 TRACK) EVENTS
AZIMUTH ϕ
CHANNELS
180°
150°
120°
90°
60°
30°
0°

FIG 26

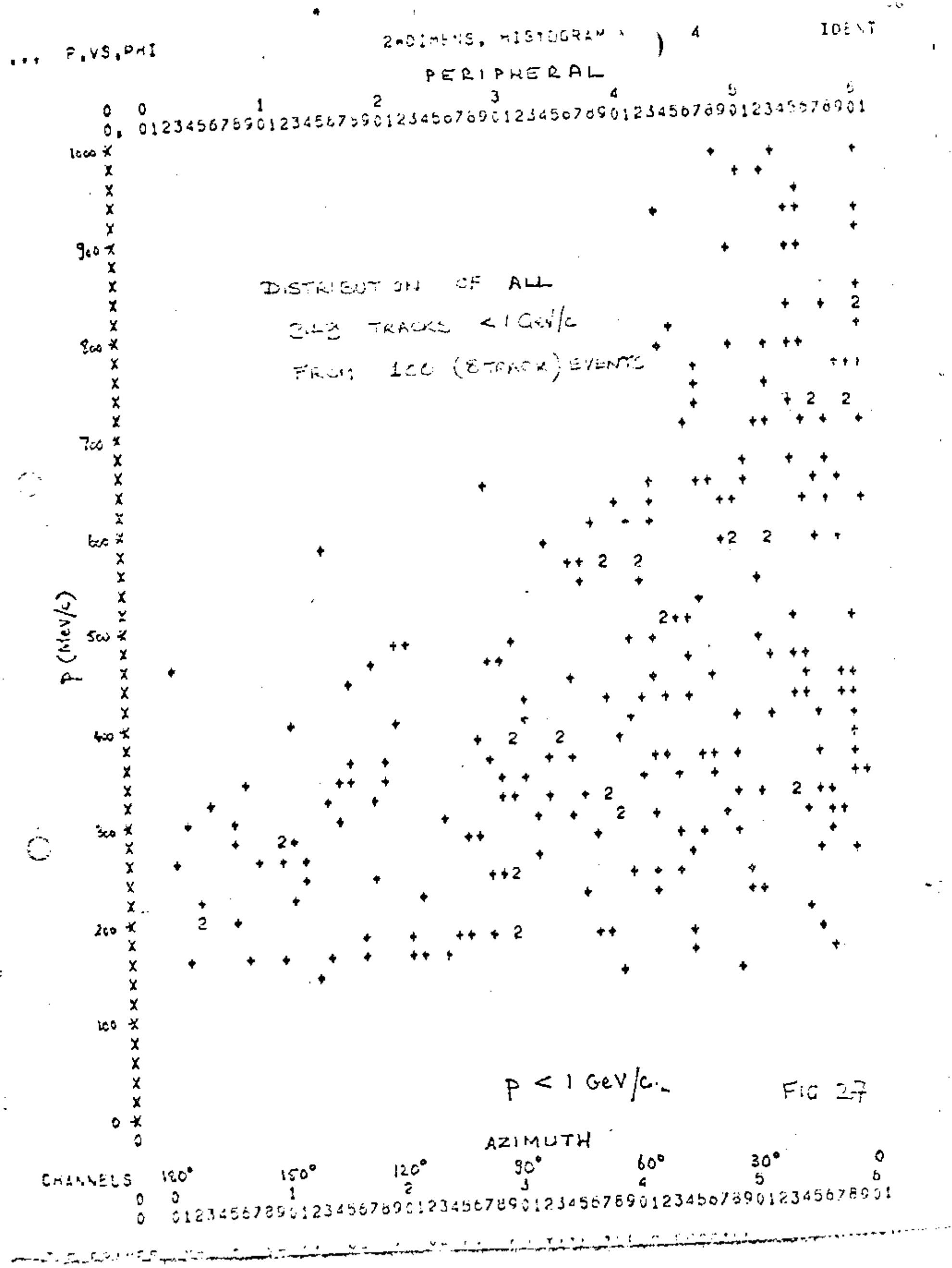
P,VS,PHI
2-DIMENS, HISTOGRAM
IDENT
PERIPHERAL
DISTRIBUTION OF ALL
348 TRACKS < 1 GeV/c
FROM 100 (8 TRACK) EVENTS
P (MeV/c)
1000
900
800
700
600
500
400
300
200
100
0
AZIMUTH
CHANNELS
180°
150°
120°
90°
60°
30°
0
P < 1 GeV/c

Fig 27

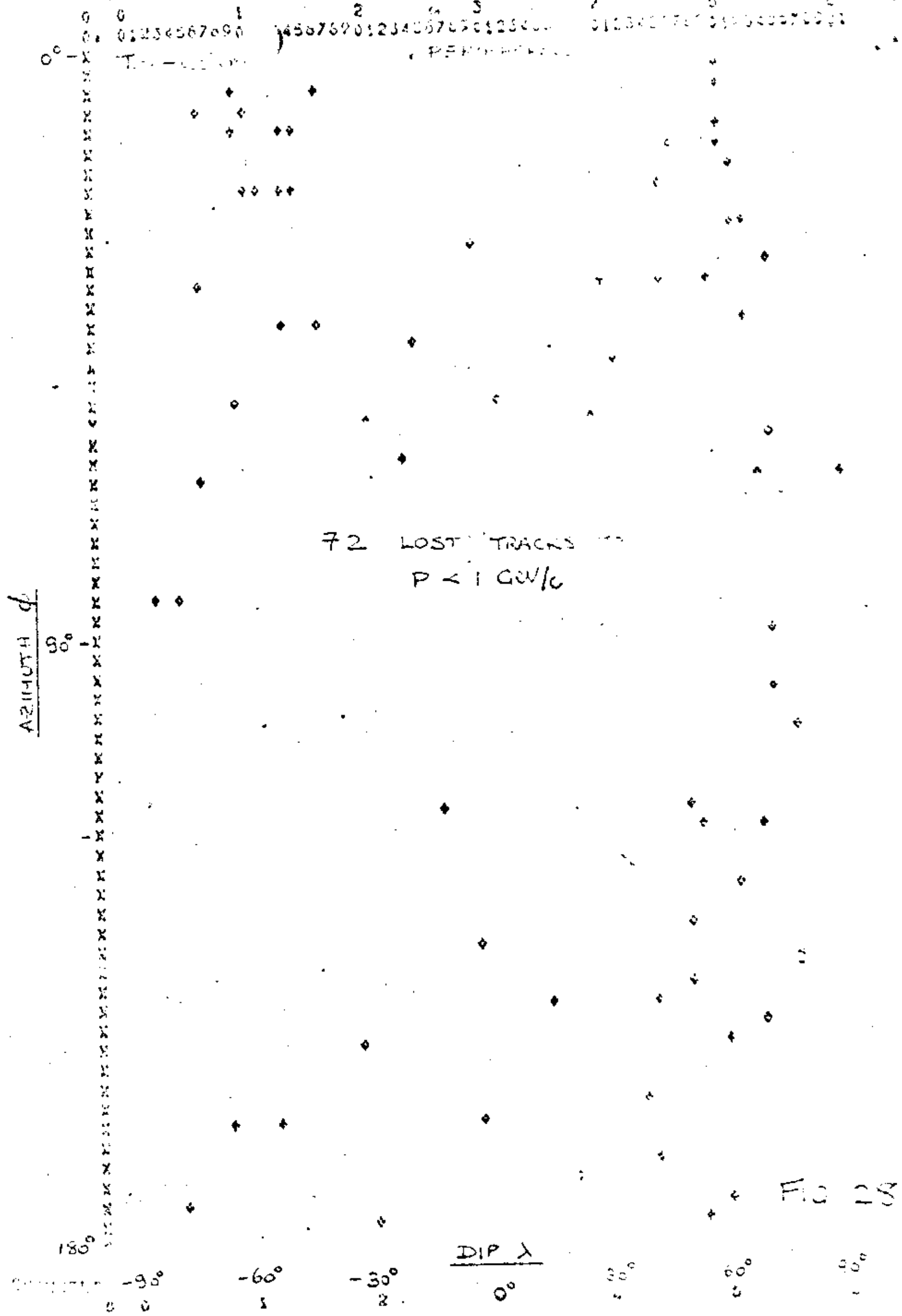
PERIPHERAL
72 LOST TRACKS
P < 1 GeV/c
AZIMUTH φ
0°
90°
180°
DIP λ
-90°
-60°
-30°
0°
30°
60°
90°

Fig 28

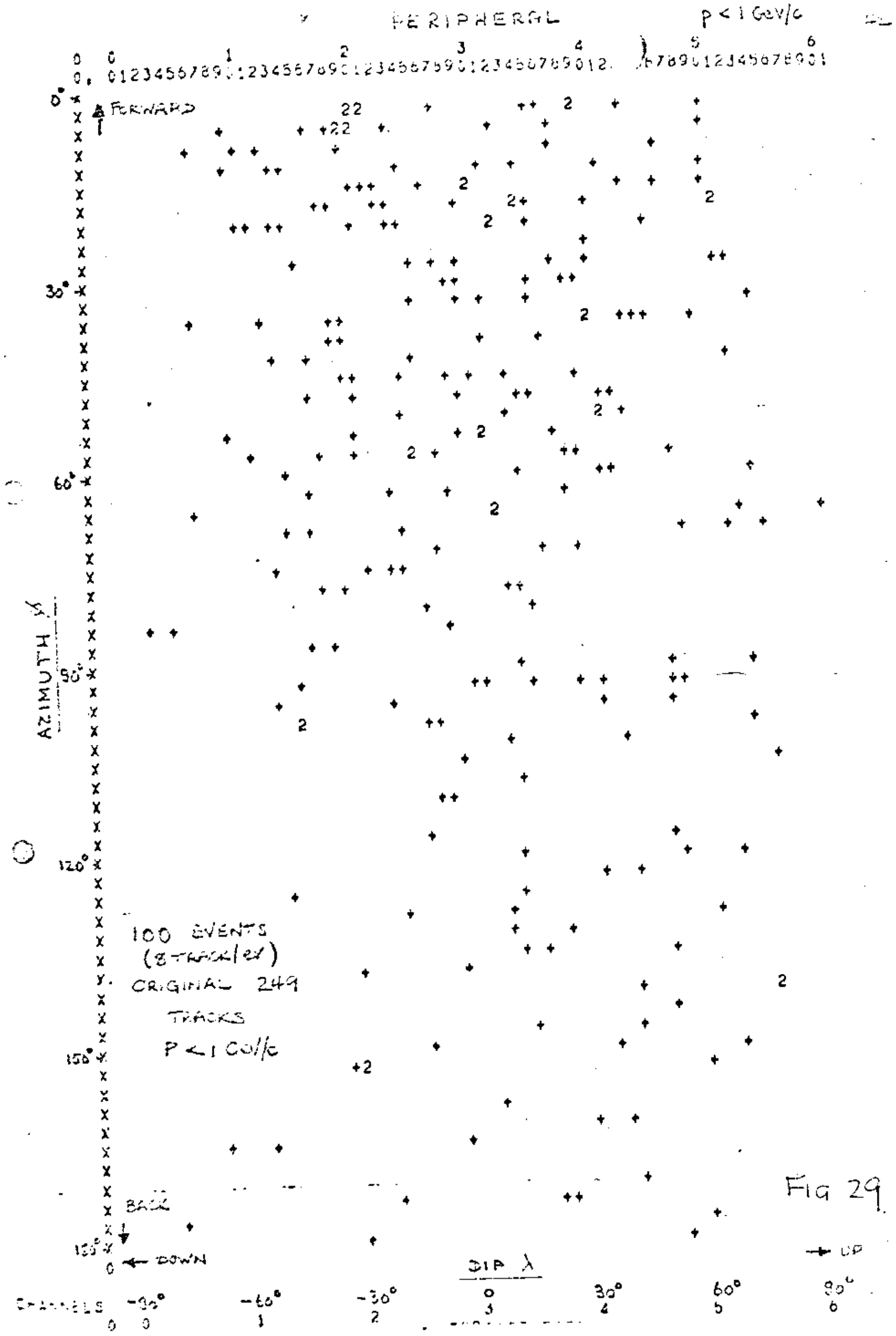
PERIPHERAL
P < 1 GeV/c
FORWARD
BACK
AZIMUTH ψ
0°
30°
60°
90°
120°
150°
180°
100 EVENTS
(8 TRACK/EV)
ORIGINAL 249
TRACKS
P < 1 GeV/c
DIP λ
← DOWN
→ UP
CHANNELS
-90°
-60°
-30°
0
30°
60°
90°

Fig 29

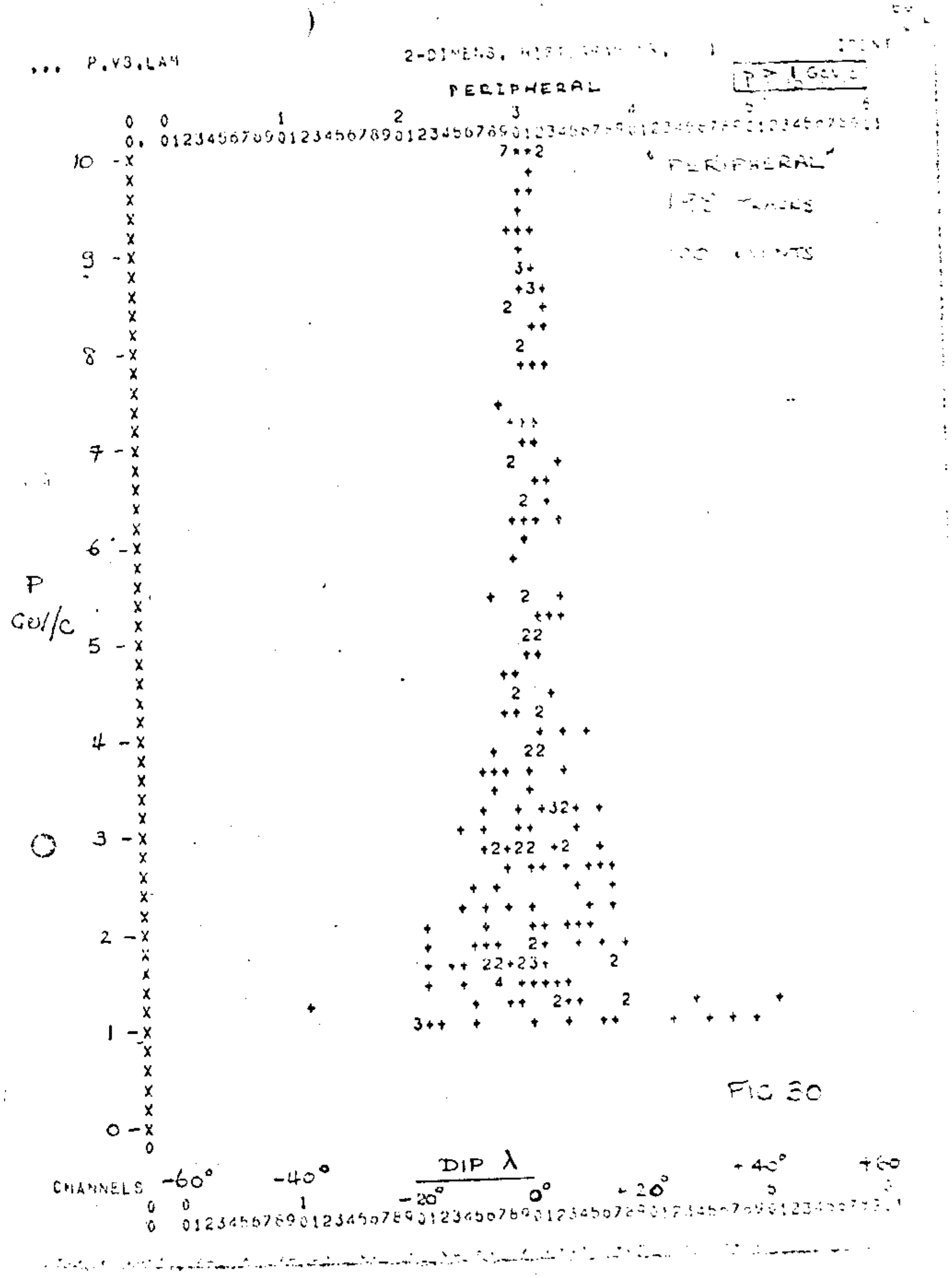
P,V3,LAM
2-DIMENS. HIST
PERIPHERAL
P > 1 GeV/c
"PERIPHERAL"
TRACKS
100 EVENTS
P
GeV/c
0
1
2
3
4
5
6
7
8
9
10
DIP λ
CHANNELS
-60°
-40°
-20°
0°
+20°
+40°
+60

Fig 30

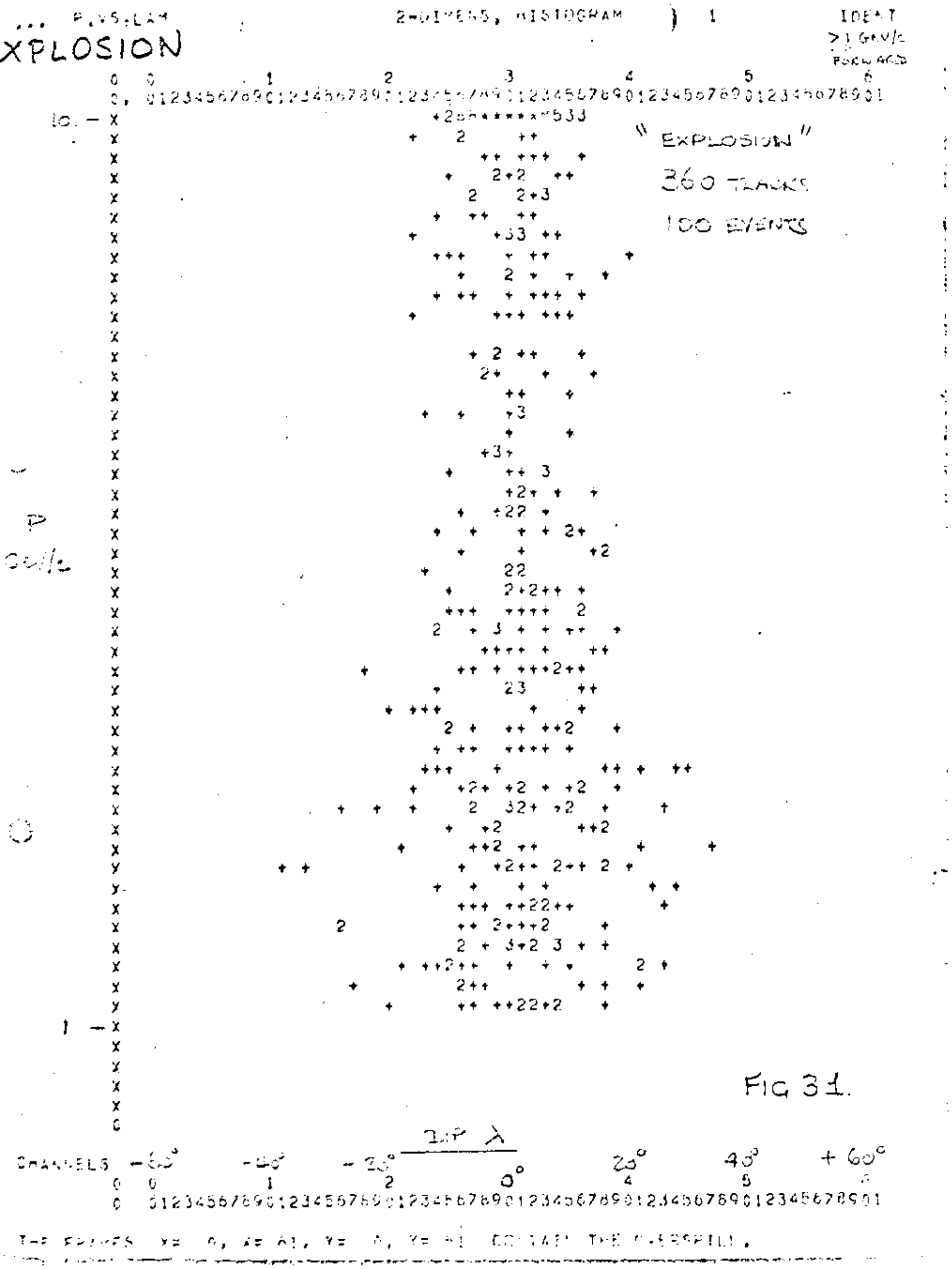

... P,VS,LAM
2-DIMENS, HISTOGRAM
IDEAL
>1 GeV/c
FORWARD
XPLOSION
" EXPLOSION "
360 TRACKS
100 EVENTS
P
GeV/c
10. –
1 –
DIP λ
CHANNELS
-60°
-40°
-20°
0°
20°
40°
+ 60°
THE FRAMES X= 0, X= 61, Y= 0, Y= 61 CONTAIN THE OVERSPILL.

FIG 31.

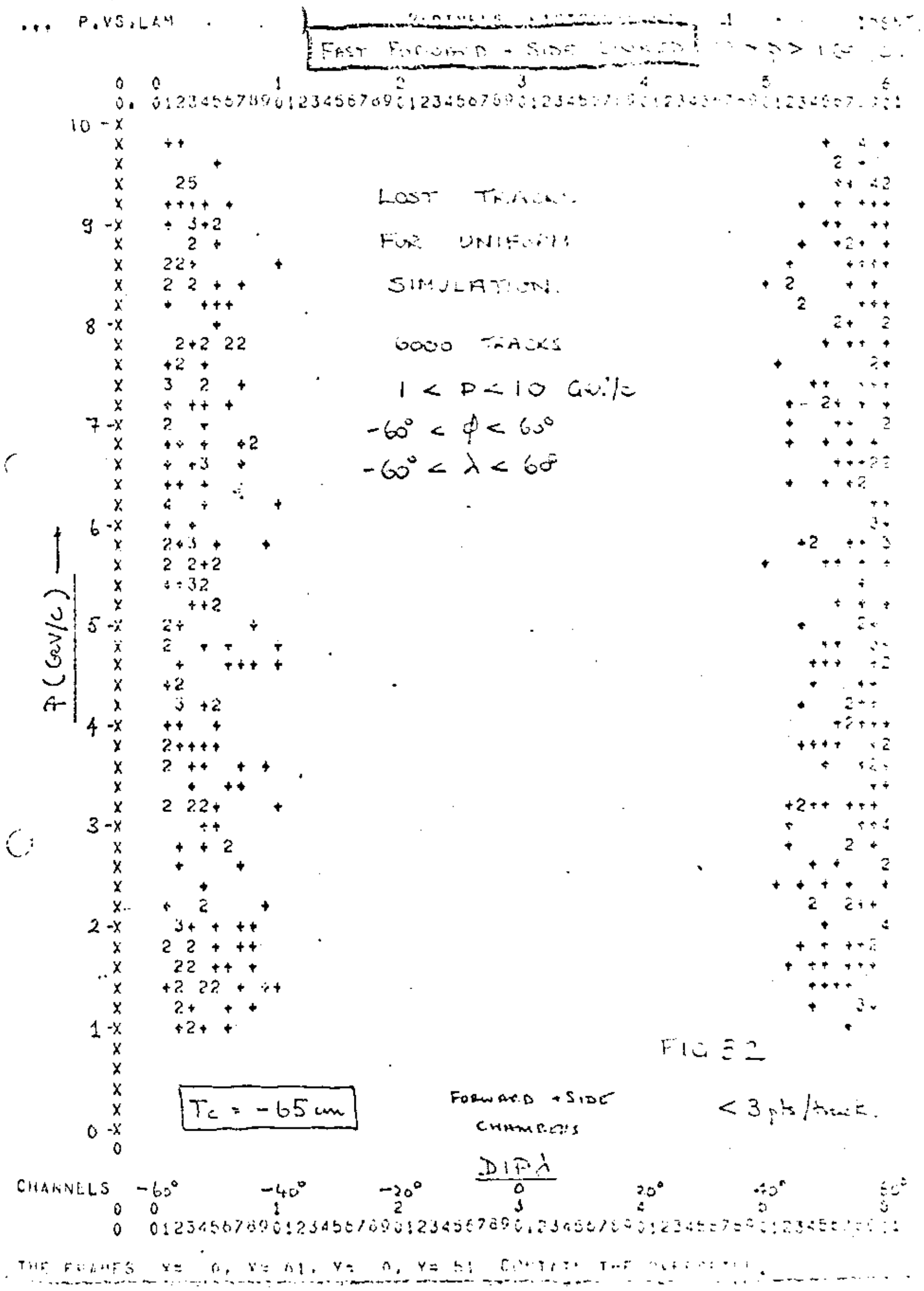

... P,VS,LAM
FAST FORWARD + SIDE LINKED
IDEAL
LOST TRACKS
FOR UNIFORM
SIMULATION.
6000 TRACKS
1 < P < 10 GeV/c
-60° < φ < 60°
-60° < λ < 60°
P (GeV/c)
Tc = -65 cm
FORWARD + SIDE CHAMBERS
< 3 pts/track.
DIP λ
CHANNELS
-60°
-40°
-20°
0
20°
40°
60°
THE FRAMES X= 0, X= 61, Y= 0, Y= 61 CONTAIN THE OVERSPILL.

FIG 32